A classification method of road transport missions and applications using the operating cycle format

Citation for the original published paper (version of record):

Romano, L., Johannesson, P., Nordström, E. et al (2022). A classification method of road transport missions and applications using the operating cycle format. IEEE Access, 10: 73087-73121. http://dx.doi.org/10.1109/ACCESS.2022.3188872

IEEE Access
Multidisciplinary | Rapid Review | Open Access Journal

Received 14 June 2022, accepted 3 July 2022, date of publication 6 July 2022, date of current version 18 July 2022.

Digital Object Identifier 10.1109/ACCESS.2022.3188872

METHODS

A Classification Method of Road Transport Missions and Applications Using the Operating Cycle Format

LUIGI ROMANO[1], PÄR JOHANNESSON[2], ERIK NORDSTRÖM[3], FREDRIK BRUZELIUS[1], RICKARD ANDERSSON[4], AND BENGT JACOBSON[1]

[1]Department of Mechanics and Maritime Sciences, Chalmers University of Technology, 41296 Gothenburg, Sweden
[2]RISE Research Institutes of Sweden, 41279 Gothenburg, Sweden
[3]Department of Physics, Umeå University, 90187 Umeå, Sweden
[4]Volvo AB, 40508 Gothenburg, Sweden

Corresponding author: Luigi Romano (luigi.romano@chalmers.se)

This work was supported by the Swedish Energy Agency and the Swedish Vehicle Research and Innovation Program (FFI) through the COVER Project under Grant 44929-1.

ABSTRACT When dealing with customers, original equipment manufacturers (OEMs) classify vehicular usage by resorting to simplified, often colloquial, descriptions that allow for a rough understanding of the operating conditions and the user's needs. In this way, the information retrieved from the customers is exploited to guide their choices in terms of vehicle design and configuration, based on the characteristics of the transport application, labeled using intuitive metrics. However, a common problem in this context is the absence of any formal connection to lower levels of representation that might effectively be used to assess vehicular energy performance in simulation, or for design optimization using mathematical algorithms. Indeed, both processes require more accurate modeling of the surroundings, including exhaustive information about the local road, weather, and traffic conditions. Therefore, starting with a detailed statistical description of the environment, this paper proposes a method for mathematical classification of transport missions and applications within the theoretical framework of the operating cycle (OC). The approach discussed in the paper combines a collection of statistical models structured hierarchically, called a stochastic operating cycle (sOC), with a bird's-eye view description of the operating environment. The latter postulates the existence of different classes, which are representative of the usage and whose definition is based on simple metrics and thresholds expressed mathematically in terms of statistical measures. Algebraic expressions, called *operating classes* in the paper, are derived analytically for all the stochastic models presented. This establishes a connection between the two levels of representation, enabling to simulate longitudinal vehicle dynamics in virtual environments generated based on the characteristics of the intended application, using log data collected from vehicles and/or information provided by customers. Additionally, the relationships between the two descriptions are formalized using elementary probability operators, allowing for an intuitive characterization of a transport operation. An example is adduced to illustrate a possible application of the proposed method, using six sOCs parametrized from log data collected during real-world missions. The proposed approach may facilitate the interaction between OEMs, customers, and road operators, allowing for planning of maintenance, and optimization of transport missions, components, and configurations using standard procedures and routines.

INDEX TERMS Autoregressive models, mission classification, operating cycle, road transport mission, stochastic modeling, stochastic operating cycle.

The associate editor coordinating the review of this manuscript and approving it for publication was Chih-Yu Hsu.

NOMENCLATURE

Symbol	Description
C	Random variable for curvature (m^{-1}).
$\mathbf{G}_R$	Generator matrix for road type.
$\mathbf{G}_V$	Generator matrix for speed sign.
H_p	Random variable for precipitation occurrence.
K	Random variable for continuous road curvature (m^{-1}).
L_h	Mean hill length (m).
L_s	Sampling length for topography (m).
L_{tot}	Total road length (km).
$\boldsymbol{L}_R$	Mean length vector for road type (km).
L_{Ri}	Mean length for road type (km).
$\boldsymbol{L}_V$	Mean length vector for speed sign (km).
L_{Vi}	Mean length for speed sign (km).
$\mathbf{P}_{H\|s_i}$	Conditional Markov matrix for precipitation occurrence.
$\mathbf{P}_R$	Markov matrix for road type.
$\mathbf{P}_V$	Markov matrix for speed signs.
R_t	Random variable for road type.
S	Random variable for season.
$\bar{T}$	Deterministic component of air temperature (°C).
$\tilde{T}$	Stochastic component of air temperature (°C).
T_{air}	Random variable for air temperature (°C).
T'_{air}	Modified random variable for air temperature (°C).
T^*_{air}	Air temperature (°C).
T_d, T_y	Daily and annual amplitudes of temperature (°C).
T_s	Random variable for stop time (s).
V	Random variable for speed sign ($km\,h^{-1}$).
V_b	Random variable for bump speed ($km\,h^{-1}$).
Y	Random variable for road grade (%).
Y'	Modified random variable for road grade (%).
a_y^{max}	Lateral comfort acceleration ($m\,s^{-2}$).
e_T	Error term for air temperature (°C).
e_Y	Error term for topography (%).
e_ρ	Error term for traffic density (km^{-1}).
e_ψ	Error term for relative humidity.
$f_{Hij\|s_i}$	Conditional number of observed transitions for precipitation occurrence.
f_{Vij}	Number of observed transitions for speed signs.
g_{Rij}	Entry of the generator matrix for road type.
g_{Vij}	Entry of the generator matrix for speed signs.
$p_{Hij\|s_i}$	Conditional Markov matrix entries for precipitation occurrence.
p_{Vij}	Markov matrix entries for speed signs.
p_{Rij}	Markov matrix entries for road type.
r_i	Road type.
r_{turn}	Minimum radius of curvature (m).
s	season.
t_s	Stop time (s).
t_{min}, t_{max}	Minimum and maximum recommended time (s).
v_b	Bump speed ($km\,h^{-1}$).
v_i	Signed speed ($km\,h^{-1}$).
v_{min}, v_{max}	Minimum and maximum recommended speed ($km\,h^{-1}$).
v_κ	Curvature speed ($m\,s^{-1}$).
y	Road grade (%).
$\bar{\Psi}$	Deterministic component of relative humidity.
$\tilde{\Psi}$	Stochastic component of relative humidity.
Ψ_{RH}	Random variable for relative humidity.
Ψ'_{RH}	Modified random variable for relative humidity.
Ψ^*_{RH}	Relative humidity.
Ψ_d, Ψ_y	Daily and annual amplitudes of relative humidity.
Λ_p	Random variable for precipitation intensity ($mm\,h^{-1}$).
$\alpha_{\Lambda_p\|s_i}$	Conditional shape parameter for precipitation intensity.
$\beta_{\Lambda_p\|s_i}$	Conditional rate parameter for precipitation intensity ($mm\,h^{-1}$).
κ	Continuous road curvature (m^{-1}).
λ_b	Speed bump intensity (km^{-1}).
λ_C	Curviness intensity (km^{-1}).
λ_p	Precipitation intensity ($mm\,h^{-1}$).
λ_s	Stop signs intensity (km^{-1}).
λ_{Ri}	Road type intensity (km^{-1}).
λ_{Vi}	Speed sign intensity (km^{-1}).
μ_C	Modified mean curvature (ln m).
μ_L	Modified mean curve length (ln m).
μ_T	Mean temperature (°C).
μ_Ψ	Mean relative humidity.
μ_ρ	Mean traffic density (km^{-1}).
$\boldsymbol{\pi}_{H\|s_i}$	Conditional stationary probability vector for precipitation occurrence.
$\pi_{H1\|s_i}$, $\pi_{H2\|s_i}$	Conditional stationary probabilities for precipitation occurrence.
$\boldsymbol{\pi}_R$	Stationary probability vector for road type.
π_{Ri}	Stationary probability for road type.
$\boldsymbol{\pi}_V$	Stationary probability vector for speed signs.
π_{Vi}	Stationary probability for speed signs.
$\bar{\rho}$	Deterministic component of traffic density (km^{-1}).
$\tilde{\rho}$	Stochastic component of traffic density (km^{-1}).
ρ_c	Critical traffic density (km^{-1}).
ρ_d	Daily traffic density amplitude (km^{-1}).
ρ_t	Random variable for traffic density (km^{-1}).
ρ'_t	Modified random variable for traffic density (km^{-1}).

ρ_{t}^{*}	Traffic density (km^{-1}).
$\phi_{T\|s_i}$	Conditional autoregressive coefficient for air temperature.
ϕ_{Y}	Autoregressive coefficient for topography.
$\phi_{\Psi\|s_i}$	Conditional autoregressive coefficient for relative humidity.
$\phi_{\rho\|s_i}$	Conditional autoregressive coefficient for traffic density.
$\varphi_{T_{\mathrm{d}}}$, $\varphi_{T_{\mathrm{y}}}$	Initial phases for air temperature (rad).
$\varphi_{\Psi_{\mathrm{d}}}$, $\varphi_{\Psi_{\mathrm{y}}}$	Initial phases for relative humidity (rad).
φ_{ρ}	Initial phase for traffic density (rad).
$\sigma_{e_T\|s_i}$	Conditional standard deviation for the innovation in the air temperature model (°C).
σ_{e_Y}	Standard deviation for the innovation in the topography model (%).
$\sigma_{e_\Psi\|s_i}$	Conditional standard deviation for the innovation for the relative humidity model.
$\sigma_{e_\rho\|s_i}$	Conditional standard deviation of the innovation for the traffic density model (km^{-1}).
σ_{C}	Modified standard deviation of curvature (ln m).
σ_{L}	Standard deviation of curvature length (ln m).
$\sigma_{\tilde{T}\|s_i}$	Conditional standard deviation for the stochastic component of air temperature (°C).
σ_{Y}	Standard deviation of topography (%).
$\sigma_{\tilde{\Psi}\|s_i}$	Conditional standard deviation for the stochastic component of relative humidity.
$\sigma_{\tilde{\rho}\|s_i}$	Conditional variance for the stochastic component of traffic density (km^{-1}).
$\bar{\omega}_{\mathrm{d}}$	Daily frequency (rad).
$\bar{\omega}_{\mathrm{y}}$	Annual frequency (rad).
$\mathcal{E}(\cdot)$	Exponential distribution.
$\mathcal{N}(\cdot,\cdot)$	Normal distribution.
$\mathcal{P}(\cdot)$	Poisson distribution.
$\mathbb{E}(\cdot)$	Expectation.
$\mathbb{P}(\cdot)$	Probability.

I. INTRODUCTION

Transport operations[1] of road vehicles may differ substantially depending on the particular properties of the mission and the geographical area where it takes place [2]–[5]. From the perspective of the intended usage, as an emblematic example, one might compare a small, relatively low-speed truck delivering within a municipality to a heavily loaded timber truck traveling long distances. The characteristics of the operating environment also stimulate vehicles differently. Topography, number and length of curves along the road, relative wind, traffic density, and many other factors all contribute to determining the vehicle's behavior, impacting important indicators like energy efficiency and (equivalent) CO_2 emissions [6]–[16].

Ideally, it would be desirable to develop individual products for every possible route and transport mission. However, due to stringent physical and economical limitations, this is impractical. Often, a viable alternative is to use a statistical approach, so that commercial vehicles are developed for typical applications and geographical regions [17], [18]. Over the years, a vast scientific literature has been produced dealing with the optimization of single components, configurations, or even fleets of road vehicles depending on the intended use [19]–[27]. Specifically, many methods proposed by researchers rely on simplified models for longitudinal vehicle dynamics in combination with reference speed profiles (called driving cycles) to simulate representative operating conditions. Starting from log data, various techniques may be employed to build driving cycles, using an assortment of measures like acceleration, mean speed and torque, cruising time, road grade, et cetera [18], [28]–[31], [31]–[53]. In particular, a first distinction may be made between rule-based methods [54], [55] and statistical ones [18], [28]–[37]. While rule-based methods are very sensitive to the experts' opinion and only replicate a limited number of characteristics from the measured driving cycles [54], [55], statistical techniques correlate synthetic speed profiles with certain operating conditions of the vehicle, such as cruising, idling, acceleration, or braking events. This enhanced approach combines different information (mostly inferred by speed and acceleration signals) to reflect the characteristics of real driving scenarios [18], [28]–[37].

In turn, methods for synthesizing driving cycles based on statistical techniques may be classified into four subcategories: micro-trip based, segment-based, pattern classification and modal cycle construction [38]. Micro-trip-based methods generate several candidate cycles from micro-trips. These are usually defined as excursions between consecutive stops, and may be chosen either randomly or based on specific modal characteristics. Then, an optimal cycle is selected based on the fulfillment of some satisfaction criterion, using a genetic algorithm [39], [40]. Driving cycles have been synthesized with the micro-trip-based methods for the cities of Hong Kong [41], Pune and Chennai, India, [35], [42] and Singapore [43].

In the segment-based method, a driving cycle is built from measured signals which are partitioned considering not only consecutive stops, but also the road characteristics and traffic conditions [9]. Segments may therefore begin and end at any speed. An inherent difficulty is that constraints on speed and acceleration must be imposed in chaining the segments together when synthesizing a new cycle [44], [45].

Pattern classification methods partition the speed data into kinematic sequences similar to micro-trips [31], [46]–[49]. With the aid of statistical techniques, these are then classified

[1] In this paper, the notions of *transport application*, *transport operation* and *transport mission* are defined according to [1]. In particular, Pettersson [1] defines the transport application as the overall purpose of a vehicle during its lifetime. This is something antecedent to the vehicle itself, and towards which specifications should be tailored. The difference between transport operation and mission is less formal. The former consists of a finite number of tasks along a given route, the latter integrates with details from the surroundings. To make sense, both operation and mission assume the existence of a vehicle, meaning that they are defined *a posteriori*.

into heterogeneous classes depending on some defined criteria. The final driving cycle is thus synthesized by combining the kinematic sequences based on the statistical properties of the classes. In several studies, new cycles have been constructed from kinematics sequences using principal component analysis (PCA) and cluster analysis [56].

Finally, in the modal cycle method, the measured speed data is clustered into snippets and classified into modal bins by using maximum likelihood estimation [31], [36], [37]. A new driving cycle is then built from chosen snippets assuming the Markov property, whose validity has also been demonstrated theoretically by [49]. In particular, two and three-dimensional Markov chains have been proposed in [36], [37]. More recently, this approach was extended in [38] by considering variable passenger loads in the synthesis of driving cycles for city buses.

Further extensions to the above-referenced works on driving cycles have also been presented in the literature to reflect variation in transport operations. For example, a procedure to generate several driving cycles starting from a single bus route was proposed in [44], [45], where the investigation was conducted concerning the number of stops [44] and variable passenger load [45]. Both factors were shown to have a significant influence over energy consumption, which appeared to be almost normally distributed. To cope with the inherent uncertainties of driving cycles, a simulation model to predict the energy demand of electric city buses was also developed in [57].

However, it should be emphasized that, in the process of generation of driving cycles, all the information about the surroundings is eventually lost when incorporated directly into a reference speed profile. From a product development and selection perspective, it would be preferable to use measures and metrics that are independent of the vehicle, and which would exhaustively describe the characteristics of the environment. Indeed, a similar approach would make no implicit assumption about the product. At the same time, it would allow for a more intuitive understanding of the main physical principles governing the longitudinal dynamics of a vehicle. In this context, detailed modeling of the surroundings appears an essential prerequisite when tailoring the design to the application. In the literature [1], the problem of building a comprehensive mathematical model that accurately replicates the driving conditions, independently of vehicle and driver, is sometimes referred to as the *representation problem*.

However, as already mentioned, road vehicles are optimized according to the overall application and do not consider individual transport missions. Hence, these should be grouped and labeled based on simple scalar metrics, implying the need for a higher-level description. Ideally, such a representation system should condense the salient characteristics of the usage, alongside with those of the operating environment, but without incorporating too many details about the physical parameters that stimulate the vehicle's behavior. For instance, some measures of interest would be general statistical descriptors of the terrain, the climate, and the mission itself. To adduce a concrete example, both Volvo and Scania have developed their own classification systems, namely the Global Transport Application (GTA) [2] and the User Factor Description (UFD). Their aim is to gain an intuitive and rough understanding of how a vehicle is operated on the road. Using relevant feedback from maintenance shops, road operators, and ultimately customers, existing vehicle categories are currently improved in an evolutionary manner. This iterative process may be further refined by using some modern mathematical tools. In fact, improvement and optimization of road vehicles can certainly be addressed in a more rigorous, systematic way, provided that a suitable representation of the operating environment exists. Unfortunately, since they were conceived to deal primarily with satisfying the needs of customers, the GTA and UFD descriptions are mostly colloquial and are based on rather informal statements. However, they may be translated in terms of frequencies and probabilities. How to systematically specify thresholds and labels to classify different missions, and how to connect these metrics with a realistic representation of the usage, is referred to as the *classification problem* in this paper.

The last aspect connects to the *variation problem*. Indeed, provided that suitable metrics can be identified, even missions belonging to the same transport application cannot be expected to be identical when interpreted as individual realizations. Ideally, it should be possible to quantify the variation within each category simply. This implies, however, the need for an intermediate level of description, which should be built around this principle and make use of elementary statistical tools. A similar stochastic approach to modeling the operating environment would naturally bridge the low-level description conceived for representation purposes and the higher-level classification system discussed previously. In this context, the three levels of representation of an operating cycle (OC) respond exactly to these needs.

A. CONTRIBUTION OF THIS PAPER

Thus far, colloquial descriptions such as the GTA and UFD have been exploited in an iterative process to improve exiting vehicle configurations based on the relevant feedback from customers and road operators. As already mentioned, the main problem connected with this approach is that the level of information (*quantized* in discrete classes) contained in such representations is not directly usable when it comes to assessing energy performance in simulation environments before physical prototypes are built, or to optimizing vehicle design using *ad-hoc* algorithms. In fact, engineers and mathematicians need to work with more refined models of the operating environment, which should ideally involve easily measurable and interpretable physical quantities.

In this context, even if the two levels of description serve different purposes, a formal connection between them may be conveniently established. In this way, information collected by customers and/or logged directly from vehicles – and

hence reflecting the characteristics of the intended application – can be easily translated into a mathematical description of the environment, allowing for a virtual representation that can be used in combination with a model for longitudinal vehicle dynamics. Such an approach would enable testing and optimization of vehicle designs and configurations based on the user's needs exploiting standard routines and tools. An effort in this direction has been attempted, for example, in [23], where the authors dealt with the optimization problem of heavy trucks for a vast combination of operating conditions, including road topography modeled using the stochastic description proposed in this paper, in combination with the corresponding classes indicated by Volvo (see Section III-A1).

Therefore, the main scope of the present work is to bridge the gap between the high and low levels of representation, enabling high-level descriptions to be used in a mathematical toolchain to optimize vehicle design depending on the features of the surroundings. This is done systematically by exploring the natural connection between a classification system for road transport missions and a stochastic approach to modeling the operating environment. Specifically, the classification and variation problems are addressed in this paper from the perspective of the OC format [1], [58], [59]. The fundamental idea is that, if the properties of the road, weather, and traffic are described using stochastic models, the same models may serve as a basis to categorize vehicular operations based on simplified measures (the same that are used when dealing with a customer). The calculation of this measures may include, for instance, statistical operators like probability and expected value. Such simplified measures would condense the mission and environment properties, establishing a non-bijective relationship between a certain category (according to some classification system), and the lower-level stochastic description. To this end, the theoretical contribution of this paper consists in deriving the analytical expressions for the above relationships, subsequently referred to as *operating classes*.

The remainder of this paper is organized as follows. Section II introduces the concept of an operating cycle and discusses the connection between its three different levels of representation. In Section III, the analytical expressions for the operating classes are derived. A systematic method of classifying individual missions and entire applications is then proposed and illustrated in Section IV. To show how the notion of an operating class may be used to label an operating cycle, an example with six operating cycles, parametrized using measured log data from heavy trucks, is then adduced considering the GTA and UFD systems. The practical application of the OC format is also illustrated by comparing two different vehicle configurations based on the characteristics of the intended transport application. A discussion on the limitations of the proposed approach, plus possible opportunities for improvement, is presented in Section V. Finally, Section VI summarizes the conclusions and outlines possible directions for future research.

II. THE OPERATING CYCLE REPRESENTATION

The OC format is a mathematical description of a road transport mission that includes relevant features from the surroundings and is independent of both vehicle and driver. Specifically, it consists of three main levels of representation, namely the *bird's-eye view*, the *stochastic operating cycle* (sOC), and the *deterministic operating cycle* (dOC), arranged in a pyramidal structure (see Figure 1). These three different descriptions address the classification, variation and representation problems, respectively. Each level will be described in detail below and the relationships between the levels will be demonstrated. A common feature of the different levels of representation is that they all distinguish between four fundamental categories: road, weather, traffic and mission. It is worth emphasizing that this paper builds upon the OC format, which has already been introduced in previous works [1], [58], [59].

A. THE BIRD'S-EYE VIEW

Descending the hierarchical order between the descriptions, the bird's-eye view collocates on the top of the pyramid. It characterizes both the individual mission and the entire application, and uses simplified metrics and labels. It is intended to be very general, allowing for straightforward classification of transport operations and applications based on a few statistical indicators [58], [60], [61]. These should be ideally chosen to represent some variation in usage, performance, or properties. The metrics and labels for the bird's-eye view may be defined from scratch or borrowed from existing classification systems, as exemplified briefly for the topography parameter. In particular, the GTA system introduced by Volvo specifies four different levels [2]:

1) `FLAT` if slopes with a grade of less than 3% occur during more than 98% of the driving distance.
2) `P-FLAT` if slopes with a grade of less than 6% occur during more than 98% of the driving distance.
3) `HILLY` if slopes with a grade of less than 9% occur during more than 98% of the driving distance.
4) `V-HILLY` if the other criteria are not fulfilled.

In the above example, the bird's-eye view labels clearly correspond to the operating classes `FLAT`, `P-FLAT` (predominantly flat), `HILLY` and `V-HILLY` (very hilly), while the metrics are the values imposed on the road grade (3%, 6% and 9%, respectively) and the probability of occurrence, always set to 0.98. On the other hand, the User Factor Description (UFD) used by Scania[2] proposes only three classes:

1) `FLAT` if max 20% of the road section inclines more than 2%.
2) `HILLY` if between 20-40% of the road section inclines more than 2%.
3) `V-HILLY` if more than 40% of the road section inclines more than 2%.

[2]The information on the User Factor Description (UFD) has kindly been supplied by Scania through personal communication.

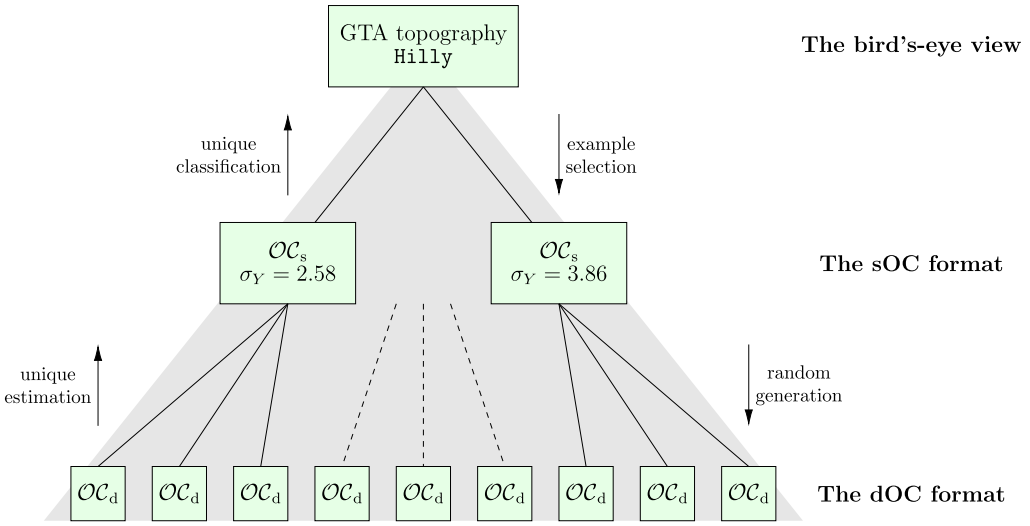

FIGURE 1. Schematic representation of the pyramidal structure of an OC. All the missions being equivalent in the sense of a GTA class belong to the same transport application from the perspective of the bird's-eye view. The individual statistical properties may however differ within the transport application (sOC). Finally, transport missions can be statistically equivalent but significantly different in practice. This is captured by the dOC representation.

In both cases, the given thresholds are ambiguous, and there is no guarantee that they can reflect any significant variation in usage or performance. Furthermore, it is worth observing that the UFD targets single road sections, while the GTA specifies the different classes based on the vehicle usage, and therefore mixes the characteristics of the environment with those of the transport operation. One main advantage of such a vague description resides in its colloquial tone. In fact, the bird's-eye view is the most appropriate representation when interfacing with the customer, who cannot be expected to have a deep understanding of stochastic models and parameters.

Formally, the complete set of bird's-eye view metrics may be defined mathematically as

$$\mathcal{OC}_b = \{\mathcal{R}_b, \mathcal{W}_b, \mathcal{T}_b, \mathcal{M}_b\}, \tag{1}$$

in which $\mathcal{R}_b$, $\mathcal{W}_b$, $\mathcal{T}_b$ and $\mathcal{W}_b$ are the sets containing all the respective bird's-eye view metrics in the road, weather, traffic, and mission categories. The subscript $(\cdot)_b$ in (1) stands for *bird's-eye view*.

B. THE STOCHASTIC OPERATING CYCLE

A stochastic model may be used to measure and mathematically reproduce variation in a transport operation [27], [29], [32]. At the mid-level, the sOC is specifically conceived as a tool to investigate the variation problem. It summarizes the statistical properties of a transport mission and consists of a collection of stochastic models organized hierarchically. In turn, the sOC models are provided with their own set of stochastic parameters, which are chosen to condense the relevant statistical properties (mean, variance, et cetera) of the corresponding physical quantity. The structure of the sOC is conceived to be as simple as possible, and the models are thought to be independent of each other, in obedience to the principle of parsimony. Disregarding the correlation between different stochastic models guarantees modularity and allows for ease of implementation and integration of new parameters, whenever required. At the same time, to balance complexity and realism, a certain level of interaction between each model is preserved by hierarchically arranging the sOC itself. Parsimony is thus achieved by defining two sets of models: primary and secondary ones (subordinate). In this way, it becomes possible to build a modular structure equipped with a high level of diversification, without the need of introducing complicated multivariate distributions. Specifically, in the sOC description, primary models for the road and weather categories relate to the notions of *road type* and *season*, as explained more extensively in Section III-B and Appendix A, respectively.

As with the bird's-eye view metrics, the complete set of sOC parameters may be defined mathematically as

$$\mathcal{OC}_s = \{\mathcal{R}_s, \mathcal{W}_s, \mathcal{T}_s, \mathcal{M}_s\}, \tag{2}$$

where $\mathcal{R}_s$, $\mathcal{W}_s$, $\mathcal{T}_s$ and $\mathcal{W}_s$ are the sets containing all the respective sOC parameters marked as road, weather, traffic and mission. Models and parameters for the road have been introduced in [58], while the weather and traffic categories have been developed more recently in [59]. The different stochastic models, plus their relative categories, are listed in in Table 1 and detailed later in Section III.

C. THE DETERMINISTIC OPERATING CYCLE

The dOC representation is the most adequate way of modeling an operating cycle when it comes to individual transport missions. It may serve as a virtual environment for realistic prediction of road vehicles' performance, virtual testing and design of control algorithms, and the development of *ad-hoc* functions.

In the dOC, the same the physical quantities that were deemed as *models* in the sOC representation[3] are interpreted as *parameters*, and are defined as discrete functions of time and position. Some parameters are only made dependent on either position or time. Some others, like the ones marked in the traffic category, depend on both. Additionally, each parameter may be represented by a scalar or a vector-valued signal (see dimensionality in Table 1). Any value between two different discrete times (or positions) may be computed by interpolation using the corresponding model in Table 1.

To formalize the dOC format mathematically, the four categories (see Table 1) may be defined as the sets containing the parameter sequences: $\mathcal{R}_\mathrm{d}$ is the set containing all sequences labeled as road, $\mathcal{W}_\mathrm{d}$ for weather, $\mathcal{T}_\mathrm{d}$ for traffic and $\mathcal{M}_\mathrm{d}$ for mission. Then, the dOC format may formalized in mathematical terms as

$$\mathcal{OC}_\mathrm{d} = \{\mathcal{R}_\mathrm{d}, \mathcal{W}_\mathrm{d}, \mathcal{T}_\mathrm{d}, \mathcal{M}_\mathrm{d}\}, \tag{3}$$

and interpolation may be defined as an operator acting on the elements in the sets. The dOC format provides a detailed view of individual transport operations without making any assumptions about the driver or vehicle. Furthermore, it is built in a modular fashion such that parameters may easily be modified, added, or removed.

D. RELATIONSHIPS BETWEEN DESCRIPTIONS

The three levels of representation discussed so far are intrinsically related, and ordered in a pyramidal structure, as already shown in Fig. 1.

The first connection which should be explored is that between the sOC and dOC descriptions. Given a set of stochastic parameters, a dOC may be interpreted as a single realization of an sOC. Indeed, by simulating its stochastic models, a fully parametrized sOC may be used to synthesize multiple dOCs. Thus, these would be equivalent in a statistical sense, but might differ significantly in practice. This also implies that the map between an sOC and a dOC is not necessarily bijective; quite the opposite. Actually, this kind of non-bijective relationship in the descending direction also persists at the higher level between the sOC and bird's-eye view representations. On the contrary, given a dOC, it is possible to estimate the corresponding stochastic parameters and hence obtain an equivalent description in terms of an sOC. This is usually done by resorting to elementary statistical methods, and assuming plausible probability distributions and stochastic models.

On the other hand, the bird's-eye view and the sOC are both statistical descriptions, but with considerably different resolutions. Indeed, while the bird's-eye view generally encompasses an entire transport application (but might also be used to classify single operations and even road sections), the sOC only targets individual missions. The formal relationship between the two levels may be elucidated by looking at the GTA classes previously introduced. Again, using the topography as an example, it is possible to estimate the process variances which yield the thresholds set by the GTA classification system, i.e. the bird's-eye view metrics (as done in Section III-A). Thus, given an sOC, the corresponding GTA class may always be deduced uniquely. The inverse operation is not possible since, for a predetermined GTA class, infinitely many sOCs may exist. More specifically, the authors of this paper are concerned with showing that, for a generic model ξ in the road, weather, and traffic OC categories, the elements in the set of sOC parameters $\mathcal{OC}_\mathrm{s}$ and the bird's-eye view metrics in the set $\mathcal{OC}_\mathrm{b}$ may be related as follows:

$$\boldsymbol{a}_\xi\left(\boldsymbol{\eta}_{\mathrm{b},\xi}\right) < \boldsymbol{g}_\xi\left(\boldsymbol{\eta}_{\mathrm{s},\xi}, \boldsymbol{\eta}_{\mathrm{b},\xi}\right) \leq \boldsymbol{b}_\xi\left(\boldsymbol{\eta}_{\mathrm{b},\xi}\right), \tag{4}$$

where $\xi \in \mathcal{X}_\mathcal{R}, \mathcal{X}_\mathcal{W}$ or $\mathcal{X}_\mathcal{T}$ is a generic sOC model, $\mathcal{X}_\mathcal{R}, \mathcal{X}_\mathcal{W}$, and $\mathcal{X}_\mathcal{T}$ denote the sets of sOC models for the road, weather, and traffic categories, respectively, $\boldsymbol{\eta}_{\mathrm{s},\xi} \in \mathcal{R}_{\mathrm{s},\xi}, \mathcal{W}_{\mathrm{s},\xi}, \mathcal{T}_{\mathrm{s},\xi}$ and $\boldsymbol{\eta}_{\mathrm{b},\xi} \in \mathcal{R}_{\mathrm{b},\xi}, \mathcal{W}_{\mathrm{b},\xi}, \mathcal{T}_{\mathrm{b},\xi}$ are vectors of sOC parameters and bird's-eye-view metrics for the model ξ, $\mathcal{R}_{\mathrm{s},\xi} \subset \mathcal{R}_\mathrm{s}$, $\mathcal{W}_{\mathrm{s},\xi} \subset \mathcal{W}_\mathrm{s}$, $\mathcal{T}_{\mathrm{s},\xi} \subset \mathcal{T}_\mathrm{s}$ are subsets of sOC parameters for the model ξ, and $\mathcal{R}_{\mathrm{b},\xi} \subset \mathcal{R}_\mathrm{b}$, $\mathcal{W}_{\mathrm{b},\xi} \subset \mathcal{W}_\mathrm{b}$, $\mathcal{T}_{\mathrm{b},\xi} \subset \mathcal{T}_\mathrm{b}$ are subset of bird's-eye-view metrics for the model ξ.

Finally, $\boldsymbol{a}_\xi(\boldsymbol{\eta}_{\mathrm{b},\xi})$ and $\boldsymbol{b}_\xi(\boldsymbol{\eta}_{\mathrm{b},\xi})$ represent lower and upper bounds for the vector-valued function $\boldsymbol{g}_\xi(\cdot,\cdot)$ appearing in (4). In this context, it should be clarified that the inequalities (4) need to be interpreted element-wise. Basically, they postulate the existence of certain relationships which mathematically formalize the so-called operating classes. It may be inferred from (4) that, for each model in each category, the corresponding operating class depends solely on the sOC parameters used to describe that model, plus the corresponding bird's-eye view metrics.

The analytical derivation of the relationships for the operating classes is carried out in Section III.

III. DERIVATION OF THE OPERATING CLASSES

The main analytical contribution of this paper lies in the derivation of the aforementioned operating classes.

In the remainder of the paper, the notation is as follows: for a generic random variable $A : \Omega_A \mapsto \mathcal{S}_A$, its realizations are denoted by a, unless specified otherwise. For continuous and discrete random variables, respectively, probability density functions (PDFs) and probability mass functions (PMFs) are denoted by $f_A(\cdot)$ and $p_A(\cdot)$, and their argument often by a. Cumulative distribution functions (CDFs) are written as $F_A(\cdot)$. For a generic function written as $f(\cdot;\cdot)$, the semicolon is used to separate variables from parameters. Multiple variables or parameters may be additionally separated using commas. The set of real numbers is denoted by $\mathbb{R}$; the sets of positive and negative real numbers are denoted by $\mathbb{R}_{\geq 0}$, $\mathbb{R}_{\leq 0}$ when including the zero and by $\mathbb{R}_{>0}$, $\mathbb{R}_{<0}$ when excluding it. The set of positive integer numbers is denoted by $\mathbb{N}$, whereas $\mathbb{N}_0$ denotes the extended set of positive integers including zero, i.e. $\mathbb{N}_0 = \mathbb{N} \cup \{0\}$. Sequences of random variables are denoted by $\{A_k\}_k$ (the subscript k is often dropped when the

[3]The relationship between the role of a physical quantity in the sOC and dOC representations is perhaps better understood from Table 1, where each entity is labeled under *model* for the sOC and *parameter* for the dOC.

TABLE 1. Stochastic models and deterministic parameters (dOC parameters) for the sOC and dOC representations. *Linear* and *constant* refer to linear and right-side continuous piecewise constant interpolation models respectively. The mathematical model of *Dirac delta* occurs when the parameter is regarded as an isolated *event*.

Model or parameter	Category	Type (for dOC)	Interp. model (for dOC)	Dim	Quantity
Speed signs	Road	Function	Constant	1	Speed limit
Altitude	Road	Function	Linear	1	Vertical coordinate
Curvature	Road	Function	Linear	1	Curvature
Ground type	Road	Function	Constant	2	Surface type, cone index
Roughness	Road	Function	Constant	2	Waviness, roughness coeff.
Stop signs	Road	Event	Dirac delta	1	Standstill time
Traffic lights	Road	Event	Dirac delta	1	Standstill time
Give way signs	Road	Event	Dirac delta	1	Standstill time
Speed bumps	Road	Event	Dirac delta	3	Length, height, angle of approach
Longitude	Road	Function	Linear	1	WGS84 longitude
Latitude	Road	Function	Linear	1	WGS84 latitude
Ambient temperature	Weather	Function	Linear	1	Temperature
Atmospheric pressure	Weather	Function	Linear	1	Pressure
Precipitation	Weather	Function	Constant	1	Precipitation amount
Wind velocity	Weather	Function	Constant	2	Velocity vector
Relative humidity	Weather	Function	Linear	1	Humidity
Traffic density	Traffic	Function	Constant	1	Density
Mission stops	Mission	Event	Dirac delta	1	Standstill time
Cargo weight	Mission	Function, event	Linear, constant	1	Payload
Power take-off	Mission	Function	Linear	1	Output power
Charging power	Mission	Function	Constant	1	Input power
Travel direction	Mission	Function	Constant	1	Driving direction

clarity allows). Indicator functions are denoted by $\mathbb{1}_{a\in\mathcal{A}}$ and assume a value of one if $a \in \mathcal{A}$ and zero otherwise.

A. ROAD CATEGORY

In the sOC description, the road category comprises stochastic models for topography, curviness, speed bumps, stop signs, road roughness, speed signs, and ground type. The corresponding operating classes are derived in the following, and connect the sOC parameters to the bird's-eye view metrics.

It is worth mentioning that all the road models presented in this paper have been chosen as a compromise between simplicity and accuracy, in obedience to the already mentioned principle of parsimony. In particular, the models for topography, curviness and road roughness are based on the extensive research presented in [10], [11], [62]–[67]. Similarly, the models for speed bumps, stop and speed signs, and road and ground types were introduced and validated in [58].

1) TOPOGRAPHY

Topography plays a major role in determining the overall energy performance of road vehicles. Indeed, positive road grades are responsible for resistive forces that oppose longitudinal motion, resulting in increased energy consumption [19]. Negative road grades, in contrast, produce forces that accelerate the vehicle downhill, and may considerably impact the life and performance of the mechanical components of the braking system. Negative slopes are also exploited by battery electric vehicles (BEVs) for regenerative braking [23]. Owing to these premises, it should not be surprising that both Volvo and Scania include the topography parameter in their classification systems.

In the sOC, the road is partitioned into $k \in \mathbb{N}$ short segments of fixed length L_s, and the grade $\{Y_k\}_{k\in\mathbb{N}}$ is regarded as a random variable on each of them. Specifically, it is restricted to assuming values between a minimum and maximum:

$$Y_k = \min\Big(\max\big(-y_c, Y'_k\big), y_c\Big), \tag{5}$$

where $y_c \in \mathbb{R}_{>0}$ is an imposed limit on the maximum road grade expressed as a percentage. By default, it may be set to $y_c = 100$. The modified topography Y'_k is then modeled using a stationary, first-order autoregressive AR(1) process as follows [10], [11]:

$$Y'_k = \phi_Y Y'_{k-1} + e_{Y,k}, \quad e_{Y,k} \sim \mathcal{N}\Big(0, \sigma^2_{e_Y}\Big), \tag{6}$$

where $\phi_Y \in (-1, 1)$ and $\sigma_{e_Y} \in (0, \infty)$ are the two characteristic parameters. According to (6), the modified road grade itself is normally distributed [68], i.e.

$$Y' \sim \mathcal{N}\Big(0, \sigma^2_Y\Big), \tag{7}$$

where the subscript k has been omitted for ease of notation.

The process variance σ^2_Y reads

$$\sigma^2_Y = \frac{\sigma^2_{e_Y}}{1 - \phi^2_Y}. \tag{8}$$

Furthermore, the autoregressive coefficient ϕ_Y may be also rewritten as a function of the hill length L_h:

$$\phi_Y = \sin\left(\frac{\pi}{2} - 2\frac{L_\mathrm{s}}{L_\mathrm{h}}\right), \tag{9}$$

where L_s is the sampling length.

Thus, the model for the topography may be equivalently parametrized using the hill length L_h and the standard deviation σ_Y defined in (8) and (9), which are easier to interpret than ϕ_Y and σ_{e_Y}. Therefore, the set of stochastic road parameters relating to the topography model may be formalized as $\mathcal{R}_{\mathrm{s},Y} = \{L_\mathrm{h}, \sigma_Y\}$.

Following the interpretation of the GTA and UFD classifications, the operating class for the topography connecting the sOC and bird's-eye view representations may be derived by considering the probability that the road grade comprises a value between a minimum and a maximum. This value of probability may range between lower and upper bounds $p_{y,\min}$ and $p_{y,\max}$, respectively. In formula: $p_{y,\min} < \mathbb{P}(y_\min < |Y| \leq y_\max) \leq p_{y,\max}$. The corresponding formula for the operating class is then given in Result 1.

Result 1 (Operating Class for Topography): For the road topography model described by (5)-(9), the following expression for the operating class may be deduced:

$$\begin{aligned} p_{y,\min} < {} & \mathbb{1}_{y_\max \in [y_\mathrm{c},\infty)} + \left[2\Phi\left(\frac{y_\max}{\sigma_Y}\right) - 1\right]\mathbb{1}_{y_\max \in [0,y_\mathrm{c})} \\ & - \left[2\Phi\left(\frac{y_\min}{\sigma_Y}\right) - 1\right]\mathbb{1}_{y_\min \in [0,y_\mathrm{c})} \\ & - \mathbb{1}_{y_\min \in [y_\mathrm{c},\infty)} \leq p_{y,\max}, \end{aligned} \tag{10}$$

where the function $\Phi(\cdot)$ is the CDF of the standard normal distribution.

Proof: Noticing that

$$\begin{aligned} \mathbb{P}(|Y| \leq y) &= F_Y(y; \sigma_Y, y_\mathrm{c}) \\ &= \mathbb{P}\Big(\big|Y'\big| \leq y\Big)\mathbb{1}_{y\in[0,y_\mathrm{c})} + \mathbb{1}_{y\in[y_\mathrm{c},\infty)}, \end{aligned} \tag{11}$$

and recalling that

$$\begin{aligned} \mathbb{P}\Big(\big|Y'\big| \leq y\Big) &= F_{Y'}(y; \sigma_Y) - F_{Y'}(-y; \sigma_Y) \\ &= 2\Phi\left(\frac{y}{\sigma_Y}\right) - 1 \end{aligned} \tag{12}$$

immediately yields (10). ∎

It may be observed that (10), despite being scalar, has the same structure of (4), and connects the elements in the set of sOC parameters for topography $\mathcal{R}_{\mathrm{s},Y} = \{L_\mathrm{h}, \sigma_Y\}$ with the bird's-eye view metrics in the set $\mathcal{R}_{\mathrm{b},Y} = \{y_\min, y_\max, p_{y,\min}, p_{y,\max}\}$.

The above inequality (10) may be solved numerically for σ_Y, once the bird's-eye view metrics have been specified. Again, adducing the example of the GTA classification system, the four different values $y_\min = 0$, $y_\max = 3$, 6 and 9 prescribed for the road grade in (10) as a percentage of the road length and the limits $p_{y,\min} = 0.98$, $p_{y,\max} = 1$ yield the values of σ_Y reported in Table 2 for the classes

TABLE 2. Topography classes according to the GTA and UFD classification systems with the corresponding intervals for the standard deviation σ_Y.

Class	GTA system	UFD system
FLAT	$\sigma_Y < 1.29$	$\sigma_Y < 1.56$
P-FLAT	$1.29 \leq \sigma_Y < 2.58$	-
HILLY	$2.58 \leq \sigma_Y < 3.87$	$1.56 \leq \sigma_Y \leq 2.38$
V-HILLY	$3.87 \leq \sigma_Y$	$2.38 < \sigma_Y$

FLAT, P-FLAT, HILLY and V-HILLY. On the other hand, as already mentioned, the UFD misses the P-FLAT class. Indeed, it only specifies one limit $y_\max = 2$ ($y_\min$ is always zero) for the road grade in (10), and two different probability thresholds $p_{y,\max} = 0.2$ and 0.4, respectively. The ranges for the standard deviation σ_Y corresponding to each topography class are listed in Table 2 for both classification systems.

It should be noted that, according to both the GTA and UFD systems, in the bird's-eye view description the hill length L_h is not included in the determination of the specific operating class. Thus, according to the bird's eye view representation, road segments with the same process variance σ_Y^2 but different hill lengths L_h are formally equivalent. A possible extension to the original definition for the operating class would be to also take into account the hill length L_h, by postulating an additional relationship of the form:

$$L_{\mathrm{h},\min} < L_\mathrm{h} \leq L_{\mathrm{h},\max}. \tag{13}$$

Together, (10) and (13) would more accurately characterize the road topography. Also in this case, (10) and (13) have the same form of (4), connecting the elements in the set $\mathcal{R}_{\mathrm{s},Y} = \{L_\mathrm{h}, \sigma_Y\}$ with the bird's-eye view metrics in $\mathcal{R}_{\mathrm{b},Y} = \{y_\min, y_\max, p_{y,\min}, p_{y,\max}, L_{\mathrm{h},\min}, L_{\mathrm{h},\max}\}$.

As an example, a comparison between measured data from a log file (corresponding to sOC 2 in Section IV-C) and the analytical PDF and CDF for the road topography according to Eqs. (11) and (12) is shown in Fig. 2.

2) CURVINESS

Lateral acceleration due to curves along the road typically induces the driver to decelerate, resulting in increased energy consumption. In this context, two main contributing phenomena may be identified: the reduced efficiency of the prime mover and the losses due to pure or combined slip conditions that take place inside the tire contact patches [69]–[71]. Moreover, lateral load due to road curvature has a substantial impact on the fatigue of the mechanical components of a vehicle, reducing their useful life [62]–[64]. Therefore, the curviness parameter is accounted for in both Volvo's and Scania's descriptions.

In the sOC, a curve is regarded as an independent event having a location, curvature (inverted radius), and length. This description – referred to as the *curviness* of the road – was adapted in [58] from [62] and is denoted in this paper by the sequence $\{X_k, C_k, L_k\}_{k\in\mathbb{N}}$. Specifically, the locations are modeled using a Poisson process, i.e.

$$X_{k+1} - X_k \sim \mathcal{E}(\lambda_C), \tag{14}$$

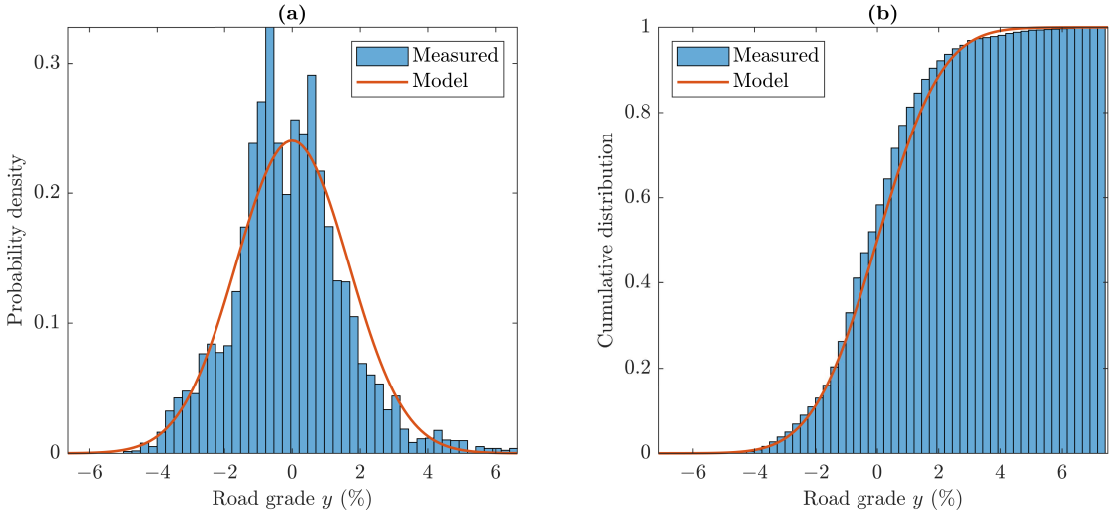

FIGURE 2. Comparison between the measured distribution and the analytical PDF and CDF of the road topography: (a) probability density; (b) cumulative distribution.

where the intensity $\lambda_C \in (0, \infty)$ should be interpreted as the mean number of curves per unit of distance. The curvatures C_k is modeled as a modified lognormal distribution as follows:

$$\frac{1}{C_k} = R'_k + r_{\text{turn}}, \quad \ln R'_k \sim \mathcal{N}\left(\mu_C, \sigma_C^2\right), \tag{15}$$

where the parameter $r_{\text{turn}} \in (0, \infty)$ appears because roads are constructed with a lower bounded radius. It should be understood that, technically, r_{turn} is not a statistical measure, but rather an inherent property of the road type. Finally, the lengths of the curve L_k are assumed to be lognormally distributed:

$$\ln L_k \sim \mathcal{N}\left(\mu_L, \sigma_L^2\right). \tag{16}$$

Therefore, in the sOC, the stochastic model for the curviness is completely described by the set of parameters $\mathcal{R}_{\text{s},C} = \{\lambda_C, r_{\text{turn}}, \mu_C, \sigma_C, \mu_L, \sigma_L\}$.

The relationship for the operating class for the curviness parameter may be derived following two different approaches, according to the GTA and UFD classification systems.

When interpreting each curve as an isolated event, an analytical expression for the operating class may be derived by imposing lower and upper bounds $\bar{n}'_{C,\min}$ and $\bar{n}'_{C,\max}$, respectively, on the expected number of curves per unit of distance that force speed reductions within a given range, depending on two specified values for the curvature $\kappa_{\min}$ and $\kappa_{\max}$. This criterion reveals to be particularly useful when assessing the impact of road curves on vehicle fatigue, since each event may be interpreted as a single loading cycle [63], [64]. A similar approach is also suggested in the UFD classification system and yields an expression for the operating class as in Result 2.

Result 2 (Operating Class for Curviness): According to the UFD system, for the road curviness model described by (14), (15) and (16), the following expression for the operating class may be deduced:

$$\begin{aligned}
&\bar{n}'_{C,\min} \\
&< \lambda_C \Big(\mathbb{1}_{\kappa_{\max} \in [1/r_{\text{turn}}, \infty)} \\
&\quad + \frac{1}{2}\left[1 - \operatorname{erf}\left(\frac{\ln(1/\kappa_{\max} - r_{\text{turn}}) - \mu_C}{\sqrt{2}\sigma_C}\right)\right] \mathbb{1}_{\kappa_{\max} \in (0, 1/r_{\text{turn}})} \\
&\quad - \frac{1}{2}\left[1 - \operatorname{erf}\left(\frac{\ln(1/\kappa_{\min} - r_{\text{turn}}) - \mu_C}{\sqrt{2}\sigma_C}\right)\right] \mathbb{1}_{\kappa_{\min} \in (0, 1/r_{\text{turn}})} \\
&\quad - \mathbb{1}_{\kappa_{\min} \in [1/r_{\text{turn}}, \infty)} \Big) \leq \bar{n}'_{C,\max}.
\end{aligned} \tag{17}$$

Proof: According to (14), the number of curves N_C along the road section behaves like a Poisson random variable, i.e. $N_C \sim \mathcal{P}(\lambda_C L_{\text{tot}})$, and assumes integer values $n_C \in \mathcal{S}_{N_C} \equiv \mathbb{N}_0$. Another Binomial variable $N'_C \sim \text{Bin}(N_C, p_\kappa)$, assuming values in $\mathcal{S}_{N'_C} = \{0, \ldots, n_C\}$ for $n_C > 0$ and $\mathcal{S}_{N'_C} = \{0\}$ for $n_C = 0$, may be used to model a subset of the total number of curves, where the quantity $p_\kappa = p_\kappa(\kappa_{\min}, \kappa_{\max}, r_{\text{turn}}, \mu_C, \sigma_C)$ should be interpreted as the probability that, for an individual curve, the curvature ranges between $\kappa_{\min} < C \leq \kappa_{\max}$. Specifically, this probability may be estimated from (15) as

$$\begin{aligned}
p_\kappa(\kappa_{\min}, \kappa_{\max}, r_{\text{turn}}, \mu_C, \sigma_C) &= \mathbb{P}\left(\kappa_{\min} < C \leq \kappa_{\max}\right) \\
&= F_C(\kappa_{\max}; r_{\text{turn}}, \mu_C, \sigma_C) \\
&\quad - F_C(\kappa_{\min}; r_{\text{turn}}, \mu_C, \sigma_C),
\end{aligned} \tag{18}$$

where

$$\begin{aligned}
&F_C(\kappa; r_{\text{turn}}, \mu_C, \sigma_C) \\
&\quad = \mathbb{P}\left(C \leq \kappa\right) \\
&\quad = \mathbb{P}\left(R' \geq 1/\kappa - r_{\text{turn}}\right) \mathbb{1}_{\kappa \in (0, 1/r_{\text{turn}})} + \mathbb{1}_{\kappa \in [1/r_{\text{turn}}, \infty)} \\
&\quad = \left[1 - F_{R'}\left(1/\kappa - r_{\text{turn}}; \mu_C, \sigma_C\right)\right] \mathbb{1}_{\kappa \in (0, 1/r_{\text{turn}})}
\end{aligned}$$

$$+ \mathbb{1}_{\kappa\in[1/r_{\text{turn}},\infty)}$$
$$= \frac{1}{2}\left[1 - \operatorname{erf}\left(\frac{\ln(1/\kappa - r_{\text{turn}}) - \mu_C}{\sqrt{2}\sigma_C}\right)\right]\mathbb{1}_{\kappa\in(0,1/r_{\text{turn}})} + \mathbb{1}_{\kappa\in[1/r_{\text{turn}},\infty)}. \quad (19)$$

From the law of total expectation, it also follows that

$$\mathbb{E}\left(\frac{N'_C}{L_{\text{tot}}}\right) = \frac{1}{L_{\text{tot}}}\mathbb{E}\Big(\mathbb{E}\big(N'_C \mid N_C\big)\Big) = \frac{1}{L_{\text{tot}}}\mathbb{E}(N_C p_\kappa) = \lambda_C p_\kappa(\kappa_{\min}, \kappa_{\max}, r_{\text{turn}}, \mu_C, \sigma_C). \quad (20)$$

Combining (18), (19) and (20) gives the result. ■

The operating class (17) connects the set of sOC parameters $\mathcal{R}_{\text{s},C} = \{\lambda_C, r_{\text{turn}}, \mu_C, \sigma_C, \mu_L, \sigma_L\}$ with that of bird's-eye view metrics $\mathcal{R}_{\text{b},C} = \{\kappa_{\min}, \kappa_{\max}, \bar{n}'_{C,\min}, \bar{n}'_{C,\max}\}$. It should be observed that μ_L and σ_L do not appear in (17), since the curves along the road are regarded as isolated events.

On the other hand, the GTA description regards the curvature $\kappa(x)$ as a function of the position along the road. In this context, the road section may be classified in respect to the curviness calculating the probability that the curvature, treated as a random variable K, assumes values between $\kappa_{\min}$ and $\kappa_{\max}$, and specifying two limits $p_{\kappa,\min}$ and $p_{\kappa,\max}$. This would be equivalent to consider a relationship of the form $p_{\kappa,\min} < \mathbb{P}(\kappa_{\min} < K \leq \kappa_{\max}) \leq p_{\kappa,\max}$. In particular, the probabilities $p_{\kappa,\min}$ and $p_{\kappa,\max}$ should be interpreted as the minimum and maximum ratios between the portion of the road for which $\kappa_{\min} < K \leq \kappa_{\max}$ and the total length of the segment, denoted by L_{tot}. In this case, an approximated expression for the operating class may be derived as in Result 3.

Result 3 (Operating Class for Curviness): According to the GTA system, for the road curviness model described by (14), (15) and (16), the following expression for the operating class may be deduced:

$$\begin{aligned} p_{\kappa,\min} < {} & \left[1 - \lambda_C \exp\left(\mu_L + \frac{\sigma_L^2}{2}\right)\right] \\ & \times \left(\mathbb{1}_{\kappa_{\max}\in[0,1/r_{\text{turn}})} - \mathbb{1}_{\kappa_{\min}\in[0,1/r_{\text{turn}})}\right) \\ & + \mathbb{1}_{\kappa_{\max}\in(0,1/r_{\text{turn}})}\frac{\lambda_C}{2}\exp\left(\mu_L + \frac{\sigma_L^2}{2}\right) \\ & \times \left[1 - \operatorname{erf}\left(\frac{\ln(1/\kappa_{\max} - r_{\text{turn}}) - \mu_C}{\sqrt{2}\sigma_C}\right)\right] \\ & - \mathbb{1}_{\kappa_{\min}\in(0,1/r_{\text{turn}})}\frac{\lambda_C}{2}\exp\left(\mu_L + \frac{\sigma_L^2}{2}\right) \\ & \times \left[1 - \operatorname{erf}\left(\frac{\ln(1/\kappa_{\min} - r_{\text{turn}}) - \mu_C}{\sqrt{2}\sigma_C}\right)\right] \\ & + \mathbb{1}_{\kappa_{\max}\in[1/r_{\text{turn}},\infty)} - \mathbb{1}_{\kappa_{\min}\in[1/r_{\text{turn}},\infty)} \leq p_{\kappa,\max}. \end{aligned} \quad (21)$$

Proof: To derive (21), it is worth observing that position along the road may be described by a random variable X, assuming values $x \in \mathcal{S}_X = [0, L_{\text{tot}}]$. The space $\mathcal{S}_X$ may be divided into two subsets $\mathcal{K}$ and $\bar{\mathcal{K}}$, corresponding to the respective portions for which the road curvature is equal to or different from zero. Clearly, $\mathcal{S}_X = \mathcal{K} \cup \bar{\mathcal{K}}$. Owing to these premises, a continuous function $K(X)$ of the random position X along the road may be constructed starting with the model for the curviness discussed in [58], whereas this paper proposes a simplified approach. In particular, the curvature K is approximated as a piecewise continuous function of X, and the effect of superimposing curves is disregarded. Therefore, the total probability $\mathbb{P}(\kappa_{\min} < K \leq \kappa_{\max})$ may be calculated starting from the relationship

$$\begin{aligned} \mathbb{P}(K \leq \kappa) = {} & \mathbb{P}\big(K \leq \kappa \mid X = x \in \bar{\mathcal{K}}\big)\,\mathbb{P}\big(X = x \in \bar{\mathcal{K}}\big) \\ & + \mathbb{P}\big(C \leq \kappa \mid X = x \in \mathcal{K}\big)\,\mathbb{P}(X = x \in \mathcal{K}) \\ = {} & \big[1 - \mathbb{P}(X = x \in \mathcal{K})\big]\mathbb{1}_{\kappa\in[0,1/r_{\text{turn}})} \\ & + \mathbb{P}\big(C \leq \kappa \mid X = x \in \mathcal{K}\big) \\ & \times \mathbb{P}(X = x \in \mathcal{K})\mathbb{1}_{\kappa\in(0,1/r_{\text{turn}})} \\ & + \mathbb{1}_{\kappa\in[1/r_{\text{turn}},\infty)}, \end{aligned} \quad (22)$$

where $\mathbb{P}(C \leq \kappa \mid X = x \in \mathcal{K})$ reads as in (19) and the probability $\mathbb{P}(X = x \in \mathcal{K})$ may be approximated using Wald's equation as

$$\mathbb{P}(X = x \in \mathcal{K}) \approx \mathbb{E}\left(\frac{1}{L_{\text{tot}}}\sum_{k=1}^{N_C} L_k\right) = \frac{1}{L_{\text{tot}}}\mathbb{E}(N_C)\,\mathbb{E}(L_1) = \lambda_C \exp\left(\mu_L + \frac{\sigma_L^2}{2}\right). \quad (23)$$

In the derivation of (23), it is worth emphasizing that, according to (14) and (16), the random variable N_C is, by construction, independent of the sequence of curve lengths $\{L_k\}_{k\in\mathbb{N}}$. Combining (18), (22) and (23) yields the desired result. ■

The relationship (21) is the expression for the operating class relating the curviness parameters $\mathcal{R}_{\text{s},C} = \{\lambda_C, r_{\text{turn}}, \mu_C, \sigma_C, \mu_L, \sigma_L\}$ of the sOC and the bird's-eye view metrics $\mathcal{R}_{\text{b},C} = \{\kappa_{\min}, \kappa_{\max}, p_{\kappa,\min}, p_{\kappa,\max}\}$ (according to the GTA representation).

Comparing (17) and (21), the classification criterion proposed by the GTA system appears more refined than that of the UFD description, since it also accounts for the length of the curves via the parameters μ_L and σ_L.

Figure 3 compares the analytical expression (22) for the CDF of the road curviness against the distribution extracted from the original log file corresponding to sOC 2 in Section IV-C.

3) SPEED BUMPS AND STOP SIGNS

In the UFD, another criterion used to classify a transport mission relates to the obstacle height of the speed bumps that may be found along the vehicle's trajectory. These force the driver to reduce their cruising speed, often resulting in increased energy consumption. A similar effect is produced by the stop signs, which clearly impose a driving speed of zero. Speed bumps and stop signs are modeled similarly in the sOC representation. They are regarded as independent events and described by the sequences $\{X_k, V_{\text{b},k}\}_{k\in\mathbb{N}}$ and $\{X_k, T_{\text{s},k}\}_{k\in\mathbb{N}}$, respectively, where X_k is again the location, $V_{\text{b},k}$ is interpreted as a recommended speed, and $T_{\text{s},k}$ as a recommended time.

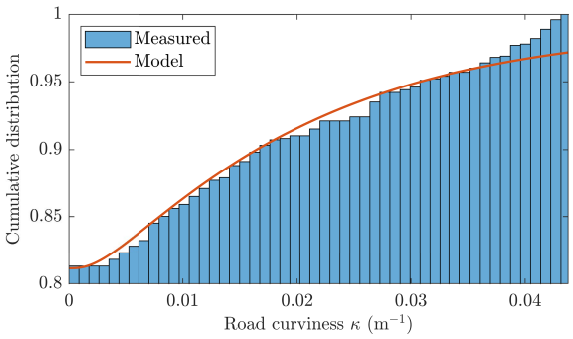

FIGURE 3. Comparison between the measured cumulative distribution and the analytical CDF obtained from the curviness model.

The distance between two consecutive events is assumed to be exponentially distributed, as in (14), but with intensities λ_b and λ_s. The recommended speed $V_{b,k}$ and time $T_{s,k}$ are supposed to be uniformly distributed between a minimum and maximum value, i.e.

$$V_{b,k} \sim \mathcal{U}(v_{min}, v_{max}), \tag{24a}$$
$$T_{s,k} \sim \mathcal{U}(t_{min}, t_{max}). \tag{24b}$$

Analogous to what done for the curviness, the road section may be characterized by imposing a limit on the expected number of speed bumps or stops that cause considerable speed reductions or prescribe sufficiently long standstill times. A similar approach is proposed in the UFD for road obstacles, whereas the GTA classification system makes no reference to either speed bumps or stop signs. Starting with the model for speed bumps, the operating class may be formalized mathematically as in Result 4.

Result 4 (Operating Class for Speed Bumps): For the speed bumps model described by (24a), the following expression for the operating class may be deduced:

$$\begin{aligned}\bar{n}'_{b,min} < \lambda_b \Bigg[& \mathbb{1}_{v_{b,max}\in[v_{max},\infty)} - \mathbb{1}_{v_{b,min}\in[v_{max},\infty)} \\ & + \left(\frac{v_{b,max}-v_{min}}{v_{max}-v_{min}}\right)\mathbb{1}_{v_{b,max}\in(v_{min},v_{max})} \\ & - \left(\frac{v_{b,min}-v_{min}}{v_{max}-v_{min}}\right)\mathbb{1}_{v_{b,min}\in(v_{min},v_{max})}\Bigg] \le \bar{n}'_{b,max}.\end{aligned} \tag{25}$$

Proof: The number of events per unit of length may be described again using a Poisson random variable, $N_b \sim \mathcal{P}(\lambda_b L_{tot})$, assuming integer values $n_b \in \mathcal{S}_{N_b} \equiv \mathbb{N}_0$. The Binomial variable $N'_b \sim \text{Bin}(N_b, p_b)$ may instead be introduced to model the number of speed bumps that impose severe speed reductions or long standstill times. It would assume integer values in the space $\mathcal{S}_{N'_b} = \{0, \dots, n_b\}$ for $n_b > 0$ and $\mathcal{S}_{N'_b} = \{0\}$ for $n_b = 0$. The quantity p_b represents the probability that the recommended speed V_b is lower than a specified threshold, and may be computed from (24a) as

$$\begin{aligned} & p_b(v_{b,min}, v_{b,max}, v_{min}, v_{max}) \\ & \triangleq \mathbb{P}(v_{b,min} < V_b \le v_{b,max}) \\ & = F_{V_b}(v_{b,max}; v_{min}, v_{max}) - F_{V_b}(v_{b,min}; v_{min}, v_{max}) \\ & = \mathbb{1}_{v_{b,max}\in[v_{max},\infty)} + \left(\frac{v_{b,max}-v_{min}}{v_{max}-v_{min}}\right)\mathbb{1}_{v_{b,max}\in(v_{min},v_{max})} \\ & \quad - \left(\frac{v_{b,min}-v_{min}}{v_{max}-v_{min}}\right)\mathbb{1}_{v_{b,min}\in(v_{min},v_{max})} - \mathbb{1}_{v_{b,min}\in[v_{max},\infty)}. \end{aligned} \tag{26}$$

Calculating $\mathbb{E}(N'_b/L_{tot})$ as in (20) and specifying lower and upper bounds $\bar{n}'_{b,min}, \bar{n}'_{b,max}$ on the expected number of speed bumps per unit of distance yields the result. ■

The expression (25) establishes a relationship between the sOC parameters $\mathcal{R}_{s,V_b} = \{\lambda_b, v_{min}, v_{max}\}$ and the bird's-eye view metrics $\mathcal{R}_{b,V_b} = \{v_b, \bar{n}'_{b,min}, \bar{n}'_{b,max}\}$. The corresponding relationship for stop signs may be derived with the same rationale:

$$\begin{aligned}\bar{n}'_{s,min} < \lambda_s \Bigg[& \mathbb{1}_{t_{s,max}\in[t_{max},\infty)} - \mathbb{1}_{t_{s,min}\in[t_{max},\infty)} \\ & + \left(\frac{t_{s,max}-t_{min}}{t_{max}-t_{min}}\right)\mathbb{1}_{t_{s,max}\in(t_{min},t_{max})} \\ & - \left(\frac{t_{s,min}-t_{min}}{t_{max}-t_{min}}\right)\mathbb{1}_{t_{s,min}\in(t_{min},t_{max})}\Bigg] \le \bar{n}'_{s,max}.\end{aligned} \tag{27}$$

4) ROAD ROUGHNESS

Road roughness plays an important role when it comes to durability and fatigue of mechanical components, but has a minor impact on energy efficiency. Nonetheless, this parameter is included in both the GTA and UFD systems.

Road profiles are traditionally modeled using Gaussian processes [72]. This choice works satisfactorily for small sections of roads, whereas variability between sections may be better explained using generalized Laplace models. These may be interpreted as Gaussian processes with randomly varying variance. In the sOC representation, the model for the road profile $Z(x)$ is based on the definition given by the ISO standard 8608 [73], which uses a two-parameter spectrum:

$$S_Z(\Omega) = C_r \left(\frac{\Omega}{\Omega_0}\right)^{-w}, \quad \Omega_1 \le \Omega \le \Omega_2, \tag{28}$$

and zero otherwise. In (28), Ω is the spatial angular frequency, $\Omega_0 = 1$, $\Omega_1 = 2\pi \cdot 0.011$, $\Omega_2 = 2\pi \cdot 2.83$ [73] are two cut frequencies expressed in radians per metre, and C_r is the degree of unevenness, also called the roughness coefficient. Finally, the waviness parameter w is assumed to be constant and set to $w = 2$. The sOC description employs a Laplace ISO model [10], [11], [65], [66], parametrized by its mean roughness C_r and the Laplace shape parameter ν_r (or, equivalently, its variance and kurtosis).

Taking inspiration from the ISO classification [73], the road may be labeled in respect to the roughness depending on the degree of unevenness C_r:

$$C_{r,min} < C_r \le C_{r,max}. \tag{29}$$

In particular, the ISO standard [73] specifies eight different road levels, ranging from class A to H in increasing roughness

order. Amongst these, however, only the first five are important for automotive applications [74]. A similar criterion is adopted in this paper to the sOC description. Accordingly, only (29) is required to establish a relationship between the set of sOC parameters $\mathcal{R}_{s,Z} = \{C_r, \nu_r\}$ and the two limits in the set $\mathcal{R}_{b,Z} = \{C_{r,\min}, C_{r,\max}\}$. It should be noted that the proposed criterion systematically neglects the effect of variability between sections, since the shape parameter ν_r does not appear in (29). By contrast, a more refined classification approach would prescribe an additional relationship including ν_r. To this end, further details on generalized Laplace distributions may be found in [67], [75].

5) SPEED SIGNS AND GROUND TYPE

The legal speed dramatically impacts the energy performance of road vehicles. In fact, while constant cruising speeds may be observed to be apparently optimal from an energy efficiency perspective, frequent variations in driving speed result in increased consumption [23].

On the other hand, the ground type and the asphalt properties play an important role in determining the maximum traction forces that the tires can generate, and have also a substantial effect on rolling resistance [76]–[79]. These two aspects are particularly significant for electric vehicles, in connection to both the higher instantaneous torques that the wheels may experience and the well-known phenomenon of range anxiety.

Accordingly, both the GTA and UFD classification systems include the above-mentioned parameters.

In the sOC description, speed signs and ground type behave as piecewise constant, right-side continuous functions of the position [58]. Since the same stochastic model is used for both entities, only the speed signs are discussed. Specifically, these are treated as a random process $V = V(x)$ along with the position $x \in \mathbb{R}$ on the road. The variable $V(x)$ is only allowed to take discrete values in the state space $\mathcal{S}_V = \{v_1, \ldots, v_{n_v}\}$, where n_v denotes the finite number of possible speed limits. The entire process is then split into two parts and modeled as a sequence of positions, with the locations of the signs, and speeds $\{X_k, V_k\}_{k\in\mathbb{N}}$.

It is also assumed that the current speed limit exerts the greater part of the influence on the upcoming limit. Thus, for the sake of simplicity, the sequence of speed limits is modeled as a Markov chain [80], [81]:

$$\begin{aligned}&\mathbb{P}\big(V_{k+1} = v_{i,k+1} \big| V_1 = v_{i,1}, V_2 = v_{i,2}, \ldots, V_k = v_{i,k}\big)\\ &\quad = \mathbb{P}\big(V_{k+1} = v_{i,k+1} \big| V_k = v_{i,k}\big),\end{aligned} \tag{30}$$

where the generic signed speed v_i is an element of the speed vector $\boldsymbol{v} = [v_1 \ \ldots \ v_{n_v}]^T$.

The Markov probability matrix $\mathbf{P}_V \in \mathbb{R}_{\geq 0}^{n_v \times n_v}$ fully characterizes the chain. An entry p_{Vij} models the conditional probability of transitioning from state i to state j and satisfies $\sum_{j=1}^{n_v} p_{Vij} = 1$. The description may be reduced further by observing that the speed limit model is embedded in that of the locations and that there are no self-transitions, so all diagonal elements are equal to zero, i.e. $p_{Vii} = 0$. Instead, the off-diagonal elements may be easily estimated from data by measuring the number of changes f_{Vij} between states i and j. Moreover, in the modeling of the road type sequence, it is assumed that there are no absorbing states. The speed sign locations may be modeled as in (14). However, each state is expected to have its own intensity: n_v states introduce n_v parameters $\lambda_{V1}, \ldots, \lambda_{Vn_v}$, which may be deduced from the mean length L_{Vi} of speed limit v_i:

$$\lambda_{Vi} = \frac{1}{L_{Vi}}. \tag{31}$$

As for the speed, the n_v mean lengths L_{Vi} may be organized into a vector $\boldsymbol{L}_V = [L_{V1} \ \ldots \ L_{Vn_v}]^T$. Thus, the complete description consists of the conditional probabilities p_{Vij} and the n_v mean lengths L_{Vi} (or, alternatively, the intensities λ_{Vi}). Furthermore, the fact that the distance $X_{k+1} - X_k$ between consecutive positions is exponentially distributed implies that $V(x)$ itself becomes a continuous-time[4] Markov chain [80]. In particular, the stationary distribution $\boldsymbol{\pi}_V$ of the overall process may be derived starting from the knowledge of the generator matrix $\mathbf{G}_V$, and satisfies the equation

$$\boldsymbol{\pi}_V \mathbf{G}_V = \mathbf{0}, \tag{32}$$

where the entries $g_{Vij} = g_{Vij}(p_{Vij}, L_{Vi})$ of $\mathbf{G}_V$ are given by

$$g_{Vij}\big(p_{Vij}, L_{Vi}\big) = \begin{cases} \lambda_{Vi} p_{Vij} = \dfrac{p_{Vij}}{L_{Vi}}, & i \neq j, \\ -\lambda_{Vi} = -\dfrac{1}{L_{Vi}}, & i = j. \end{cases} \tag{33}$$

Form a bird's-eye view perspective, the operating class may be defined by considering the probability that the speed over the road section ranges between a minimum $\hat{v}_{\min}$ and a maximum $\hat{v}_{\max}$. This probability value may be constrained between lower and upper bounds $p_{v,\min}$ and $p_{v,\max}$, i.e. $p_{v,\min} < \mathbb{P}(\hat{v}_{\min} < V \leq \hat{v}_{\max}) \leq p_{v,\max}$. This criterion is similar to that used in the UFD representation system. Denoting by $\mathcal{I}_{(\hat{v}_{\min}, \hat{v}_{\max}]}$ the set comprising the values of i such that $v_i \in (\hat{v}_{\min}, \hat{v}_{\max}]$, the relationship connecting the sOC parameters $\mathcal{R}_{s,V} = \{\boldsymbol{v}, \mathbf{P}_V, \boldsymbol{L}_V\}$ to the bird's-eye view metrics $\mathcal{R}_{b,V} = \{\hat{v}_{\min}, \hat{v}_{\max}, p_{v,\min}, p_{v,\max}\}$ may be found in the form

$$p_{v,\min} < \sum_{i \in \mathcal{I}_{(\hat{v}_{\min}, \hat{v}_{\max}]}} \pi_{Vi}(\mathbf{P}_V, \boldsymbol{L}_V) \leq p_{v,\max}, \tag{34}$$

subjected to the constraint $\sum_{i=1}^{n_v} \pi_{Vi} = 1$.

Instead, the GTA description proposes that a transport mission should be classified based on the expected number of transitions between speeds along the road, per unit of length. To formalize this mathematically, the variable N_{f_V}, assuming values in $\mathcal{S}_{N_{f_V}} \equiv \mathbb{N}_0$, is introduced to model the number of speed changes occurring on a road of total

[4]Continuous Markov chains are traditionally called *continuous-time Markov chains*, even though, in the present case, the dimension being considered is space rather than time.

length L_{tot}. This criterion may be integrated with information about the mean legal speed along the road, thus imposing also $\hat{v}_{\min} < \mathbb{E}(V) \leq \hat{v}_{\max}$. The two conditions yield the set of analytical expressions for the operating class as in Result 5

Result 5 (Operating Class for Speed Signs): According to the GTA system, for the speed signs model described by (30)-(33), the following expressions for the operating class may be deduced:

$$\bar{n}_{f_V,\min} < \frac{1}{L_{\text{tot}}} \sum_{n_{f_V}=0}^{\infty} \sum_{j=1}^{n_v} \sum_{i=1}^{n_v} n_{f_V} \hat{p}_{ij}\left(n_{f_V}; L_{\text{tot}}\right) \times \pi_{Vi}(\mathbf{P}_V, \boldsymbol{L}_V) \leq \bar{n}_{f_V,\max}, \tag{35a}$$

$$\hat{v}_{\min} < \sum_{i=1}^{n_v} v_i \pi_{Vi}(\mathbf{P}_V, \boldsymbol{L}_V) \leq \hat{v}_{\max}. \tag{35b}$$

Proof: The probability $\hat{p}_{ij}(n_{f_V}; L_{\text{tot}}) \triangleq \mathbb{P}(N_{f_V} = n_{f_V} \cap V(L_{\text{tot}}) = v_j \mid V(0) = v_i)$ of having exactly $n_{f_V} > 0$ number of transitions when $V(L_{\text{tot}}) = v_j$ conditioned to $V(0) = v_i$ may be calculated as [82], [83]

$$\hat{p}_{ij}\left(n_{f_V}; L_{\text{tot}}\right) = \sum_{k \neq i} \int_0^{L_{\text{tot}}} \mathrm{e}^{g_{Vii}(p_{Vij}, L_{Vi})(L_{\text{tot}}-L)} \times g_{Vik}\left(p_{Vij}, L_{Vi}\right) \hat{p}_{kj}\left(n_{f_V} - 1; L\right) \mathrm{d}L, \tag{36}$$

with initial condition $\hat{p}_{ij}(0; L_{\text{tot}}) = p_{Vij} \mathrm{e}^{g_{ii}(p_{Vij}, L_{Vi}) L_{\text{tot}}}$ [83]. Supposing that the initial probability of being in the state v_i coincides with the stationary one, the total probability $\hat{p}_j(n_{f_V}; L_{\text{tot}}) \triangleq \mathbb{P}(N_{f_V} = n_{f_V} \cap V(L_{\text{tot}}) = v_j)$ of having exactly n_{f_V} transitions when $V(L_{\text{tot}}) = v_j$ then becomes

$$\begin{aligned}
&\hat{p}_j\left(n_{f_V}; L_{\text{tot}}\right) \\
&\quad = \sum_{i=1}^{n_v} \mathbb{P}\left(N_{f_V} = n_{f_V} \cap V(L_{\text{tot}}) = v_j \;\middle|\; V(0) = v_i\right) \\
&\qquad \times \pi_{Vi}(\mathbf{P}_V, \boldsymbol{L}_V) \\
&\quad = \sum_{i=1}^{n_v} \hat{p}_{ij}\left(n_{f_V}; L_{\text{tot}}\right) \pi_{Vi}(\mathbf{P}_V, \boldsymbol{L}_V).
\end{aligned} \tag{37}$$

Summing over j yields the probability of having exactly n_{f_V} speed jumps along a road of length L_{tot}, i.e. the PMF

$$\begin{aligned}
&p_{N_{f_V}}\left(n_{f_V}; p_{Vij}, \boldsymbol{L}_V, L_{\text{tot}}\right) \\
&\quad = \sum_{j=1}^{n_v} \hat{p}_j\left(n_{f_V}; L_{\text{tot}}\right) \\
&\quad = \sum_{j=1}^{n_v} \sum_{i=1}^{n_v} \hat{p}_{ij}\left(n_{f_V}; L_{\text{tot}}\right) \pi_{Vi}(\mathbf{P}_V, \boldsymbol{L}_V).
\end{aligned} \tag{38}$$

Accordingly, the expected value of speed transitions per unit of length $\mathbb{E}(N_{f_V}/L_{\text{tot}})$ reads

$$\begin{aligned}
\mathbb{E}\left(\frac{N_{f_V}}{L_{\text{tot}}}\right) &= \frac{1}{L_{\text{tot}}} \sum_{n_{f_V}=0}^{\infty} n_{f_V} p_{N_{f_V}}\left(n_{f_V}; \mathbf{P}_V, \boldsymbol{L}_V, L_{\text{tot}}\right) \\
&= \frac{1}{L_{\text{tot}}} \sum_{n_{f_V}=0}^{\infty} \sum_{j=1}^{n_v} \sum_{i=1}^{n_v} n_{f_V} \hat{p}_{ij}\left(n_{f_V}; L_{\text{tot}}\right) \\
&\quad \times \pi_{Vi}(\mathbf{P}_V, \boldsymbol{L}_V),
\end{aligned} \tag{39}$$

which gives (35a). The derivation of (35b) is trivial and hence omitted. ■

The inequalities (35) relate the set of sOC parameters $\mathcal{R}_{\text{s},V} = \{\boldsymbol{v}, \mathbf{P}_V, \boldsymbol{L}_V\}$ with that of bird's-eye view metrics, denoted by $\mathcal{R}_{\text{b},V} = \{\hat{v}_{\min}, \hat{v}_{\max}, \bar{n}_{f_V,\min}, \bar{n}_{f_V,\max}\}$. It may be observed that (39) yields a rather complicated expression for the total number of transitions per unit of length. A simpler approach would be to approximate the number of transitions to the state i considering the asymptotic or limiting distribution, i.e. $\mathbb{E}(N_{f_V}/L_{\text{tot}}) \approx \sum_{i=1}^{n_v} \pi_{Vi}/L_{Vi}$, so that (35a) becomes

$$\bar{n}_{f_V,\min} < \sum_{i=1}^{n_v} \frac{\pi_{Vi}(\mathbf{P}_V, \boldsymbol{L}_V)}{L_{Vi}} \leq \bar{n}_{f_V,\max}. \tag{40}$$

The above relationship (40) may be used in place of (35a) to establish a formal expression of the operating class.

TABLE 3. Probabilities p_{s_i} for each season assuming that the year is always composed of 365 days.

Probability p_{s_i}	Boreal hemisphere	Austral hemisphere
p_{s_1}	90/365	92/365
p_{s_2}	92/365	91/365
p_{s_3}	92/365	90/365
p_{s_4}	91/365	92/365

B. WEATHER CATEGORY

As briefly mentioned in Section II-B, in the sOC format, a hierarchical order is introduced to preserve the interaction between the weather models without needing to introduce complicated multivariate formulations. A composite structure is achieved by defining the season as the primary weather model. The parameters describing each physical quantity then inherit their values depending upon the specific seasonal setting. This concept is illustrated graphically in Fig. 4, where the four seasons (primary model) are shown together with the set of stochastic parameters for each secondary weather model.

In this context, the season may be also regarded as a random variable S, whose possible realisations are $s \in \mathcal{S}_S = \{s_1, s_2, s_3, s_4\}$ with probabilities p_{s_i}, $i = 1, 2, 3, 4$, respectively.[5] It is worth emphasizing that the seasons considered in this paper are the meteorological ones, as opposed to the astronomical. Hence, the probabilities p_{s_i} should be calculated differently depending on the location of the road segment (boreal or austral hemisphere), and are given in Table 3.

Based on these premises, using A to denote a generic random variable (either continuous or discrete) for a weather model, the total probability $\mathbb{P}(A)$ may be computed starting from the conditional probabilities $\mathbb{P}(A \mid S = s_i)$ as

$$\mathbb{P}(A) = \sum_{i=1}^{4} \mathbb{P}\left(A \;\middle|\; S = s_i\right) \mathbb{P}\left(S = s_i\right)$$

[5] In this paper, the realizations s_i, $i = 1, 2, 3, 4$ correspond to winter, spring, summer and autumn, in that order.

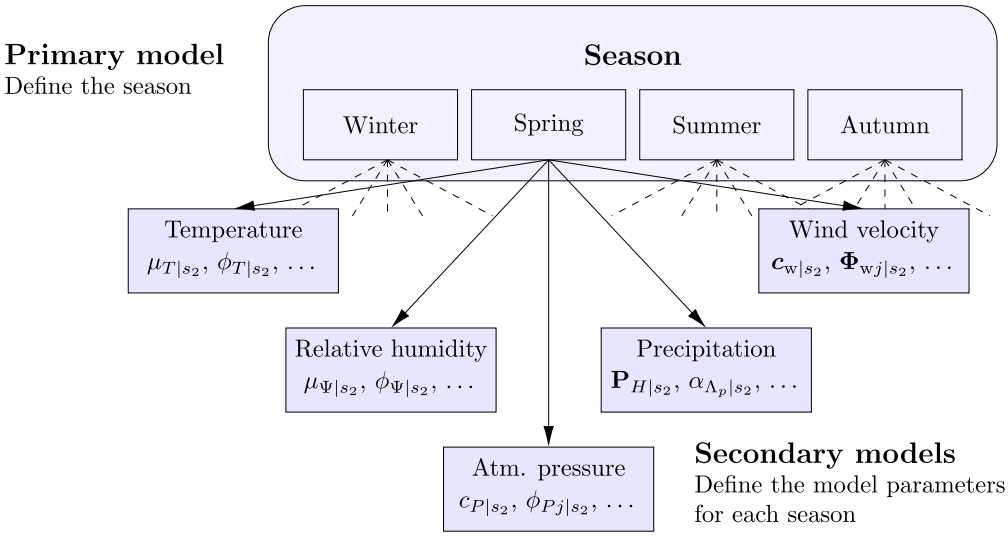

FIGURE 4. The season is the primary weather model. The other parameters are treated as ancillary and inherit their values depending on the season.

$$= \sum_{i=1}^{4} \mathbb{P}\big(A \mid S = s_i\big) p_{s_i}. \tag{41}$$

Since the sOC parameters used also depend on the specific seasonal setting, the notation $\zeta_{|s_i}$ is used to emphasize that $\zeta_{|s_i}$ is the conditional version of the parameter ζ for $S = s_i$.

The stochastic models for the weather category discussed in this paper are based on the formulations presented in [59], and were validated using data collected from the Swedish Meteorological and Hydrological Institute (SMHI).

1) AIR TEMPERATURE AND ATMOSPHERIC HUMIDITY

Air temperature and humidity have a profound impact on the performance of the engine and on the batteries of BEVs [12]. Thermal management strategies also need to be adapted based on the combined effect of both quantities, especially for vehicles operating in cold climates [84], [85]. In addition, the air temperature has a secondary effect on air drag. Not surprisingly, the UFD and GTA classification systems take into account both temperature and humidity in their simplified descriptions of the environment.

In the sOC representation, the models for air temperature and atmospheric humidity are introduced simultaneously, since they are similar. More specifically, they are described by two sequences $\{T_{\mathrm{air},k}\}_{k\in\mathbb{N}}$, $\{\Psi_{\mathrm{RH},k}\}_{k\in\mathbb{N}}$ assuming values $T^*_{\mathrm{air},k}$ and $\Psi^*_{\mathrm{RH},k}$ in their respective spaces $\mathcal{S}_{T_{\mathrm{air}}}$ and $\mathcal{S}_{\Psi_{\mathrm{RH}}}$. In both cases, the time resolution may be expressed as a fraction of hour $1/K$, with $K \in \mathbb{N}$. Accordingly, the value $k = 1$ refers to the first fraction of the first hour of a first year assumed as a reference. Furthermore, limits are imposed on both quantities to satisfy physical constraints:

$$T_{\mathrm{air},k} = \max\Big(T_0, T'_{\mathrm{air},k}\Big), \tag{42a}$$

$$\Psi_{\mathrm{RH},k} = \min\Big(\max\Big(0, \Psi'_{\mathrm{RH},k}\Big), 1\Big), \tag{42b}$$

where $T_0 = -273.15°\mathrm{C}$ represents the zero point for thermodynamic temperature, and $T'_{\mathrm{air},k}$, $\Psi'_{\mathrm{RH},k}$ may be in turn decomposed as

$$T'_{\mathrm{air},k} = \bar{T}_k + \tilde{T}_k, \tag{43a}$$

$$\Psi'_{\mathrm{RH},k} = \bar{\Psi}_k + \tilde{\Psi}_k, \tag{43b}$$

in which $\bar{T}$, $\bar{\Psi}$ and $\tilde{T}$, $\tilde{\Psi}$ capture the deterministic and stochastic components of the air temperature and humidity, respectively.

In particular, the deterministic trends $\bar{T}_k$ and $\bar{\Psi}_k$ in (43) are modeled using a composition of two sine waves as follows [59], [61]:

$$\bar{T}_k = \mu_T + T_{\mathrm{d}} \sin\big(\bar{\omega}_{\mathrm{d}} k + \varphi_{T_{\mathrm{d}}}\big) + T_{\mathrm{y}} \sin\big(\bar{\omega}_{\mathrm{y}} k + \varphi_{T_{\mathrm{y}}}\big), \tag{44a}$$

$$\bar{\Psi}_k = \mu_\Psi + \Psi_{\mathrm{d}} \sin\big(\bar{\omega}_{\mathrm{d}} k + \varphi_{\Psi_{\mathrm{d}}}\big) + \Psi_{\mathrm{y}} \sin\big(\bar{\omega}_{\mathrm{y}} k + \varphi_{\Psi_{\mathrm{y}}}\big), \tag{44b}$$

where μ_T and μ_Ψ represent the average temperature and humidity over the year, T_{d}, T_{y} and Ψ_{d}, Ψ_{y} are the amplitudes of the daily and annual deterministic component, and $\bar{\omega}_{\mathrm{d}} = 2\pi/(24 \cdot K)$, $\bar{\omega}_{\mathrm{y}} = 2\pi/(24 \cdot 365 \cdot K)$ the daily and annual frequency, respectively. It should be noticed that the deterministic parameters in (44) are not season-dependent. On the other hand, the stochastic parts $\tilde{T}_k$ and $\tilde{\Psi}_k$ are both modeled using a stationary AR(1) process:

$$\tilde{T}_k = \phi_{T|s_i} \tilde{T}_{k-1} + e_{T,k}, \quad e_{T,k} \sim \mathcal{N}\Big(0, \sigma^2_{e_T|s_i}\Big), \tag{45a}$$

$$\tilde{\Psi}_k = \phi_{\Psi|s_i} \tilde{\Psi}_{k-1} + e_{\Psi,k}, \quad e_{\Psi,k} \sim \mathcal{N}\Big(0, \sigma^2_{e_\Psi|s_i}\Big), \tag{45b}$$

with the characteristic parameters $\phi_{T|s_i}$, $\sigma_{e_T|s_i}$ and $\phi_{\Psi|s_i}$, $\sigma_{e_\Psi|s_i}$ depending explicitly upon the specific season s_i, $i = 1, 2, 3, 4$. The stochastic components themselves are normally distributed, i.e. $\tilde{T} \sim \mathcal{N}(0, \sigma^2_{e_T|s_i})$, $\tilde{\Psi} \sim \mathcal{N}(0, \sigma^2_{e_\Psi|s_i})$, where the process variances $\sigma^2_{\tilde{T}|s_i}$ and $\sigma^2_{\tilde{\Psi}|s_i}$ are given

respectively by

$$\sigma^2_{\tilde{T}|s_i} = \frac{\sigma^2_{e_T|s_i}}{1-\phi^2_{T|s_i}}, \tag{46a}$$

$$\sigma^2_{\tilde{\Psi}|s_i} = \frac{\sigma^2_{e_\Psi|s_i}}{1-\phi^2_{\Psi|s_i}}, \tag{46b}$$

and may be used in place of $\sigma^2_{e_T|s_i}$ and $\sigma^2_{e_\Psi|s_i}$ to parametrize the temperature and humidity models, since they are easier to interpret.

In both cases, the operating classes may be established starting from the known probability that each quantity ranges between a minimum and a maximum value. Considering the air temperature T_{air}, this statement may be formalized by calculating the probability that $T^*_{\min} < T_{\text{air}} \leq T^*_{\max}$ during the whole year, and imposing lower and upper bounds $p_{T^*_{\text{air}},\min}$ and $p_{T^*_{\text{air}},\max}$, respectively. This translates mathematically into $p_{T^*_{\text{air}},\min} < \mathbb{P}(T^*_{\min} < T_{\text{air}} \leq T^*_{\max}) \leq p_{T^*_{\text{air}},\max}$. The analytical expression for the corresponding operating class reads as in Result 6.

Result 6 (Operating Class for Air Temperature): For the air temperature model described by (42a), (43a), (44a), (45a), and (46a), the following expression for the operating class may be deduced:

$$\begin{aligned} &p_{T^*_{\text{air}},\min} \\ &< \sum_{i=1}^{4} \sum_{\bar{T}_k \in \mathcal{S}_{\bar{T}|s_i}} p_{\bar{T}_k|s_i} p_{s_i} \mathbb{1}_{T^*_{\max} \in [T_0,\infty)} \\ &\quad \times \Phi\left(\frac{T^*_{\max} - \bar{T}_k\left(\mu_T, T_{\text{d}}, T_{\text{y}}, \varphi_{T_{\text{d}}}, \varphi_{T_{\text{y}}}\right)}{\sigma_{\tilde{T}|s_i}} \right) \\ &\quad - \sum_{i=1}^{4} \sum_{\bar{T}_k \in \mathcal{S}_{\bar{T}|s_i}} p_{\bar{T}_k|s_i} p_{s_i} \mathbb{1}_{T^*_{\min} \in [T_0,\infty)} \\ &\quad \times \Phi\left(\frac{T^*_{\min} - \bar{T}_k\left(\mu_T, T_{\text{d}}, T_{\text{y}}, \varphi_{T_{\text{d}}}, \varphi_{T_{\text{y}}}\right)}{\sigma_{\tilde{T}|s_i}} \right) \leq p_{T^*_{\text{air}},\max}. \end{aligned} \tag{47}$$

Proof: According to (41), the total probability that the air temperature is between $T^*_{\min}$ and $T^*_{\max}$ may be computed by summation over $s_i \in \mathcal{S}_S$ of the conditional probabilities relating to each season. From (42a), it follows that

$$\begin{aligned} &\mathbb{P}\left(T^*_{\min} < T_{\text{air}} \leq T^*_{\max} \,\middle|\, S = s_i\right) \\ &\quad = \mathbb{P}\left(T'_{\text{air}} \leq T^*_{\max} \,\middle|\, S = s_i\right) \mathbb{1}_{T^*_{\max} \in [T_0,\infty)} \\ &\qquad - \mathbb{P}\left(T'_{\text{air}} \leq T^*_{\min} \,\middle|\, S = s_i\right) \mathbb{1}_{T^*_{\min} \in [T_0,\infty)}. \end{aligned} \tag{48}$$

For each season, the conditional probabilities in (48) may be determined considering the number of different solutions $\bar{T}_k \in \mathcal{S}_{\bar{T}|s_i}$ of the deterministic component $\bar{T}$ obtained as k varies in each seasonal subsets $\mathcal{S}_{k|s_i} \subseteq \mathbb{N}_{>0}$, plus their probabilities $p_{\bar{T}|s_i}$. To this end, it should be observed that the two sine waves in (44a) are periodic over the day and the year, respectively. Since $\bar{\omega}_{\text{d}}$ is an integer multiple of $\bar{\omega}_{\text{y}}$, the total period coincides with the year itself, and thus the solutions $\bar{T}_k$ may be deduced considering each season once only and in isolation. This is equivalent to considering the seasonal subsets relating to a single year, for example $\mathcal{S}_{k|s_i} \subset \{1, \ldots, 24 \cdot 365 \cdot K\}$. Indeed, the sets $\mathcal{S}_{k|s_i}$ comprise the values assumed by k for a generic season, independently of the year.[6] Thus, a generic conditional probability $\mathbb{P}(T'_{\text{air}} \leq T^*_{\text{air}} \mid S = s_i)$ may be written as

$$\begin{aligned} &\mathbb{P}\left(T'_{\text{air}} \leq T^*_{\text{air}} \,\middle|\, S = s_i\right) \\ &\quad = \sum_{\bar{T}_k \in \mathcal{S}_{\bar{T}|s_i}} \mathbb{P}\left(\bar{T} + \tilde{T} \leq T^*_{\text{air}} \,\middle|\, S = s_i \cap \bar{T} = \bar{T}_k\right) \\ &\quad = \sum_{\bar{T}_k \in \mathcal{S}_{\bar{T}|s_i}} F_{\tilde{T}}\left(T^*_{\text{air}} - \bar{T}_k\left(\mu_T, T_{\text{d}}, T_{\text{y}}, \varphi_{T_{\text{d}}}, \varphi_{T_{\text{y}}}\right); \sigma_{e_T|s_i}\right) \\ &\qquad \times p_{\bar{T}_k|s_i}, \end{aligned} \tag{49}$$

with

$$\begin{aligned} &F_{\tilde{T}}\left(T^*_{\text{air}} - \bar{T}_k\left(\mu_T, T_{\text{d}}, T_{\text{y}}, \varphi_{T_{\text{d}}}, \varphi_{T_{\text{y}}}\right); \sigma_{e_T|s_i}\right) \\ &\quad = \Phi\left(\frac{T^*_{\text{air}} - \bar{T}_k\left(\mu_T, T_{\text{d}}, T_{\text{y}}, \varphi_{T_{\text{d}}}, \varphi_{T_{\text{y}}}\right)}{\sigma_{\tilde{T}|s_i}} \right). \end{aligned} \tag{50}$$

Combining (41) with (48), (49) and (50) yields the result. ■

The expression for the operating class (47) relates the sOC parameters $\mathcal{W}_{\text{s},T_{\text{air}}} = \{\mu_T, T_{\text{d}}, T_{\text{y}}, \varphi_{T_{\text{d}}}, \varphi_{T_{\text{y}}}, \phi_{T|s_i}, \sigma_{\tilde{T}|s_i}\}$ and the set of bird's-eye view metrics $\mathcal{W}_{\text{b},T_{\text{air}}} = \{T^*_{\min}, T^*_{\max}, p_{T^*_{\text{air}},\min}, p_{T^*_{\text{air}},\max}\}$. Once again, it should be observed that the autoregressive coefficients $\phi_{T|s_i}$ do not appear in (47).

A similar equation may be derived for the atmospheric humidity considering the probability that Ψ_{RH} ranges between $\Psi^*_{\min}$ and $\Psi^*_{\max}$. In this case, the conditional probability reads

$$\begin{aligned} &\mathbb{P}\left(\Psi^*_{\min} < \Psi_{\text{RH}} \leq \Psi^*_{\max} \,\middle|\, S = s_i\right) \\ &\quad = \mathbb{1}_{\Psi^*_{\max} \in [1,\infty)} + \mathbb{P}\left(\Psi'_{\text{RH}} \leq \Psi^*_{\max} \,\middle|\, S = s_i\right) \mathbb{1}_{\Psi^*_{\max} \in [0,1)} \\ &\qquad - \mathbb{P}\left(\Psi'_{\text{RH}} \leq \Psi^*_{\min} \,\middle|\, S = s_i\right) \mathbb{1}_{\Psi^*_{\min} \in [0,1)} - \mathbb{1}_{\Psi^*_{\min} \in [1,\infty)}. \end{aligned} \tag{51}$$

Hence, analogous calculations as previously yield the following relationship:

$$\begin{aligned} p_{\Psi^*_{\text{RH}},\min} \;<\; &\mathbb{1}_{\Psi^*_{\max} \in [1,\infty)} + \sum_{i=1}^{4} \sum_{\bar{\Psi}_k \in \mathcal{S}_{\bar{\Psi}|s_i}} p_{\bar{\Psi}_k|s_i} p_{s_i} \mathbb{1}_{\Psi^*_{\max} \in [0,1)} \\ &\times \Phi\left(\frac{\Psi^*_{\max} - \bar{\Psi}_k\left(\mu_\Psi, \Psi_{\text{d}}, \Psi_{\text{y}}, \varphi_{\Psi_{\text{d}}}, \varphi_{\Psi_{\text{y}}}\right)}{\sigma_{\tilde{\Psi}|s_i}} \right) \\ &- \sum_{i=1}^{4} \sum_{\bar{\Psi}_k \in \mathcal{S}_{\bar{\Psi}|s_i}} p_{\bar{\Psi}_k|s_i} p_{s_i} \mathbb{1}_{\Psi^*_{\min} \in [0,1)} \end{aligned}$$

[6] For example, for $s = s_1$, $\mathcal{S}_{k|s_i}$ is given by $\mathcal{S}_{k|s_1} = \{1, \ldots, 24 \cdot 59 \cdot K\} \cup \{24 \cdot 334 \cdot K, \ldots, 24 \cdot 365 \cdot K\}$ in the boreal hemisphere and by $\mathcal{S}_{k|s_1} = \{24 \cdot 153 \cdot K, \ldots, 24 \cdot 244 \cdot K\}$ in the austral hemisphere.

$$\times \Phi\left(\frac{\Psi^*_{\min} - \bar{\Psi}_k\left(\mu_\Psi, \Psi_\mathrm{d}, \Psi_\mathrm{y}, \varphi_{\Psi_\mathrm{d}}, \varphi_{\Psi_\mathrm{y}}\right)}{\sigma_{\tilde{\Psi}|s_i}}\right) - \mathbb{1}_{\Psi^*_{\max}\in[1,\infty)} \leq p_{\Psi^*_{\mathrm{RH}},\max}, \tag{52}$$

which again connects the set of sOC parameters $\mathcal{W}_{\mathrm{s},\Psi_{\mathrm{RH}}} = \{\mu_\Psi, \Psi_\mathrm{d}, \Psi_\mathrm{y}, \varphi_{\Psi_\mathrm{d}}, \varphi_{\Psi_\mathrm{y}}, \phi_{\Psi|s_i}, \sigma_{\tilde{\Psi}|s_i}\}$ to that of bird's-eye view metrics $\mathcal{W}_{\mathrm{b},\Psi_{\mathrm{RH}}} = \{\Psi^*_{\min}, \Psi^*_{\max}, p_{\Psi^*_{\mathrm{RH}},\min}, p_{\Psi^*_{\mathrm{RH}},\max}\}$. Analogous to (47), the terms $\bar{\Psi}_k$ in (52) represent the different solutions for the deterministic component of the atmospheric humidity obtained by letting k vary in each seasonal subset $\mathcal{S}_{k|s_i}$, and $p_{\bar{\Psi}_k|s_i}$ the corresponding probabilities.

As an example, the temperature distributions for the city of Gothenburg, Sweden, in 2019, obtained using data collected from the SMHI, are compared to the analytical PDF and CDF derived according to Eqs. (49) and (50) in Fig. 5. The relative humidity exhibits a similar trend.

2) PRECIPITATION

The intensity of the atmospheric precipitation highly conditions the driver's choice of speed [86], [87], which is clearly reflected in the prime mover operating conditions and, ultimately, in its energy efficiency. Moreover, precipitation accumulated on the ground is responsible for variations in the friction coefficient [88] (usually decreased by the presence of thin layers of water or ice), impacting the tire performance and their ability to produce tractive and braking forces, and exciting the well-known phenomenon of hydroplaning. For these reasons, Scania explicitly accounts for the intensity of precipitation in the UFD description.

According to the sOC representation, the sequence for atmospheric precipitation is modeled in a two-step process [59], [61]. In the first step, the occurrence of the event $\{H_{\mathrm{p},k}\}_{k\in\mathbb{N}}$ is simulated, and then a suitable probability distribution is used to fit the intensity $\{\Lambda_{\mathrm{p},k}\}_{k\in\mathbb{N}}$, which corresponds to the precipitation amount expressed in millimeters per hour (it assumes value $\lambda_{\mathrm{p},k} \in \mathcal{S}_{\Lambda_\mathrm{p}} \subseteq \mathbb{R}_{>0}$). In particular, the occurrence is modeled by using a Markov chain of fixed interval, similar to what was done in [89], [90]. The stochastic variable $H_{\mathrm{p},k}$ is allowed to take states from the finite space $\mathcal{S}_{H_\mathrm{p}} = \{1, 2\}$, where 1 and 2 correspond to the *dry* and *wet* events. The Markov process for the precipitation is fully characterized by a transition matrix $\mathbf{P}_{H|s_i} \in \mathbb{R}^{2\times 2}_{\geq 0}$. The model for precipitation has only two states, and hence the two following conditions also hold:

$$p_{H12|s_i} = 1 - p_{H11|s_i}, \tag{53a}$$

$$p_{H21|s_i} = 1 - p_{H22|s_i}. \tag{53b}$$

The transition probabilities $p_{H11|s_i}$ and $p_{H22|s_i}$ may be estimated by counting the number of transitions for the dry and wet events.

For the wet event, the intensity (that is the amount of precipitation per hour) is finally modeled using a Gamma distribution [91], [92]:

$$\Lambda_{\mathrm{p},k|s_i} \sim \mathrm{Ga}\left(\alpha_{\Lambda_\mathrm{p}|s_i}, \beta_{\Lambda_\mathrm{p}|s_i}\right). \tag{54}$$

Hence, for each season, the precipitation model is fully described by the coefficients $p_{Hij|s_i}$ of the matrix $\mathbf{P}_{H|s_i}$ and the shape and rate parameters $\alpha_{\Lambda_\mathrm{p}|s_i} \in (0, \infty)$ and $\beta_{\Lambda_\mathrm{p}|s_i} \in (0, \infty)$.

The corresponding operating class may be formalized by prescribing that the probability that the precipitation amount per hour ranges between $\lambda_{\mathrm{p,min}}$, $\lambda_{\mathrm{p,max}}$ and should be lower and upper-bounded by $p_{\lambda_\mathrm{p},\max}$ and $p_{\lambda_\mathrm{p},\min}$, i.e. $p_{\lambda_\mathrm{p},\min} < \mathbb{P}(\lambda_{\mathrm{p,min}} < \Lambda_\mathrm{p} \leq \lambda_{\mathrm{p,max}}) \leq p_{\lambda_\mathrm{p},\max}$. This yields the expression in Result 7.

Result 7 (Operating Class for Precipitation): For the precipitation model described by (53) and (54), the following expression for the operating class may be deduced:

$$\begin{aligned} p_{\lambda_\mathrm{p},\min} < {} & \sum_{i=1}^{4} \pi_{H1|s_i}\left(\mathbf{P}_{H|s_i}\right) p_{s_i}\left[\mathbb{1}_{\lambda_{\mathrm{p,max}}\in\mathbb{R}_{\geq 0}} - \mathbb{1}_{\lambda_{\mathrm{p,min}}\in\mathbb{R}_{\geq 0}}\right] \\ & + \sum_{i=1}^{4} \frac{1}{\Gamma\left(\alpha_{\Lambda_\mathrm{p}|s_i}\right)} \gamma\left(\alpha_{\Lambda_\mathrm{p}|s_i}, \beta_{\Lambda_\mathrm{p}|s_i}\lambda_{\mathrm{p,max}}\right) \\ & \times \pi_{H2|s_i}\left(\mathbf{P}_{H|s_i}\right) p_{s_i} \mathbb{1}_{\lambda_{\mathrm{p,max}}\in\mathbb{R}_{>0}} \\ & - \sum_{i=1}^{4} \frac{1}{\Gamma\left(\alpha_{\Lambda_\mathrm{p}|s_i}\right)} \gamma\left(\alpha_{\Lambda_\mathrm{p}|s_i}, \beta_{\Lambda_\mathrm{p}|s_i}\lambda_{\mathrm{p,min}}\right) \\ & \times \pi_{H2|s_i}\left(\mathbf{P}_{H|s_i}\right) p_{s_i} \mathbb{1}_{\lambda_{\mathrm{p,min}}\in\mathbb{R}_{>0}} \leq p_{\lambda_\mathrm{p},\max}, \end{aligned} \tag{55}$$

where $\Gamma(\cdot)$ and $\gamma(\cdot, \cdot)$ are the Gamma function and the Lower Incomplete Gamma function, respectively.

Proof: The probability $\mathbb{P}(\lambda_{\mathrm{p,min}} < \Lambda_\mathrm{p} \leq \lambda_{\mathrm{p,max}})$ may be worked out analytically by considering the stationary distribution for the wet and dry events during each season. In particular, the conditional stationary distributions $\boldsymbol{\pi}_{H|s_i}$ correspond to the left eigenvector for the matrices $\mathbf{P}_{H|s_i}$:

$$\boldsymbol{\pi}_{H|s_i}\mathbf{P}_{H|s_i} = \boldsymbol{\pi}_{H|s_i}, \tag{56}$$

subject to the constraint $\pi_{H1|s_i} + \pi_{H2|s_i} = 1$. Solving (56) yields

$$\pi_{H1|s_i}\left(\mathbf{P}_{H|s_i}\right) = \frac{1 - p_{H22|s_i}}{2 - p_{H11|s_i} - p_{H22|s_i}}, \tag{57a}$$

$$\pi_{H2|s_i}\left(\mathbf{P}_{H|s_i}\right) = \frac{1 - p_{H11|s_i}}{2 - p_{H11|s_i} - p_{H22|s_i}}. \tag{57b}$$

Therefore, for each season, the conditional probability $\mathbb{P}(\lambda_{\mathrm{p,min}} < \Lambda_\mathrm{p} \leq \lambda_{\mathrm{p,max}} \mid S = s_i)$ may be calculated starting from the relationship

$$\begin{aligned} & \mathbb{P}\left(\Lambda_\mathrm{p} \leq \lambda_\mathrm{p} \mid S = s_i\right) \\ & = \mathbb{P}\left(\Lambda_\mathrm{p} \leq \lambda_\mathrm{p} \mid S = s_i \cap H_\mathrm{p} = 1\right) \mathbb{P}\left(H_\mathrm{p} = 1 \mid S = s_i\right) \\ & \quad + \mathbb{P}\left(\Lambda_\mathrm{p} \leq \lambda_\mathrm{p} \mid S = s_i \cap H_\mathrm{p} = 2\right) \mathbb{P}\left(H_\mathrm{p} = 2 \mid S = s_i\right) \\ & = \pi_{H1|s_i}\left(\mathbf{P}_{H|s_i}\right) \mathbb{1}_{\lambda_\mathrm{p}\in\mathbb{R}_{\geq 0}} \\ & \quad + F_{\Lambda_\mathrm{p}}\left(\lambda_\mathrm{p}; \alpha_{\Lambda_\mathrm{p}|s_i}, \beta_{\Lambda_\mathrm{p}|s_i}\right) \pi_{H2|s_i}\left(\mathbf{P}_{H|s_i}\right) \mathbb{1}_{\lambda_\mathrm{p}\in\mathbb{R}_{>0}}. \end{aligned} \tag{58}$$

Recalling (41) and combining (54), (57) and (58) leads to the result. ∎

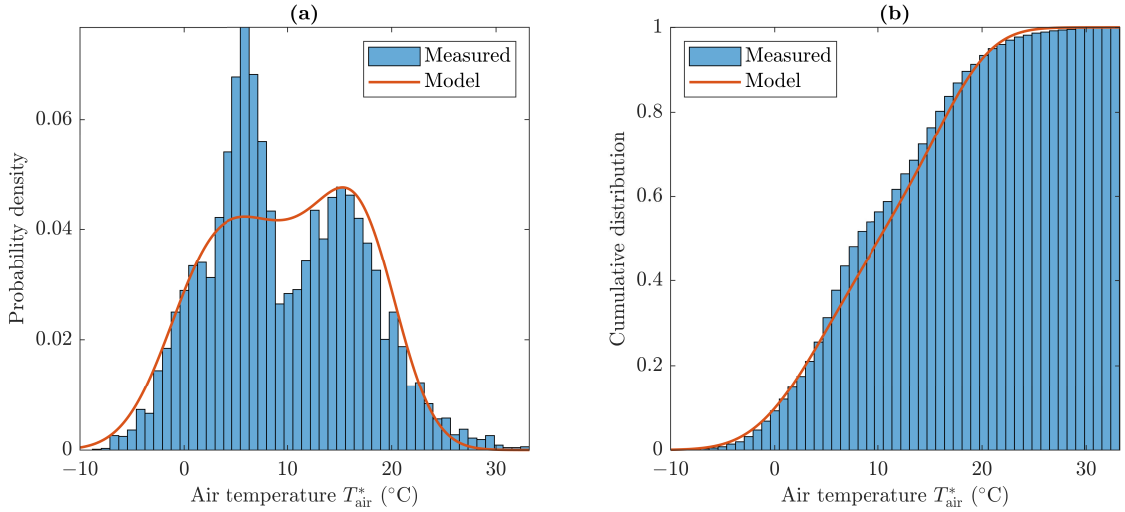

FIGURE 5. Comparison between the measured and analytical temperature distributions for the city of Gothenburg, Sweden, in 2019: (a) probability density; (b) cumulative distribution.

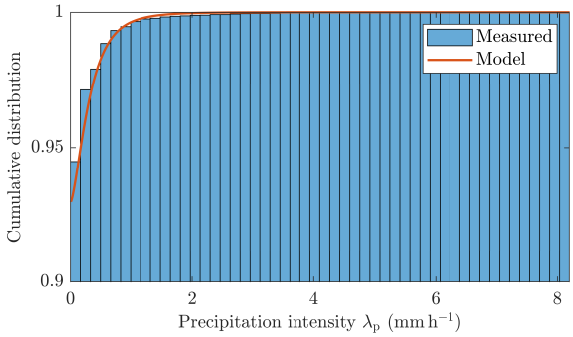

FIGURE 6. Comparison between the measured cumulative distribution for the precipitation in Gothenburg (2019) and the analytical CDF derived from the precipitation model.

Inequality (55) establishes the relationships between the set of sOC parameters $\mathcal{W}_{\text{s},H_{\text{p}}} = \{\mathbf{P}_{H|s_i}, \alpha_{\Lambda_{\text{p}}|s_i}, \beta_{\Lambda_{\text{p}}|s_i}\}$ and the bird's-eye view metrics $\mathcal{W}_{\text{b},H_{\text{p}}} = \{\lambda_{\text{p,min}}, \lambda_{\text{p,max}}, p_{\lambda_{\text{p}},\text{min}}, p_{\lambda_{\text{p}},\text{max}}\}$.

The measured cumulative distribution for the precipitation in Gothenburg for the year 2019, obtained again using SMHI data, is compared to the analytical CDF of Eq. (58) in Fig. 6.

C. TRAFFIC CATEGORY

Especially in highly-congested scenarios, road traffic excites frequent fluctuations in the driver's choice of speed. As a consequence, the prime mover becomes subjected to transient dynamics and operates in suboptimal conditions. From the perspective of energy efficiency, detailed modeling of the interaction between individual vehicles is not usually required, whereas a macroscopic approach is sufficient [9].

More specifically, in the sOC representation, the traffic flow is assumed to be stationary on the road section, and thus the unique variable to be considered becomes the so-called density, denoted by ρ_{t} expressed as a number of vehicles per distance. Moreover, in the sOC format, given a road, the parameters used to describe the traffic are also supposed to depend upon the season, and therefore a relationship analogous to (41) holds for ρ_{t}.

1) TRAFFIC DENSITY

For each road segment, the traffic density is modeled[7] as a sequence $\{\rho_{\text{t},k}\}_{k\in\mathbb{N}}$ assuming non negative values $\rho^*_{\text{t},k} \in \mathcal{S}_{\rho_{\text{t}}}$:

$$\rho_{\text{t},k} = \min\Big(\max\Big(0, \rho'_{\text{t},k}\Big), \rho_{\text{c}}\Big) \tag{59}$$

where ρ_{c} is a critical value for the density, and ρ'_k is the sum of a deterministic and stochastic component:

$$\rho'_{\text{t},k} = \bar{\rho}_k + \tilde{\rho}_k. \tag{60}$$

with

$$\bar{\rho}_k = \mu_{\rho|s_i} + \rho_{\text{d}|s_i} \sin\Big(\bar{\omega}_{\text{d}} k + \varphi_{\rho_{\text{d}}|s_i}\Big), \tag{61a}$$

$$\tilde{\rho}_k = \phi_{\rho|s_i}\tilde{\rho}_{k-1} + e_{\rho,k}, \quad e_{\rho,k} \sim \mathcal{N}\Big(0, \sigma^2_{e_\rho|s_i}\Big). \tag{61b}$$

In (61), $\mu_{\rho|s_i}$ is the average density on a specific road segment during the season, $\rho_{\text{d}|s_i}$ is the amplitude of the daily variation, $\bar{\omega}_{\text{d}}$ is again the daily frequency, $\varphi_{\rho_{\text{d}}|s_i}$ the initial phase. It should be noted that, as opposed to the models for the air temperature and humidity, the deterministic parameters in this case depend explicitly upon the seasonal setting. Thus, in the sOC description, the traffic density is parametrized by the deterministic quantities $\mu_{\rho|s_i}$, $\rho_{\text{d}|s_i}$, $\varphi_{\rho_{\text{d}}|s_i}$ and the stochastic coefficients $\phi_{\rho|s_i}$, $\sigma_{e_\rho|s_i}$. As usual, the

[7]The stocastic model for traffic density discussed in this paper is based on that presented in [59], and was validated using data collected from the Trafikverket.

error variance $\sigma^2_{e_\rho|s_i}$ may be rewritten in terms of the process variance as

$$\sigma^2_{\tilde{\rho}|s_i} = \frac{\sigma^2_{e_\rho|s_i}}{1-\phi^2_{\rho|s_i}}, \tag{62}$$

which, for each season, actually represents the variance of the stochastic component of the traffic density, i.e. $\tilde{\rho} \sim \mathcal{N}(0, \sigma^2_{\tilde{\rho}|s_i})$.

In the bird's-eye view representation, the relative metrics may again be derived by imposing $p_{\rho_t^*,\min} < \mathbb{P}(\rho^*_{\min} < \rho_t \leq \rho^*_{\max}) \leq p_{\rho_t^*,\max}$, where $\rho^*_{\min}$, $\rho^*_{\max}$ are prescribed thresholds, and the probabilities $p_{\rho_t^*,\min}, p_{\rho_t^*,\max}$ should be interpreted as the limiting fractions of the day for which the traffic density is comprised between $\rho^*_{\min}$ and $\rho^*_{\max}$. These two values may be deduced starting from some empirical or analytical model that relates density to speed variation.

Due to the above premises, the derivation of the relationship for the operating class may be worked out exactly as in Section III-B1 and is hence omitted. The final inequality is

$$\begin{aligned} p_{\rho_t^*,\min} < {} & \mathbb{1}_{\rho^*_{\max}\in[\rho_c,\infty)} + \sum_{i=1}^{4} \sum_{\bar{\rho}_k \in \mathcal{S}_{\tilde{\rho}|s_i}} p_{\bar{\rho}_k|s_i} p_{s_i} \mathbb{1}_{\rho^*_{\max}\in[0,\rho_c)} \\ & \times \Phi\left(\frac{\rho^*_{\max} - \bar{\rho}_k\left(\mu_{\rho|s_i}, \rho_{d|s_i}, \varphi_{\rho_d|s_i}\right)}{\sigma_{\tilde{\rho}|s_i}} \right) \\ & - \sum_{i=1}^{4} \sum_{\bar{\rho}_k \in \mathcal{S}_{\tilde{\rho}|s_i}} p_{\bar{\rho}_k|s_i} p_{s_i} \mathbb{1}_{\rho^*_{\min}\in[0,\rho_c)} \\ & \times \Phi\left(\frac{\rho^*_{\min} - \bar{\rho}_k\left(\mu_{\rho|s_i}, \rho_{d|s_i}, \varphi_{\rho_d|s_i}\right)}{\sigma_{\tilde{\rho}|s_i}} \right) \\ & - \mathbb{1}_{\rho^*_{\min}\in[\rho_c,\infty)} \leq p_{\rho_t^*,\max}, \end{aligned} \tag{63}$$

which connects the set of sOC parameters $\mathcal{T}_{s,\rho_t} = \{\mu_{\rho|s_i}, \rho_{d|s_i}, \varphi_{\rho_d|s_i}, \phi_{\rho|s_i}, \sigma_{\tilde{\rho}|s_i}\}$ to the bird's-eye view metrics $\mathcal{T}_{b,\rho_t} = \{\rho^*_{\min}, \rho^*_{\max}, p_{\rho_t^*,\min}, p_{\rho_t^*,\max}\}$.

D. MISSION CATEGORY

In the sOC description, there is presently no stochastic model for the mission category. However, for classifying road transport missions, the traveled distance might be used as a first indicator. This paper proposes the same approach as the GTA system, which prescribes four different levels:

1) `STOP&GO` if the mean distance between delivery or pickup of goods/passengers is shorter than 0.5 km.
2) `LOCAL` if the mean distance between delivery or pickup of goods/passengers is longer than 0.5 km but shorter than 5 km.
3) `REGIONAL` if the mean distance between delivery or pickup of goods/passengers is longer than 5 km but shorter than 50 km.
4) `L-DISTANCE` if the mean distance between delivery or pickup of goods/passengers is longer than 50 km.

The mission length is a delicate parameter, since it produces a significant effect on nondimensional indicators [1].

The complete set of operating class relationships derived in this paper, plus the corresponding sOC parameters and bird's-eye view metrics, are summarized in Table 4 for each model in the road, weather, and traffic categories.

IV. MATHEMATICAL CLASSIFICATION OF ROAD TRANSPORT MISSIONS AND APPLICATIONS

The theoretical framework developed in Section III may be used to label individual transport missions, but also to encompass entire transport applications, starting from available measurements logged during vehicular operations. To illustrate this, two examples are adduced using the GTA and UFD representations.

A. THE GTA AND UFD CLASSIFICATION SYSTEMS

The derivation of the analytical expressions for the operating classes in Section III was inspired by the interpretation from two already-existing classification systems: the GTA and the UFD representations. In the scope of product development and selection, they may serve as a preliminary but powerful tool to gain a rough idea of the vehicle usage, and evaluate the salient characteristics of its operating environment. As they are both colloquial in nature, with some exceptions they do not prescribe the precise thresholds of the operating classes, whereas an informal approach is often preferred. An option would be to establish the corresponding metrics using some fundamental intuition about the effect that some physical quantities produce on the vehicle's performance or driver's behavior. Tables 5 and 6 list the values for the probabilities and limits imposed on some of the operating classes according to the GTA and UFD interpretations. The numbers highlighted in bold refer to values not specified in the original classification system, but which were either deduced in the paper based on some simple physical model, or guessed. On the other hand, the expression 'n.s.' has been used when the threshold is not specified and no simple model was available from which to infer a plausible numerical value.

Starting from the topography model, it should be observed that both the GTA and UFD systems define the operating classes with great precision, as briefly mentioned in Section III-A1 and exemplified in Section IV. This may well be ascribed to the topography's considerable impact on such important indicators as energy efficiency [58]. The number of curves and local curvature of the road also play a major effect in determining the overall performance of the vehicle [58]. In spite of this, the classification approach appears to be less refined for the curviness parameter. In particular, the GTA system only sets the limits for the probabilities $p_{\kappa,\min}$ and $p_{\kappa,\max}$, while no exhaustive information is provided by the UFD representation. Hence, the maximum value for the curvature $\kappa_{\max} = 0.008\ \mathrm{m}^{-1}$ in Tables 5 and 6 was estimated from the steady-state relationship $\kappa_{\max} = a_y^{\max}/v_\kappa^2$, which connects a comfort threshold for the lateral acceleration $a_y^{\max}$ with a reference speed in a curve v_κ. In the present case, the

TABLE 4. Model interpretation, operating class relationships, sOC parameters and bird's-eye view metrics for the models presented in Section III. It should be observed that the operating classes for the topography and curviness parameters are determined using two relationships. While for the topography the inequality for the hill length may complement that on the process variance, the two relationships for the road curviness and speed signs should be used separately, depending on the specific classification system in use (UFD or GTA).

Model	Mathematical interpretation	Operating class relationships	sOC parameters $\mathcal{OC}_\mathrm{s}$	Bird's-eye view metrics $\mathcal{OC}_\mathrm{b}$
		Road category		
Topography	$p_{y,\min} < \mathbb{P}(y_\min < \lvert Y\rvert \leq y_\max) \leq p_{y,\max}$	Equation (10)	L_h, σ_Y	$y_\min$, $y_\max$, $p_{y,\min}$, $p_{y,\max}$, $L_{\mathrm{h},\min}$, $L_{\mathrm{h},\max}$
Curviness	$\bar{n}'_{C,\min} < \mathbb{E}\left(\frac{N'_C}{L_\mathrm{tot}}\right) \leq \bar{n}'_{C,\max}$,	Equation (17)	λ_C, μ_C, σ_C,	$\bar{n}'_{C,\min}$, $\bar{n}'_{C,\max}$,
	$p_{\kappa,\min} < \mathbb{P}(\kappa_\min < C \leq \kappa_\max) \leq p_{\kappa,\max}$	Equation (21)	μ_L, σ_L, r_turn	$\kappa_\min$, $\kappa_\max$, $p_{\kappa,\min}$, $p_{\kappa,\max}$
Speed bumps	$\bar{n}'_{\mathrm{b},\min} < \mathbb{E}\left(\frac{N'_\mathrm{b}}{L_\mathrm{tot}}\right) \leq \bar{n}'_{\mathrm{b},\max}$	Equation (25)	λ_b, $v_\min$, $v_\max$	$v_{\mathrm{b},\min}$, $v_{\mathrm{b},\max}$, $\bar{n}'_{\mathrm{b},\min}$, $\bar{n}'_{\mathrm{b},\max}$
Stop signs	$\bar{n}'_{\mathrm{s},\min} < \mathbb{E}\left(\frac{N'_\mathrm{s}}{L_\mathrm{tot}}\right) \leq \bar{n}'_{\mathrm{s},\max}$	Equation (27)	λ_s, $t_\min$, $t_\max$	$t_{\mathrm{s},\min}$, $t_{\mathrm{s},\max}$, $\bar{n}'_{\mathrm{s},\min}$, $\bar{n}'_{\mathrm{s},\max}$
Road roughness	$C_{\mathrm{r},\min} < \mathbb{E}(Z) \leq C_{\mathrm{r},\max}$	Equation (29)	C_r, ν_r	$C_{\mathrm{r},\min}$, $C_{\mathrm{r},\max}$
Speed signs	$p_{v,\min} < \mathbb{P}(\hat{v}_\min < V \leq \hat{v}_\max) \leq p_{v,\max}$	Equation (34)	$\boldsymbol{v}$, $\mathbf{P}_V$, $\boldsymbol{L}_V$	$\hat{v}_\min$, $\hat{v}_\max$, $p_{v,\min}$, $p_{v,\max}$
	$\hat{v}_\min < \mathbb{E}(V) \leq \hat{v}_\max$	Equation (35b)		
	$\bar{n}_{f_V,\min} < \mathbb{E}\left(\frac{N_{f_V}}{L_\mathrm{tot}}\right) \leq \bar{n}_{f_V,\max}$	Equation (35a) or (40)		$\bar{n}_{f_V,\min}$, $\bar{n}_{f_V,\max}$
		Weather category		
Air temperature	$p_{T^*_\mathrm{air},\min} < \mathbb{P}(T^*_\min < T_\mathrm{air} \leq T^*_\max) \leq p_{T^*_\mathrm{air},\max}$	Equation (47)	μ_T, T_d, T_y, φ_{T_d}, φ_{T_y}, $\phi_{T\mid s_i}$, $\sigma_{\tilde{T}\mid s_i}$,	$T^*_\min$, $T^*_\max$, $p_{T^*_\mathrm{air},\min}$, $p_{T^*_\mathrm{air},\max}$
Atm. humidity	$p_{\Psi^*_\mathrm{RH},\min} < \mathbb{P}(\Psi^*_\min < \Psi_\mathrm{RH} \leq \Psi^*_\max) \leq p_{\Psi^*_\mathrm{RH},\max}$	Equation (52)	μ_Ψ, Ψ_d, Ψ_y, $\varphi_{\Psi_\mathrm{d}}$, $\varphi_{\Psi_\mathrm{y}}$, $\phi_{\Psi\mid s_i}$, $\sigma_{\tilde{\Psi}\mid s_i}$,	$\Psi^*_\min$, $\Psi^*_\max$, $p_{\Psi^*_\mathrm{RH},\min}$, $p_{\Psi^*_\mathrm{RH},\max}$
Precipitation	$p_{\lambda_\mathrm{p},\min} < \mathbb{P}(\lambda_{\mathrm{p},\max} < \Lambda_\mathrm{p} \leq \lambda_{\mathrm{p},\max}) \leq p_{\lambda_\mathrm{p},\max}$	Equation (55)	$\mathbf{P}_{H\mid s_i}$, $\alpha_{\Lambda_\mathrm{p}\mid s_i}$, $\beta_{\Lambda_\mathrm{p}\mid s_i}$	$\lambda_{\mathrm{p},\min}$, $\lambda_{\mathrm{p},\max}$ $p_{\lambda_\mathrm{p},\min}$, $p_{\lambda_\mathrm{p},\max}$
		Traffic category		
Traffic density	$p_{\rho^*_\mathrm{t},\min} < \mathbb{P}(\rho^*_\min < \rho_\mathrm{t} \leq \rho^*_\max) \leq p_{\rho^*_\mathrm{t},\max}$	Equation (63)	$\mu_{\rho\mid s_i}$, $\rho_{\mathrm{d}\mid s_i}$, $\phi_{\rho_\mathrm{d}\mid s_i}$, $\phi_{\rho\mid s_i}$, $\sigma_{\tilde{\rho}\mid s_i}$	$\rho^*_\min$, $\rho^*_\max$ $p_{\rho^*_\mathrm{t},\min}$, $p_{\rho^*_\mathrm{t},\max}$

latter two quantities were assumed to be $a_y^\max = 2\ \mathrm{m\,s^{-2}}$ and $v_\kappa = 54\ \mathrm{km\,h^{-1}}$, respectively. These are only indicative values, and correspond specifically to a speed reduction of about 20% when driving at 70 $\mathrm{km\,h^{-1}}$. The value for the maximum number of curves $n'_{C,\max}$ (expressed in events per 100 km) marking the transition from the LOW to the HIGH class in the UFD system was simply set as equal to 20, analogous to the first limit for the stop signs. The same rationale was applied in determining the limits for the number of speed bumps, with the difference that in this case three levels are specified, namely LOW, HIGH and V−HIGH. For the latter two models, the speed and waiting time thresholds $v_{\mathrm{b},\min}$, $v_{\mathrm{b},\max}$, $t_{\mathrm{s},\min}$, $t_{\mathrm{s},\max}$ were assumed to be equal to the maximum recommended speed and time $v_\max$, $t_\max$, meaning that all the speed bumps and stop signs are considered in defining a class. The values for $C_{\mathrm{r},\min}$ and $C_{\mathrm{r},\max}$ in the road roughness model were deduced from the first four levels specified by the ISO standard [73]. Finally, regarding the model for speed signs, no limits $\hat{v}_\min$, $\hat{v}_\max$ were assumed for the GTA system, and the classes LOW, HIGH and V−HIGH were only determined based on the number of expected speed transitions. The values $\bar{n}_{f_V,\min}$ and $\bar{n}_{f_V,\min}$ were inspired by those for the stop signs. The probabilities $p_{v,\min}$ and $p_{v,\max}$ in the UFD description were always set to 0.7 and 1, respectively.

Regarding the weather models, there was no easily identifiable metric for atmospheric humidity and precipitation. However, the different levels and thresholds for air temperature are detailed in Appendix VI-B. In theory, it should be possible to correlate the amount of precipitation with the driver speed variation using some physical or empirical model, but no attempt was made in this paper. Alternatively, a more refined system would be preferable; one that distinguishes between more than just two classes. An example would be specifying four categories according to the Manual of Surface Observations [93].

Ultimately, the traffic model was omitted, since the GTA and UFD do not specify any density level along the road. However, a simple approach would be to relate travel speed to density according to some equilibrium equation assuming, say, a fundamental diagram for the different road types. This is also suggested in [59].

TABLE 5. Mathematical interpretations, operating classes and bird's-eye view metrics for the sOC models according to the GTA classification system. The values in bold refer to values that are not specified in the original classification system, but have been guessed in the paper. The values for $\kappa_{\min}$, $\kappa_{\max}$ in the curviness model are expressed in m^{-1}; for $\bar{n}_{f_V,\min}$, $\bar{n}_{f_V,\max}$ in the stop and speed signs models in number of events per 100 km; for is $\hat{v}_{\min}$ and $\hat{v}_{\max}$ in the speed signs model in $\mathrm{km\,h}^{-1}$.

Model	Relationship	Operating Class	Bird's-eye view metrics $\mathcal{OC}_\mathrm{b}$
		Road category	
Topography	Equation (10)	FLAT	$y_{\min} < 0$, $y_{\max} = 3$, $p_{y,\min} = 0.98$, $p_{y,\max} = 1$
		P-FLAT	$y_{\min} < 0$, $y_{\max} = 6$, $p_{y,\min} = 0.98$, $p_{y,\max} = 1$
		HILLY	$y_{\min} < 0$, $y_{\max} = 9$, $p_{y,\min} = 0.98$, $p_{y,\max} = 1$
		V-HILLY	else
Curviness	Equation (21)	LOW	$\kappa_{\min} < 0$, $\kappa_{\max} = \mathbf{0.008}$, $p_{\kappa,\min} = 0.8$, $p_{\kappa,\max} = 1$
		HIGH	else
Road roughness	Equation (29)	SMOOTH	$C_{\mathrm{r},\min} = 0$, $C_{\mathrm{r},\max} = \mathbf{16 \cdot 10^{-6}}$
		ROUGH	$C_{\mathrm{r},\min} = \mathbf{16 \cdot 10^{-6}}$, $C_{\mathrm{r},\max} = \mathbf{64 \cdot 10^{-6}}$
		V-ROUGH	$C_{\mathrm{r},\min} = \mathbf{64 \cdot 10^{-6}}$, $C_{\mathrm{r},\max} = \mathbf{256 \cdot 10^{-6}}$
		OFF-ROAD	$C_{\mathrm{r},\min} = \mathbf{256 \cdot 10^{-6}}$, $C_{\mathrm{r},\max} \to \infty$
Speed signs	Equation (35b) and (35a) or (40)	LOW	$\hat{v}_{\min} = 0$, $\hat{v}_{\max} = \mathbf{60}$, $\bar{n}_{f_V,\min} = 0$, $\bar{n}_{f_V,\max} = \mathbf{50}$
		HIGH	$\hat{v}_{\min} = \mathbf{60}$, $\hat{v}_{\max} = \mathbf{90}$, $\bar{n}_{f_V,\min} = \mathbf{50}$, $\bar{n}_{f_V,\max} = \mathbf{100}$
		V-HIGH	$\hat{v}_{\min} = \mathbf{90}$, $\hat{v}_{\max} \to \infty$, $\bar{n}_{f_V,\min} = \mathbf{100}$, $\bar{n}_{f_V,\max} \to \infty$
		Weather category	
Air temperature	Equation (47)	Appendix B	Appendix B

TABLE 6. Mathematical interpretations, operating classes and bird's-eye view metrics for the sOC models according to the UFD classification system. If the metrics are present, but their numerical values is not specified, 'n.s.' is used. The values in bold refer to values that are not specified in the original classification system, but have been guessed in the paper. The values for $\kappa_{\min}$, $\kappa_{\max}$ in the curviness model are expressed in m^{-1}; for $\bar{n}'_{\mathrm{b},\min}$, $\bar{n}'_{\mathrm{b},\max}$ and $\bar{n}'_{\mathrm{s},\min}$, $\bar{n}'_{\mathrm{s},\max}$ in the speed bumps and stop signs models in number of events per 100 km; for is $\hat{v}_{\min}$ and $\hat{v}_{\max}$ in the speed signs model in $\mathrm{km\,h}^{-1}$.

Model	Relationship	Operating Class	Bird's-eye view metrics $\mathcal{OC}_\mathrm{b}$
		Road category	
Topography	Equation (10)	FLAT	$y_{\min} = 2$, $y_{\max} \to \infty$, $p_{y,\min} = 0$, $p_{y,\max} = 0.2$
		HILLY	$y_{\min} = 2$, $y_{\max} \to \infty$, $p_{y,\min} = 0.2$, $p_{y,\max} = 0.4$
		V-HILLY	else
Curviness	Equation (17)	LOW	$\kappa_{\min} < 0$, $\kappa_{\max} = \mathbf{0.008}$, $\bar{n}'_{C,\min} = 0$, $\bar{n}'_{C,\max} = \mathbf{20}$
		HIGH	else
Speed bumps	Equation (25)	LOW	$\bar{n}'_{\mathrm{b},\min} = 0$, $\bar{n}'_{\mathrm{b},\max} = \mathbf{20}$, $v_{\mathrm{b},\min} = v_{\mathrm{b},\max} = \boldsymbol{v}_{\max}$
		HIGH	$\bar{n}'_{\mathrm{b},\min} = \mathbf{20}$, $\bar{n}'_{\mathrm{b},\max} = \mathbf{50}$, $v_{\mathrm{b},\min} = v_{\mathrm{b},\max} = \boldsymbol{v}_{\max}$
		V-HIGH	$\bar{n}'_{\mathrm{b},\min} = \mathbf{50}$, $\bar{n}'_{\mathrm{b},\max} \to \infty$, $v_{\mathrm{b},\min} = v_{\mathrm{b},\max} = \boldsymbol{v}_{\max}$
Stop signs	Equation (27)	FLUID	$\bar{n}'_{\mathrm{s},\min} = 0$, $\bar{n}'_{\mathrm{s},\max} = 20$, $t_{\mathrm{s},\min} = t_{\mathrm{s},\max} = \boldsymbol{t}_{\max}$
		LIGHT	$\bar{n}'_{\mathrm{s},\min} = 20$, $\bar{n}'_{\mathrm{s},\max} = 50$, $t_{\mathrm{s},\min} = t_{\mathrm{s},\max} = \boldsymbol{t}_{\max}$
		RESIDENTIAL	$\bar{n}'_{\mathrm{s},\min} = 50$, $\bar{n}'_{\mathrm{s},\max} = 150$, $t_{\mathrm{s},\min} = t_{\mathrm{s},\max} = \boldsymbol{t}_{\max}$
		DENSE	$\bar{n}'_{\mathrm{s},\min} = 150$, $\bar{n}'_{\mathrm{s},\max} = 250$, $t_{\mathrm{s},\min} = t_{\mathrm{s},\max} = \boldsymbol{t}_{\max}$
		START&STOP	$\bar{n}'_{\mathrm{s},\min} = 250$, $\bar{n}'_{\mathrm{s},\max} = 500$, $t_{\mathrm{s},\min} = t_{\mathrm{s},\max} = \boldsymbol{t}_{\max}$
		VF-START&STOP	$\bar{n}'_{\mathrm{s},\min} = 500$, $\bar{n}'_{\mathrm{s},\max} \to \infty$, $t_{\mathrm{s},\min} = t_{\mathrm{s},\max} = \boldsymbol{t}_{\max}$
Road roughness	Equation (29)	SMOOTH	$C_{\mathrm{r},\min} = 0$, $C_{\mathrm{r},\max} = \mathbf{16 \cdot 10^{-6}}$
		ROUGH	$C_{\mathrm{r},\min} = \mathbf{16 \cdot 10^{-6}}$, $C_{\mathrm{r},\max} = \mathbf{64 \cdot 10^{-6}}$
		V-ROUGH	$C_{\mathrm{r},\min} = \mathbf{64 \cdot 10^{-6}}$, $C_{\mathrm{r},\max} = \mathbf{256 \cdot 10^{-6}}$
		OFF-ROAD	$C_{\mathrm{r},\min} = \mathbf{256 \cdot 10^{-6}}$, $C_{\mathrm{r},\max} \to \infty$
Speed signs	Equation (34)	LOW	$\hat{v}_{\min} = 0$, $\hat{v}_{\max} = 50$, $p_{v,\min} = \mathbf{0.7}$, $p_{v,\max} = \mathbf{1}$
		MODERATE	$\hat{v}_{\min} = 50$, $\hat{v}_{\max} = 70$, $p_{v,\min} = \mathbf{0.7}$, $p_{v,\max} = \mathbf{1}$
		HIGH	$\hat{v}_{\min} = 70$, $\hat{v}_{\max} = 90$, $p_{v,\min} = \mathbf{0.7}$, $p_{v,\max} = \mathbf{1}$
		V-HIGH	$\hat{v}_{\min} = 90$, $\hat{v}_{\max} \to \infty$, $p_{v,\min} = \mathbf{0.7}$, $p_{v,\max} = \mathbf{1}$
		Weather category	
Air temperature	Equation (47)	Appendix B	Appendix B
Atm. humidity	Equation (52)	LOW	$\Psi^*_{\min} < 0$, $\Psi^*_{\max} = $ n.s., $p_{\Psi^*_{\mathrm{RH}},\min} = 0$, $p_{\Psi^*_{\mathrm{RH}},\max} = $ n.s.
		HIGH	else
Precipitation	Equation (55)	LOW	$\lambda_{\mathrm{p},\min} < 0$, $\lambda_{\mathrm{p},\max} = $ n.s., $p_{\lambda_{\mathrm{p}},\min} = 0$, $p_{\lambda_{\mathrm{p}},\max} = $ n.s.
		HIGH	else

B. CLASSIFICATION OF TRANSPORT APPLICATIONS

To illustrate the potential of the combined sOC and bird's-eye view descriptions, a first example was aimed at classifying an entire transport application. For the sake of simplicity, only the mission length and topography parameters were considered. Fig. 7 shows the distribution of 192 road transport

missions carried out by a Volvo FH16 during a period of approximately six months.[8] The operations were classified using the relationship for the OC class given by (10). Specifically, Fig. 7(a) and Fig. 7(b) refer to the distributions obtained according to the GTA and UFD thresholds for the standard deviation σ_Υ of the road grade, as listed in Table 2. While the total distance may be deduced immediately from log data, the topography parameters should be estimated using *ad-hoc* tools, such as the Wafo package [94], [95].

Looking at Fig. 7, it may be observed that the two systems yield rather different results. In particular, the UFD description misses the P−FLAT level; the transport operations are, therefore, spread across the remaining categories. This generally increases the number of FLAT and HILLY missions, compared to the distribution obtained by using the GTA metrics. Specifically, the HILLY category seems to be predominant in Fig. 7(b), whereas the majority of the mission is labeled as P−FLAT in Fig. 7(a). On the other hand, the distribution of V−HILLY missions is characterized by a similar trend for both classification systems.

In both cases, the entire application may be characterized starting with the estimated parameters for the individual missions, combined with their distributions. Independently of the classification system, the application is labeled as L−DISTANCE in respect of the mission length, with an average distance traveled of 52.4 km. On the other hand, the GTA and UFD systems classify the application respectively as P−FLAT and HILLY in reference to the topography class. Additional details about the individual missions are given in Table 11 in Appendix C1.

C. CLASSIFICATION OF TRANSPORT MISSIONS

Considering individual road missions, an idealized representation in terms of a dOC may be built starting from measured data. An equivalent statistical description in the form of an sOC may then be derived for each dOC by estimating the stochastic parameters of the road models presented in Section III.

The following example analyzes six different sOCs, parameterized using data collected during real vehicular operations [58], [96]. To obtain a more accurate description of the operating environment, the sOC parameters were estimated for different road types (urban, rural, highway). These were determined based on the legal speed values for different sections (more details may be found in Appendix A). The complete set of parameters for each reference sOC is listed in Tables 12, 13, 14, 15, 16 and 17 in Appendix C2. In general, it may be observed that each road type has its own characteristics. For instance, urban roads generally appear to be curvy, whereas rural and highway sections are mainly straight, and characterized by longer and larger curves. Also, the frequency of stop signs may be expected to correlate to the road type, as confirmed by the value of the parameters in Appendix C2. The classification of individual road types was then carried out directly by utilizing the expressions for the operating classes derived in this paper. These, combined with (66) and (68) in Appendix C2, were finally used to categorize each road mission (sOC).

The six operating cycles thus parametrized were then classified, taking four different parameters into account: topography, curviness, stop and speed signs. Starting from the values for the probabilities and metrics reported in Tables 5 and 6, the estimated classes for each combination of parameter and road type are listed in Table 7. Specifically, while both the GTA and UFD systems set their own thresholds on the model for topography, curviness, and speed signs, it should be observed that the GTA lacks the operating classes for the stop signs. Therefore, the corresponding road types and the overall sOC were only labeled according to the metrics used in the UFD representation. For each operating cycle, the road types were first categorized individually, and then used together to classify the overall mission according to the methodology illustrated in Appendix A. The percentages describing the road composition in the second column correspond to the stationary probabilities $\boldsymbol{\pi}_R\mathbf{G}_R = \mathbf{0}$ for the continuous-time Markov process describing the sequence of road types in Appendix. A. Generally speaking, it may be observed highways are the predominant road composition for most of the operating cycles. As a result, the total probabilities and expectations calculated using (66) are largely determined by the stochastic parameters for the highways. These are often characterized by relatively higher velocities, smoother curves, reduced hilliness, and fewer stops. Thus, the stochastic operating cycles themselves inherit the same characteristics, and are labeled accordingly. This justifies to a large extent the fact that they quite often seem to fall in the same categories as the corresponding highway roads. In particular, the two parameters that deserve special attention are the topography and the speed signs. Concerning the former, the road types and stochastic operating cycles of the example are noticeably categorized in the P−FLAT level according to the GTA system. However, this category is absent in the UFD representation, which systematically assigns the labels FLAT or HILLY. Again, this discrepancy is interesting, and confirms that the two systems conflict most of the time. A similar phenomenon may be observed in respect of the speed signs (to ensure a fair comparison, only the criterion on the mean speed in (35b) was included in the example, while the number of transitions was disregarded). By construction, urban sections are always labeled in the LOW category according to both the GTA and UFD descriptions. According to the UFD metrics, rural and highway roads are alternatively labeled as MODERATE and HIGH or HIGH and V−HIGH, respectively, whereas the UFD system often replaces the MODERATE level with the HIGH class, except for sOC 6. For the case under consideration, all the rural sections were labeled as MODERATE using the UFD criterion, whereas the highways, excluded sOC 5, as HIGH. The GTA system also classifies as V−HIGH the highway section

[8] Since the example excludes the weather parameters, six months has been assumed a sufficient period of time to span the overall application.

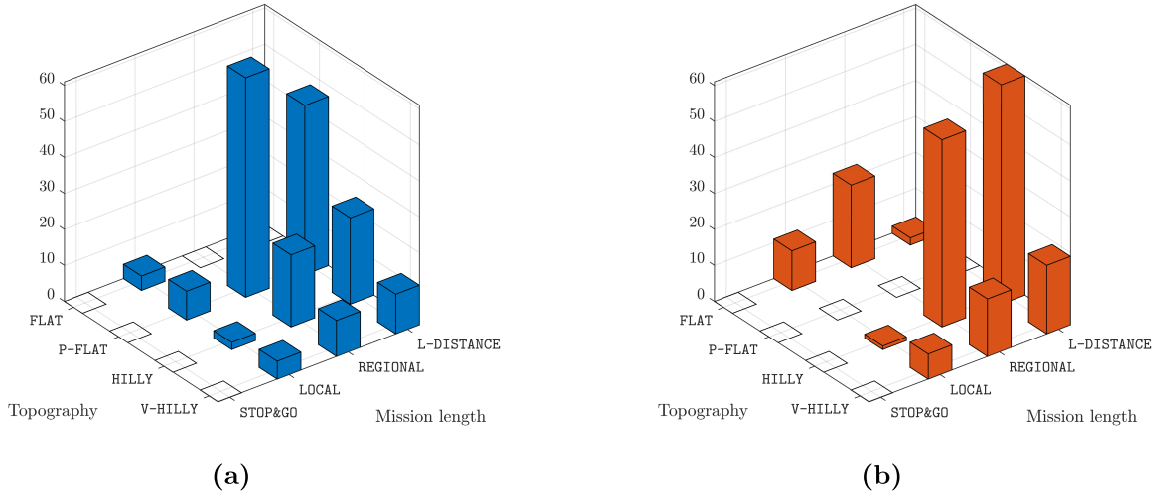

FIGURE 7. Distribution of road transport mission according to the GTA (a) and UFD (b) classification systems.

of sOC 4. At any rate, the stochastic operating cycles always inherited the HIGH label. Two striking exceptions are sOC 2 and sOC 5, which did not satisfy any criterion based on the classification established by the UFD system. Indeed, no speed range of those in Table 5 dominates for more than 70% of the traveled distance. This unexpected result is symptomatic and highlights the need for a refined classification system, plus more scientific definitions of both the notion of a class *per se* and its corresponding metrics. Conversely, the GTA system tends to assign the label V−HIGH to urban or rural sections, which are characterized by more frequent transitions between speeds. In this case, highway roads also exerted the majority of the influence in determining the level of the entire operating cycles, which were always classified as LOW except for sOC 5.

D. A CASE-STUDY EXAMPLE OF APPLICATION

While a complete, rigorous optimization problem is beyond the scope of this paper, a simple example is adduced to illustrate the practical application of the OC format for the purpose of vehicle design selection. For the sake of simplicity, only two different configurations are considered and compared in the following: a rigid Volvo FH16 750 and a FH13 540. The two configuration are similar, with the Volvo FH13 540 being equipped with a smaller engine. Additional details about both configurations may be found, for example, in the Volvo specification sheets [97].

The energy performance of the two different powertrains may be assessed considering a typical transport application, given for example in the form of a distribution as in Section IV-B. To this end, multiple dOCs (either original or synthetic) may be used as an input to a complete simulation model for longitudinal vehicle dynamics, including a dynamic driver model. For the case study presented in this paper, the VehProp environment [98] was used to model and simulate both trucks. To reduce the dimension of the problem, a few sOCs were selected appropriately to be representative of the actual usage. More specifically, using the GTA description as a reference classification system, the first three sOC in Section IV-C, parametrised based on real data logged from the Volvo FH16 750, were employed to assess variability in fuel consumption (measured in $l\,10^{-1}km^{-1}$)[9] depending on the characteristics of each mission and on the specific configuration. In this context, it may be easily observed that all the three missions are classified as P−FLAT in the topography category, which is the predominant class. In turn, the selected sOCs were used to synthesize 200 dOCs for each reference mission.

The resulting distributions are plotted in Figures 8 and 9. In particular, in Figure 8, the histograms of the fuel consumption are shown (blue for the FH16 750 and orange for the FH13 540), along with the mean value μ and the two bandwidths $\mu \pm \sigma$ and $\mu \pm 2\sigma$ (the corresponding mean values are listed in Table 8 for both trucks), whereas Figure 9 compares the energy performance of the two configurations for each reference mission. Generally speaking, it may be observed that the total fuel consumption calculated by simulating the reference dOCs is lower than the mean value resulting from the corresponding distribution. For the first two missions, the fuel consumption in output from the reference dOCs is still contained within a single standard deviation bandwidth, whereas for the third missions is contained between two standard deviations for both vehicle configurations. Therefore, the reference dOCs may be fairly considered as typical operation for the first two transport missions. In all cases, it may be concluded that the FH13 540 outperforms the FH16 750 in terms of energy efficiency, implying that, all the other

[9] 10 km correspond to one Swedish mil.

TABLE 7. Operating classes for the six different stochastic operating cycles in the example of Section IV-C. The term *composition* refers to the composition of the road (percentages of urban, rural and highway types) according to the distributions calculated as explained in Section VI-A. The classification is carried out in respect of both the individual road types and the total transport operation. The topography and curviness parameters are classified using the GTA and UFD system in turn; the stop signs are only classified using the metrics from the UFD.

			Operating class						
			Topography		*Curviness*		*Stop signs*	*Speed signs*	
sOC	**Road type**	**Composition**	GTA	UFD	GTA	UFD		GTA	UFD
1	*Urban*	3.6%	P-FLAT	HILLY	HIGH	LOW	FLUID	LOW	LOW
	Rural	4.6%	HILLY	V-HILLY	LOW	LOW	FLUID	HIGH	MODERATE
	Highway	91.8%	P-FLAT	HILLY	LOW	LOW	FLUID	HIGH	HIGH
	Total	100%	P-FLAT	HILLY	LOW	LOW	FLUID	HIGH	HIGH
2	*Urban*	19.7%	HILLY	V-HILLY	HIGH	LOW	FLUID	LOW	LOW
	Rural	18.9%	P-FLAT	FLAT	LOW	LOW	FLUID	HIGH	MODERATE
	Highway	61.4%	FLAT	FLAT	LOW	LOW	FLUID	HIGH	HIGH
	Total	100%	P-FLAT	FLAT	LOW	LOW	FLUID	HIGH	-
3	*Urban*	11.5%	P-FLAT	HILLY	HIGH	LOW	FLUID	LOW	LOW
	Rural	1.5%	FLAT	FLAT	HIGH	LOW	FLUID	HIGH	MODERATE
	Highway	87%	P-FLAT	FLAT	LOW	LOW	FLUID	HIGH	HIGH
	Total	100%	P-FLAT	FLAT	LOW	LOW	LIGHT	HIGH	HIGH
4	*Urban*	3.8%	P-FLAT	FLAT	HIGH	LOW	LIGHT	LOW	LOW
	Rural	9.5%	P-FLAT	HILLY	HIGH	LOW	FLUID	HIGH	MODERATE
	Highway	86.7%	P-FLAT	HILLY	LOW	LOW	FLUID	V-HIGH	HIGH
	Total	100%	P-FLAT	HILLY	LOW	LOW	FLUID	HIGH	HIGH
5	*Urban*	12.1%	FLAT	HILLY	LOW	LOW	DENSE	LOW	LOW
	Rural	45.6%	P-FLAT	HILLY	HIGH	LOW	LIGHT	HIGH	MODERATE
	Highway	42.4%	P-FLAT	HILLY	LOW	LOW	FLUID	V-HIGH	V-HIGH
	Total	100%	P-FLAT	HILLY	LOW	LOW	LIGHT	HIGH	-
6	*Urban*	14.5%	HILLY	FLAT	HIGH	LOW	FLUID	LOW	LOW
	Rural	6.2%	HILLY	V-HILLY	LOW	LOW	RESIDENTIAL	LOW	MODERATE
	Highway	79.3%	P-FLAT	HILLY	LOW	LOW	FLUID	HIGH	HIGH
	Total	100%	HILLY	V-HILLY	LOW	LOW	FLUID	HIGH	HIGH

TABLE 8. Fuel consumption ($l\,10^{-1}\,km^{-1}$).

		Mean μ	Standard deviation σ
Mission 1:	measured:	6.3386	-
	ref dOC FH16 750:	6.5293	-
	ref dOC FH13 540:	6.3706	-
	Generated dOCs FH16 750:	6.7900	0.7243
	Generated dOCs FH13 540:	6.4443	0.5836
Mission 2:	measured:	6.6587	-
	ref dOC FH16 750:	6.7580	-
	ref dOC FH13 540:	6.3283	-
	Generated dOCs FH16 750:	7.1658	0.6219
	Generated dOCs FH13 540:	6.6130	0.5929
Mission 3:	measured:	4.5473	-
	ref dOC FH16 750:	4.4874	-
	ref dOC FH13 540:	3.9123	-
	Generated dOCs FH16 750:	5.2973	0.5372
	Generated dOCs FH13 540:	4.6496	0.5097

things being equal, the FH13 540 configuration would be preferable to purchase.[10]

It should be emphasized that, since only two different configurations were considered in the previous example, it was possible to easily compare the energy performance on the whole population of generated dOCs. This approach would not be feasible when dealing with a complex optimization problem involving thousands of decision variables and possible vehicle designs. In the latter case, the vehicle should be optimized by considering dOCs that are optimally representative of both the mission characteristics and the energy usage, that is a synthetically generated mission yielding, in simulation, mean or close-to-mean energy consumption. Such approach as been already applied by other scholars, for example in [21]–[23], [26] (in particular, it is interesting to observe that the OC model for topography was already included in [23], with the corresponding classes defined according to the GTA system). Moreover, if log data from idividual or single vehicles are available, typical dOCs may be properly selected as already explained in the previous example. The representativeness in terms of energy consumption for an optimized configuration may be instead evaluated *a posteriori* on the same population of road operations.

[10]In general, no substantial difference between the vehicles's speed could be observed in simulation.

V. DISCUSSION

The examples in Section IV were aimed at illustrating how the dual description bird's-eye view/sOC can be made to work in practice when addressing the classification problem. This section discusses two extremely delicate aspects related to the proposed approach.

A. SCIENTIFIC DEFINITION OF METRICS AND LABELS

The example discussed in Section IV was emblematic in underlining the need for a classification system that could appropriately reflect the usage. To clarify this concept, one

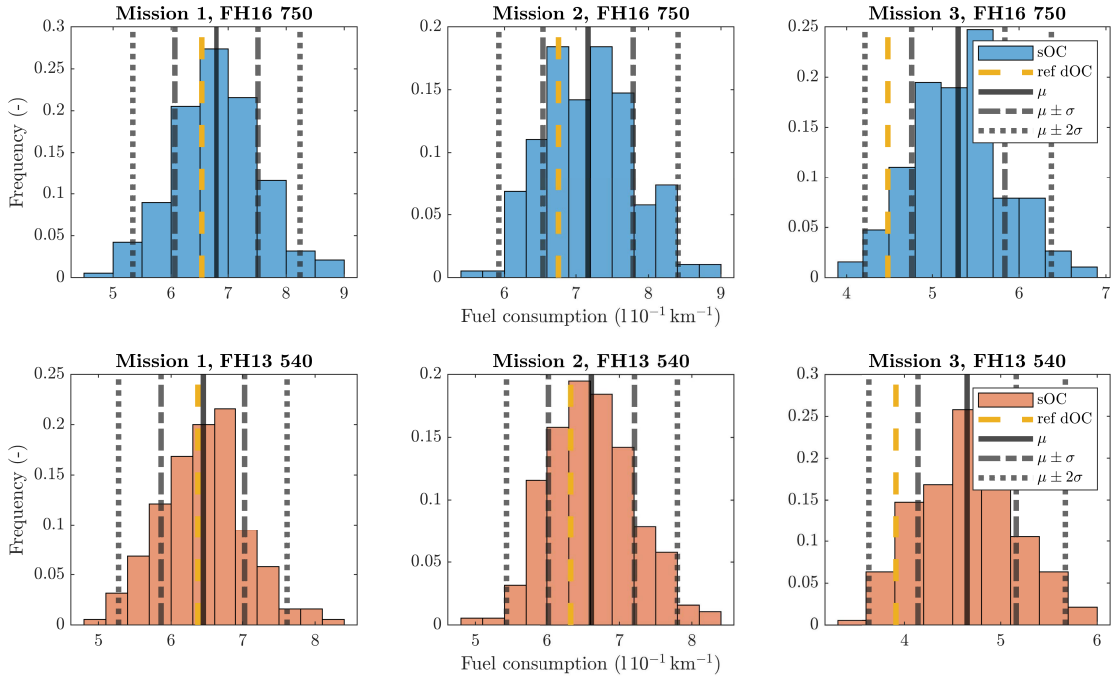

FIGURE 8. Distribution of the fuel consumption for both configurations.

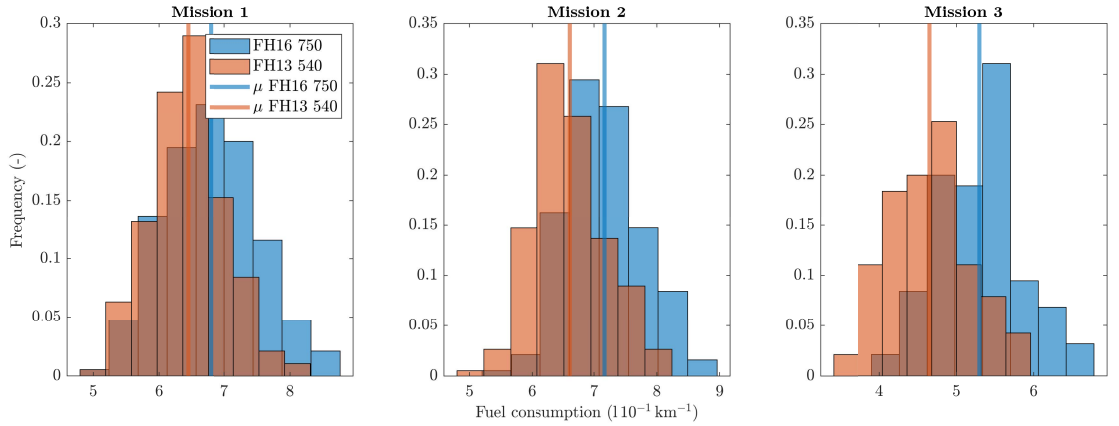

FIGURE 9. Comparison between the distribution of the fuel consumption for each reference mission.

may think of a customer who, based on the known properties of the intended transport application, needs to choose a new vehicle. Assuming that an optimization problem to find standard configurations that better suit the application has already been solved, the customer simply has to choose from the available optimal designs. However, the outcome of the optimization problem would be highly dependent on how the operating classes and their metrics have been established. Both the GTA and UFD representations set their own systems of thresholds mostly on empirical bases. The reason for this lies in the fact that both classifications have been developed over many years as a result of mutual interaction between manufacturers and customers. Their non-mathematical nature reflects the stakeholders' necessities. In this context, the substantial discrepancy between the metrics from the GTA and UFD systems might lead to very different solutions in terms of the best design. This might be overcome if a systematic, scientific method of specifying labels and limits for the operating classes were to be established.

For those models whose metrics are prescribed in terms of expectation, as in (17), (25) and (27), the problem merely reduces to finding the right sequence of limits for the expected number of events. This operation might seem trivial in theory, but, from a practical perspective, it is not obvious how to proceed. When the classes are specified in terms of probabilities, on the other hand, the issue may become rather thorny.

Often, the GTA and UFD systems only set one bound. In this case, as with the road topography, the levels are always well-defined, and it is possible to assign a unique set of sOC parameters to a certain operating class. In a more general situation, lower and upper bounds on both the probability and the parameter itself should be prescribed to span the entire range of possibilities. However, this also multiplies the number of classes needed, increasing the complexity of such a classification system. To keep the structure of a bird's-eye view description as simple as possible, it becomes obvious that the thresholds values cannot be imposed based on pure mathematical considerations, whereas a heuristic approach is required.

B. FEASIBLE SETS OF sOC PARAMETERS

It was briefly mentioned in Section II-D that the relationship between the bird's-eye view and sOC representations is not bijective in the ascending direction. In particular, while a given set of sOC parameters should ideally correspond uniquely to a certain class, the opposite does not hold. Fixing a probability threshold, or equivalently the number of expected events, the analytical expression for an operating class may be interpreted as a hypersurface having multiple solutions. Broadly speaking, there exist infinite different sets of sOC parameters that categorize a mission in the same operating class. Mathematically, this certainly appears logical. The physical interpretation, on the other hand, is not so obvious: some combinations of sOC parameters may make no sense. An emblematic situation where this becomes problematic is in dealing directly with customers, with no prior information about the intended usage: they may have a rough idea of the characteristics of the operating environment, but would be unable to indicate a precise estimate of the topography variance. The manufacturer might suggest an optimal configuration for the truck based on the bird's-eye view description provided by the customer, but the optimization problem should have been already solved assuming a set of possible values for the topography variance. In this context, how to ascertain that a solution is feasible from the physical interpretation perspective is a highly intriguing question. One possibility is to resort almost exclusively to sets of parameters extracted from real vehicular operations, or from data collected by external servers. Single missions might, therefore, be used as a basis to build a large, reliable dataset of parameters.

VI. CONCLUSION

Classifying individual transport missions at an individual level, as well as entire vehicular applications, is crucial when it comes to designing and selecting single components and configurations, and in the planning of maintenance and optimization of road operations. This paper addressed the classification problem from the perspective of the operating cycle (OC) description by exploring the relationship between two of its three levels of representation, namely the bird's-eye view and the stochastic operating cycle (sOC). While the former is characterized by a rather colloquial tone and aims to provide an intuitive understanding of the usage by resorting to simple metrics and labels, the latter is the most adequate descriptive tool in reflecting variation in the operating environment, drivers' attitudes, and overall vehicle performance. Specifically, the non-technical language of the bird's-eye view relies naturally on vague statements, which might be interpreted in terms of elementary statistics. On the other hand, the sOC represents the surroundings, including the road, weather, and traffic properties, using a vast set of independent stochastic models structured in a modular, hierarchical fashion.

In this paper, the natural connection between the sOC and the bird's-eye view was therefore formulated in terms of elementary statistical operators, such as probability $\mathbb{P}(\cdot)$ and expectation $\mathbb{E}(\cdot)$. Starting from the stochastic modeling approach typical of the sOC, these were calculated analytically in Section III for the different models in the road, weather, and traffic categories, establishing algebraic expressions, renamed in this paper as *operating classes*, which relate the two levels of description. The result is a collection of analytical relationships, which are easy to understand in terms of frequencies, probabilities, and expected number of events that a driver may encounter along the road or during a mission. In particular, the mathematical derivation of the expressions for the operating classes was based on intuition gained from examining some existing classification systems, like the Global Transport Application (GTA) introduced by Volvo and the User Factor Description (UFD) used by Scania. The purpose of the operating class is twofold. Exploiting the relationship between the sOC and the bird's-eye view in the ascending direction, road transport missions categorized according to the operating classes may be labeled directly starting from, say, log data or non-technical information retrieved from customers. This enables classification not only of road operations seen in isolation, but also the entire application, allowing for a high level of standardization. On the other hand, the non-bijective nature of the inverse relationship (in the descending direction) may facilitate optimization of the vehicle's configuration, starting from a rough understanding of the usage. A typical case is that of a vehicle manufacturer dealing with a customer, who cannot be expected to have a deep knowledge of stochastic models and statistical operators. Asking simple questions about the typical operating environment and characteristics of the mission, engineers may use information from the answers to parametrize several sOCs, and, in turn, dOCs. These may be combined with vehicle and driver models into virtual simulation environments to conduct statistical studies and solve optimization problems.

To illustrate the potential of the proposed approach, an example with six stochastic operating cycles parametrized from log data, plus an entire transport application, was discussed in Section IV, using the GTA and UFD systems for comparison. While it was shown how to take advantage of the dual-level of description bird's-eye view/sOC to categorize both individual roads and missions, the example also

highlighted some weaknesses of the classification systems currently used. In particular, the need for more refined classification criteria emerged in conjunction with the impossibility of labeling certain missions, at least according to the metrics defined in the GTA and UFD representations. How to prescribe probabilities and thresholds scientifically is however an open problem, which has not so far been explored in context. Moreover, a unique operating class according to the bird's-eye view description may correspond to sets of sOC parameters that are unfeasible from a physical perspective. Further research is needed to investigate both aspects in greater detail.

Another interesting direction for future studies connects to the possibility of including more stochastic models and parameters when addressing the classification problem of energy usage of road vehicles. For example, factors like road width, visibility, snow accumulation, wind speed and direction, and daily traveled distance also play an important role in determining the vehicle's response in terms of energy efficiency. However, they are not currently considered by the existing classification systems. Therefore, the need for extending the stochastic operating cycle representation to incorporate these variables should be carefully evaluated.

Finally, the potential of the new formalism established in the paper should also be tested on large, complicated optimization problems, similar to those solved by Ghandriz *et al.* [23], where the effect of the road topography was investigated using the stochastic model discussed in Section III-A1. With the novel operating classes derived in Section III, the analysis conducted in [23] could be easily extended to account for the contribution of other road and weather parameters.

APPENDIX

A. ROAD TYPES AND TOTAL PROBABILITY

The notion of an operating class introduced in Sections II, and III may be used to categorize either a road mission or an individual road section, hereinafter referred to as *type*. In the latter case, the road type may be regarded as a primary model for the road, and would work similarly to the season for the weather category. Depending on the road type, different sets of stochastic parameters may then be used for the models illustrated in Section III, which would be treated as secondary ones. This approach is often used in the sOC representation, as discussed also in [58]. A graphical representation of the hierarchical structure of the road type, plus the sOC parameters for the secondary road models, is shown in Fig. 10. More specifically, the modeling of the road types may be related to the notion of speed signs, and represented as a stochastic process starting from the speed limit [99]. The existence of n_r different road types r_t may be firstly postulated, i.e. $\{r_1, \ldots, r_{n_r}\}$, based on a sequence of $n_r - 1$ characteristic speeds, ordered in ascending magnitude. These would mark the transition from one road type to the next, implying that each speed sign would belong uniquely to a given road type. Accordingly, the road type would itself become a random variable R_t, assuming values $r_\mathrm{t} \in \mathcal{S}_{R_\mathrm{t}} = \{r_1, \ldots, r_{n_r}\}$, as a function of the speed sign $V(x)$, and would in turn depend on the position along the road. A specific number $n_{v|r_i}$ of speed signs may be associated with each road type. Modeling the locations X_k for the road types as in (14), the model would be described by a continuous-time Markov chain, and completely parametrized by the entries p_{Rij} of the single-step transition matrix $\mathbf{P}_R \in \mathbb{R}_{\geq 0}^{n_r \times n_r}$ and the n_r intensities λ_{Ri}, reading

$$\lambda_{Ri} = \frac{1}{L_{Ri}}, \tag{64}$$

being L_{Ri} the mean length of the road type r_i. Again, the n_r mean lengths L_{Ri} may be collected in a vector $\boldsymbol{L}_R = [L_{R1} \ \ldots \ L_{Rn_r}]^\mathrm{T}$.

If a similar approach is preferred, analogous to that in Section III-A5, the stationary $\boldsymbol{\pi}_R$ distribution of the overall process should be derived as the solution of $\boldsymbol{\pi}_R \mathbf{G}_R = \mathbf{0}$, where the entries $g_{Rij} = g_{Rij}(p_{Rij}, L_{Ri})$ of the generator matrix $\mathbf{G}_R$ would be given by

$$g_{Rij}(p_{Rij}, L_{Ri}) = \begin{cases} \lambda_{Ri} p_{Rij} = \dfrac{p_{Rij}}{L_{Ri}}, & i \neq j, \\ -\lambda_{Ri} = -\dfrac{1}{L_{Ri}}, & i = j. \end{cases} \tag{65}$$

To classify an operating cycle, it would therefore be necessary to compute the total probabilities or expectations by summation over the different road types. Indeed, road segments belonging to the same road type should be described using the same values for the sOC parameters. The total probability and expectation for a generic random variable A in the road or weather categories would become

$$\begin{aligned} \mathbb{P}(A) &= \sum_{i=1}^{n_r} \mathbb{P}(A \mid R_\mathrm{t} = r_i)\, \mathbb{P}(R_\mathrm{t} = r_i) \\ &= \sum_{i=1}^{n_r} \mathbb{P}(A \mid R_\mathrm{t} = r_i) \pi_{Ri}(\mathbf{P}_R, \boldsymbol{L}_R), \end{aligned} \tag{66a}$$

$$\begin{aligned} \mathbb{E}(A) &= \sum_{i=1}^{n_r} \mathbb{E}(A \mid R_\mathrm{t} = r_i)\, \mathbb{P}(R_\mathrm{t} = r_i) \\ &= \sum_{i=1}^{n_r} \mathbb{E}(A \mid R_\mathrm{t} = r_i) \pi_{Ri}(\mathbf{P}_R, \boldsymbol{L}_R), \end{aligned} \tag{66b}$$

where the analytical expressions for the probabilities $\mathbb{P}(A \mid R_\mathrm{t} = r_i)$ and the expectations $\mathbb{E}(A \mid R_\mathrm{t} = r_i)$ would coincide with those for the operating classes derived in Section III. It should be emphasized that, in (66), the probabilities $\mathbb{P}(R_\mathrm{t} = r_i)$ may be set equal to the stationary ones for the road types, given a generic sOC. This should be the preferred approach when referring to an sOC, which is an abstract entity. In this context, it could be mentioned that calculation of the number of transitions between speeds should be modified to include also the number of transitions between different road types. Introducing a new variable

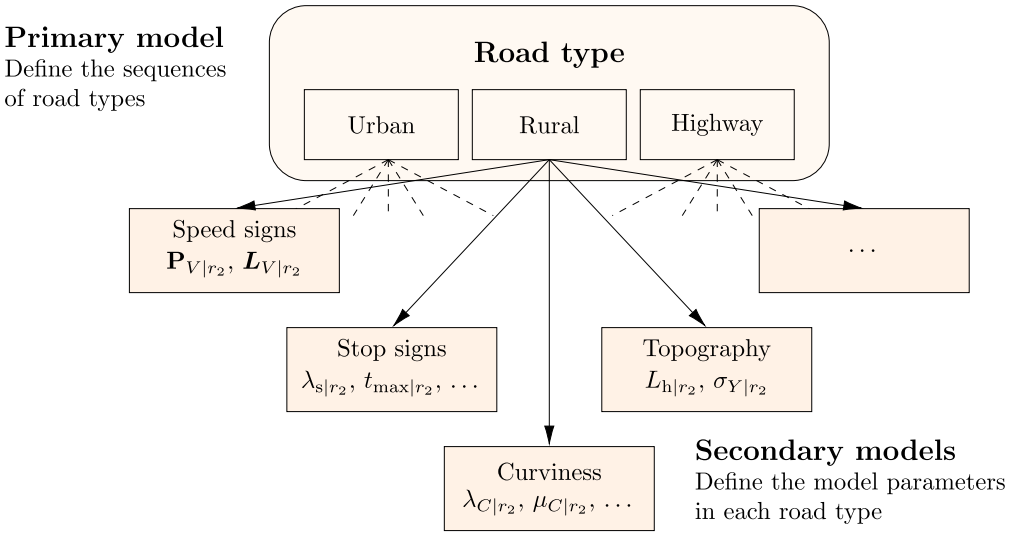

FIGURE 10. Graphical illustration of the primary road model.

TABLE 9. Upper and lower limits on the air temperature according to the GTA classification system.

Upper limit	Lower limit
$T^*_{\max} = 40°\mathrm{C}$	$T^*_{\min} = -15°\mathrm{C}$
$T^*_{\max} > 40°\mathrm{C}$	$T^*_{\min} = -25°\mathrm{C}$
	$T^*_{\min} = -40°\mathrm{C}$
	$T^*_{\min} < -40°\mathrm{C}$

$N_{fV+fR} = N_{fV} + N_{fR}$, accounting for both types of speed jumps, the expected number of total transitions may be estimated as

$$\begin{aligned}\mathbb{E}\left(\frac{N_{fV+fR}}{L_{\text{tot}}}\right) &= \sum_{i=1}^{n_r} \mathbb{E}\left(\frac{N_{fV}}{L_{\text{tot}}} \,\middle|\, R_{\text{t}} = r_i\right) \mathbb{P}(R_{\text{t}} = r_i) \\ &\quad + \mathbb{E}\left(\frac{N_{fR}}{L_{\text{tot}}}\right) \\ &= \sum_{i=1}^{n_r} \mathbb{E}\left(\frac{N_{fV}}{L_{\text{tot}}} \,\middle|\, R_{\text{t}} = r_i\right) \pi_{Ri}(\mathbf{P}_R, \boldsymbol{L}_R) \\ &\quad + \mathbb{E}\left(\frac{N_{fR}}{L_{\text{tot}}}\right), \end{aligned} \tag{67}$$

where $\mathbb{E}(N_{fV}/L_{\text{tot}} \mid R_{\text{t}} = r_i)$ reads as in (39) and $\mathbb{E}(N_{fR}/L_{\text{tot}})$ may be calculated with similar relationships to (36), (37), (38) and (39).

Finally, the traffic density also deserves special attention, since its parameters would depend not only on road type but also speed signs. Since each speed sign may be uniquely associated with a single road type, the total probability $\mathbb{P}(\rho^*_{\min} < \rho_{\text{t}} \leq \rho^*_{\max})$ would be calculated as

$$\begin{aligned}&\mathbb{P}(\rho^*_{\min} < \rho_{\text{t}} \leq \rho^*_{\max}) \\ &\quad = \sum_{i=1}^{n_r} \sum_{j=1}^{n_{v|r_i}} \mathbb{P}(\rho^*_{\min} < \rho_{\text{t}} \leq \rho^*_{\max} \mid R_{\text{t}} = r_i \cap V = v_j) \\ &\qquad \times \mathbb{P}(V = v_j \mid R_{\text{t}} = r_i)\, \mathbb{P}(R_{\text{t}} = r_i) \\ &\quad = \sum_{i=1}^{n_r} \sum_{j=1}^{n_{v|r_i}} \mathbb{P}(\rho^*_{\min} < \rho_{\text{t}} \leq \rho^*_{\max} \mid R_{\text{t}} = r_i \cap V = v_j) \\ &\qquad \times \pi_{Vj}(\mathbf{P}_{V|r_i}, \boldsymbol{L}_{V|r_i}) \pi_{Ri}(\mathbf{P}_R, \boldsymbol{L}_R), \end{aligned} \tag{68}$$

where the formal expression for $\mathbb{P}(\rho^*_{\min} < \rho_{\text{t}} \leq \rho^*_{\max} \mid R_{\text{t}} = r_i \cap V = v_j)$ would read exactly as in (63).

TABLE 10. The operating classes for the air temperature parameter in the UFD description. The `V-COLD`, `COLD`, `WARM` and `V-WARM` classes are defined by three relationships of the same type. On the other hand, the `MIXED` class only needs two inequalities to be completely defined.

Air temperature classes in the UFD description					
Operating class	Number of relationship i	UFD thresholds $T^{*(i)}_{\min}$	$T^{*(i)}_{\max}$	$p^{(i)}_{T^*_{\text{air}},\min}$	$p^{(i)}_{T^*_{\text{air}},\max}$
`V-COLD`	1	$-\infty$	$-30°\mathrm{C}$	0	**0.5**
	2	$20°\mathrm{C}$	∞	0	**0.2**
	3	$30°\mathrm{C}$	∞	0	0
`COLD`	1	$-\infty$	$-15°\mathrm{C}$	0	**0.5**
	2	$25°\mathrm{C}$	∞	0	**0.2**
	3	$30°\mathrm{C}$	∞	0	0
`MIXED`	1	$-\infty$	$-15°\mathrm{C}$	0	**0.2**
	3	$30°\mathrm{C}$	∞	0	**0.2**
`WARM`	1	$-\infty$	$5°\mathrm{C}$	0	**0.5**
	2	$-\infty$	$0°\mathrm{C}$	0	0
	3	$40°\mathrm{C}$	∞	0	**0.2**
`V-WARM`	1	$-\infty$	$15°\mathrm{C}$	0	**0.2**
	2	$-\infty$	$0°\mathrm{C}$	0	0
	3	$45°\mathrm{C}$	∞	0	**0.5**

B. THE AIR TEMPERATURE PARAMETER IN THE GTA AND UFD CLASSIFICATION SYSTEMS

The temperature parameter in the GTA and UFD classification systems is treated differently and deserves special attention. In particular, the GTA description specifies the lower and upper bound on the thresholds $T^*_{\min}$ and $T^*_{\max}$ (Table 9). From Table 9, it may be understood there are eight possible combinations between the upper and lower limits,

TABLE 11. Travelled distance and standard deviation for topography σ_Y for the road transport missions in the example of Section IV.

Mission	Distance (km)	σ_Y (%)	Mission	Distance (km)	σ_Y (%)	Mission	Distance (km)	σ_Y (%)	Mission	Distance (km)	σ_Y (%)
1	14.710	1.438	49	16.240	2.404	97	67.205	2.056	145	52.120	1.742
2	88.620	2.502	50	78.310	3.530	98	41.545	1.978	146	45.530	1.822
3	85.270	2.377	51	34.380	2.864	99	44.095	1.534	147	16.220	1.795
4	85.740	2.022	52	11.525	1.541	100	1.195	1.156	148	26.375	1.816
5	8.310	1.464	53	3.770	4.598	101	162.485	2.091	149	58.135	2.351
6	16.360	2.417	54	105.650	1.712	102	8.665	2.955	150	34.675	1.923
7	61.545	2.372	55	7.940	1.469	103	182.665	2.098	151	122.995	1.917
8	152.645	1.937	56	15.125	1.702	104	13.955	1.434	152	145.705	2.458
9	47.375	1.933	57	5.965	1.877	105	35.010	2.588	153	38.270	1.822
10	28.140	2.141	58	20.450	1.716	106	56.685	2.557	154	0.865	0.956
11	20.915	1.686	59	111.815	3.187	107	26.920	2.382	155	37.675	1.833
12	9.285	2.608	60	58.095	3.742	108	23.135	1.491	156	2.705	4.853
13	20.595	1.698	61	8.150	2.513	109	4.365	4.420	157	39.015	1.811
14	1.875	1.262	62	91.440	3.220	110	60.485	2.295	158	26.825	1.955
15	8.580	2.151	63	8.315	1.420	111	26.735	2.128	159	24.265	1.347
16	3.115	1.411	64	51.535	2.003	112	93.050	1.814	160	20.485	1.426
17	39.020	2.449	65	89.515	2.490	113	79.525	2.000	161	36.945	1.604
18	52.005	2.280	66	18.655	2.740	114	133.070	1.938	162	77.545	2.305
19	75.180	2.218	67	52.825	2.534	115	133.070	1.938	163	17.395	1.531
20	86.185	2.005	68	24.535	1.426	116	16.025	2.379	164	44.450	2.279
21	13.570	1.432	69	1.195	1.560	117	169.090	1.992	165	100.310	1.954
22	55.555	3.534	70	1.230	1.394	118	8.295	1.780	166	93.595	1.853
23	89.020	1.835	71	20.480	1.718	119	64.245	2.124	167	56.940	3.016
24	31.255	2.453	72	20.535	1.697	120	86.165	1.952	168	119.880	2.048
25	75.380	1.970	73	1.065	1.251	121	18.685	2.541	169	1.270	1.539
26	20.950	1.692	74	83.095	1.606	122	49.925	2.643	170	1.160	1.221
27	143.035	1.889	75	86.150	1.641	123	55.660	2.255	171	84.715	2.074
28	99.410	1.924	76	7.705	1.357	124	91.275	1.482	172	53.570	2.164
29	6.205	1.475	77	95.270	2.059	125	1.220	1.192	173	29.475	2.068
30	126.380	2.254	78	13.235	2.467	126	1.240	1.085	174	34.795	1.766
31	6.745	1.570	79	13.430	2.274	127	115.550	2.562	175	29.970	1.796
32	22.205	1.643	80	131.310	2.722	128	104.525	1.866	176	21.435	1.274
33	88.475	1.964	81	3.495	4.707	129	77.080	1.801	177	124.260	2.155
34	131.575	1.837	82	73.825	3.285	130	19.100	2.323	178	13.785	2.877
35	219.235	1.900	83	17.025	2.345	131	118.690	1.982	179	84.270	1.893
36	81.095	1.958	84	8.270	1.626	132	32.065	1.559	180	66.455	1.844
37	20.960	1.710	85	128.980	1.854	133	152.805	2.107	181	16.420	1.581
38	8.265	1.925	86	0.725	5.007	134	107.790	1.963	182	94.310	2.111
39	183.045	2.331	87	19.700	1.627	135	141.945	2.147	183	54.885	1.540
40	1.665	3.057	88	122.915	2.272	136	44.170	2.361	184	22.670	1.621
41	105.925	1.877	89	7.680	1.264	137	10.250	1.510	185	17.060	1.581
42	96.850	1.956	90	6.365	1.434	138	8.535	1.931	186	51.215	2.354
43	1.005	0.950	91	102.610	2.509	139	44.680	2.251	187	48.480	1.695
44	7.560	1.298	92	49.055	2.129	140	117.220	2.150	188	5.635	1.560
45	78.560	3.268	93	24.455	2.288	141	119.720	2.451	189	42.040	1.845
46	64.335	3.534	94	32.860	3.224	142	30.350	2.008	190	62.865	1.901
47	1.030	3.382	95	13.965	1.477	143	42.240	2.213	191	32.395	1.987
48	93.220	2.430	96	86.020	2.277	144	9.045	1.793	192	27.110	1.663

TABLE 12. sOC parameters for road transport missions 1.

Model	Parameter	Value (per road type)			Unit
		Urban	*Rural*	*Highway*	
Road type	L_{Ri}	1.35	1.74	34.58	km
	p_{Rij}	$[0 \quad 0 \quad 1]$	$[1 \quad 0 \quad 0]$	$[0 \quad 1 \quad 0]$	-
Speed signs	v_i	30, 50	70	80	km h^{-1}
	L_{Vi}	$[1.22 \quad 0.26]$	-	-	km
	p_{Vij}	$\begin{bmatrix} 0 & 1 \\ 1 & 0 \end{bmatrix}$	-	-	-
Stop signs	λ_s	0.74	0	0.03	km^{-1}
	t_{min}, t_{max}	19, 38.5	-	2, 10	s
Curviness	λ_C	12.6	2.9	0.03	km^{-1}
	μ_C	4.14	4.56	2.50	ln m
	σ_C	0.98	1.12	0	ln m
	r_{turn}	12.5	12.5	12.5	m
	μ_L	3.60	4.35	4.32	ln m
	σ_L	0.74	0.75	0	ln m
Topography	L_h	25	25	25	m
	σ_Y	2.04	3.49	1.78	%

TABLE 13. sOC parameters for road transport missions 2.

Model	Parameter	Value (per road type)			Unit
		Urban	*Rural*	*Highway*	
Road type	L_{Ri}	3.16	3.02	9.83	km
	p_{Rij}	$\begin{bmatrix} 0 & 0 & 1 \end{bmatrix}$	$\begin{bmatrix} \frac{3}{4} & 0 & \frac{1}{4} \end{bmatrix}$	$\begin{bmatrix} \frac{1}{4} & \frac{3}{4} & 0 \end{bmatrix}$	-
Speed signs	v_i	30, 50	70	80	km h^{-1}
	L_{Vi}	$\begin{bmatrix} 1.37 & 5.84 \end{bmatrix}$	-	-	km
	p_{Vij}	$\begin{bmatrix} 0 & 1 \\ 1 & 0 \end{bmatrix}$	-	-	-
Stop signs	λ_{s}	0.44	0.17	0	km^{-1}
	t_{min}, t_{max}	2, 25	4, 10	-	s
Curviness	λ_C	10.6	0.58	0.28	km^{-1}
	μ_C	3.81	3.88	4.31	ln m
	σ_C	0.91	1.01	1.04	ln m
	r_{turn}	12.5	12.5	12.5	m
	μ_L	3.86	4.72	4.60	ln m
	σ_L	0.73	0.84	0 .95	ln m
Topography	L_{h}	25	25	25	m
	σ_Y	3.63	1.51	0.97	%

TABLE 14. sOC parameters for road transport missions 3.

Model	Parameter	Value (per road type)			Unit
		Urban	*Rural*	*Highway*	
Road type	L_{Ri}	1.97	0.51	14.9	km
	p_{Rij}	$\begin{bmatrix} 0 & \frac{1}{2} & \frac{1}{2} \end{bmatrix}$	$\begin{bmatrix} 0 & 0 & 1 \end{bmatrix}$	$\begin{bmatrix} 1 & 0 & 0 \end{bmatrix}$	-
Speed signs	v_i	30, 50	60, 70	80	km h^{-1}
	L_{Vi}	$\begin{bmatrix} 1.18 & 0.79 \end{bmatrix}$	$\begin{bmatrix} 0.35 & 0.16 \end{bmatrix}$	-	km
	p_{Vij}	$\begin{bmatrix} 0 & 1 \\ 1 & 0 \end{bmatrix}$	$\begin{bmatrix} 0 & 1 \\ 1 & 0 \end{bmatrix}$	-	-
Stop signs	λ_{s}	0.51	2.0	0	km^{-1}
	t_{min}, t_{max}	4, 6	1, 3	-	s
Curviness	λ_C	8.7	11.9	0.13	km^{-1}
	μ_C	3.89	3.44	3.50	ln m
	σ_C	0.93	1.24	1.14	ln m
	r_{turn}	12.5	12.5	12.5	m
	μ_L	3.81	3.87	5.05	ln m
	σ_L	0.66	0.54	1.34	ln m
Topography	L_{h}	25	25	25	m
	σ_Y	2.29	0.84	1.4	%

TABLE 15. sOC parameters for road transport missions 4.

Model	Parameter	Value (per road type)			Unit
		Urban	*Rural*	*Highway*	
Road type	L_{Ri}	0.4	1.0	13.7	km
	p_{Rij}	$\begin{bmatrix} 0 & \frac{2}{3} & \frac{1}{3} \end{bmatrix}$	$\begin{bmatrix} \frac{2}{3} & 0 & \frac{1}{3} \end{bmatrix}$	$\begin{bmatrix} \frac{1}{2} & \frac{1}{2} & 0 \end{bmatrix}$	-
Speed signs	v_i	30, 50	70, 80	90	km h^{-1}
	L_{Vi}	$\begin{bmatrix} 1.0 & 0.7 \end{bmatrix}$	$\begin{bmatrix} 2.4 & 0.5 \end{bmatrix}$	-	km
	p_{Vij}	$\begin{bmatrix} 0 & 1 \\ 1 & 0 \end{bmatrix}$	$\begin{bmatrix} 0 & 1 \\ 1 & 0 \end{bmatrix}$	-	-
Stop signs	λ_{s}	2.30	0.35	0.04	km^{-1}
	t_{min}, t_{max}	8, 100	77, 95	29, 37	s
Curviness	λ_C	8.8	15.3	3.4	km^{-1}
	μ_C	5.3	5.7	6.2	ln m
	σ_C	1.2	0.9	0.3	ln m
	r_{turn}	12.5	12.5	12.5	m
	μ_L	4.2	4.1	3.7	ln m
	σ_L	0.6	0.5	0.3	ln m
Topography	L_{h}	170	450	1010	m
	σ_Y	1.47	1.99	1.88	%

TABLE 16. sOC parameters for road transport missions 5.

Model	Parameter	Value (per road type)			Unit
		Urban	*Rural*	*Highway*	
Road type	L_{Ri}	2	6	7	km
	p_{Rij}	$\begin{bmatrix} 0 & \frac{3}{4} & \frac{1}{4} \end{bmatrix}$	$\begin{bmatrix} \frac{2}{5} & 0 & \frac{3}{5} \end{bmatrix}$	$\begin{bmatrix} \frac{1}{2} & \frac{1}{2} & 0 \end{bmatrix}$	-
Speed signs	v_i	30, 50	60, 70, 80	90, 100, 110	km h^{-1}
	L_{Vi}	$\begin{bmatrix} 0.3 & 1.5 \end{bmatrix}$	$\begin{bmatrix} 1 & 5 & 2 \end{bmatrix}$	$\begin{bmatrix} 3 & 3 & 4 \end{bmatrix}$	km
	p_{Vij}	$\begin{bmatrix} 0 & 1 \\ 1 & 0 \end{bmatrix}$	$\begin{bmatrix} 0 & \frac{3}{4} & \frac{1}{4} \\ \frac{8}{11} & 0 & \frac{3}{11} \\ \frac{2}{5} & \frac{3}{5} & 0 \end{bmatrix}$	$\begin{bmatrix} 0 & \frac{1}{2} & \frac{1}{2} \\ \frac{1}{5} & 0 & \frac{4}{5} \\ \frac{1}{3} & \frac{2}{3} & 0 \end{bmatrix}$	-
Stop signs	λ_{s}	2.0	0.4	0	km^{-1}
	t_{min}, t_{max}	5, 20	5, 10	-	s
Curviness	λ_C	3.0	1.0	0.4	km^{-1}
	μ_C	3.0	4.5	6.0	ln m
	σ_C	1.2	1.0	1.0	ln m
	r_{turn}	12.5	12.5	12.5	m
	μ_L	3.2	4.6	5.5	ln m
	σ_L	1.1	1.6	2.0	ln m
Topography	L_{h}	250	200	1100	m
	σ_Y	1.0	2.5	2.0	%

TABLE 17. sOC parameters for road transport missions 6.

Model	Parameter	Value (per road type)			Unit
		Urban	*Rural*	*Highway*	
Road type	L_{Ri}	1.10	0.94	12.0	km
	p_{Rij}	$\begin{bmatrix} 0 & \frac{2}{3} & \frac{1}{3} \end{bmatrix}$	$\begin{bmatrix} 1 & 0 & 0 \end{bmatrix}$	$\begin{bmatrix} 1 & 0 & 0 \end{bmatrix}$	-
Speed signs	v_i	50	60	70	km h^{-1}
	L_{Vi}	-	-	-	km
	p_{Vij}	-	-	-	-
Stop signs	λ_{s}	0	0.53	0	km^{-1}
	t_{min}, t_{max}	-	25, 31	-	s
Curviness	λ_C	3.3	0	0.25	km^{-1}
	μ_C	2.94	-	3.80	ln m
	σ_C	1.60	-	0.74	ln m
	r_{turn}	12.5	12.5	12.5	m
	μ_L	3.82	-	4.76	ln m
	σ_L	0.75	-	0.22	ln m
Topography	L_{h}	167	226	281	m
	σ_Y	3.56	3.14	2.22	%

and therefore eight possible classes.[11] Accordingly, each operating class only needs one relationship to be completely determined.

On the other hand, the UFD description uses a more sophisticated strategy. Five levels are specified as follows:

1) `V-COLD` if sometimes colder than −30°C, rarely warmer than 20°C and never warmer than 30°C.
2) `COLD` if sometimes colder than −15°C, rarely warmer than 25°C, and never warmer than 25°C.
3) `MIXED` if rarely colder than −15°C and rarely warmer than 30°C.
4) `WARM` if sometimes colder than 5°C, never colder than 0°C and rarely warmer than 40°C.
5) `V-WARM` if rarely colder than 15°C, never colder than 0°C and sometimes warmer than 45°C.

However, in the list above, the classes are formulated rather vaguely, since 'sometimes' and 'rarely' are not specified in terms of frequencies or probabilities. As a first interpretation, they may be assumed to indicate frequencies of around fifty and twenty percent, respectively (in bold in Table 10). Moreover, in the UFD system, each class is determined using multiple conditions on the limits T^*_{min}, T^*_{max} and the probability $p_{T^*_{\mathrm{air}}}$. These conditions may be numbered consecutively using superscript $^{(i)}$, with $i = 1, 2, 3$ for the `V-COLD`, `COLD`, `WARM` and `V-WARM` classes, and $i = 1, 2$ for the `MIXED` class. Table 10 summarizes the operating classes for the air temperature parameter according to the UFD interpretation.

However, in respect of the operating classes defined using the values in Tables 9 and 10, however, it should be observed that the relationship (47) does not guarantee absolute lower

[11] In each case, the corresponding probability $p_{T^*_{\mathrm{air}},\mathrm{max}}$ could be assumed to be close to the unity (for example $p_{T^*_{\mathrm{air}},\mathrm{max}} = 0.99$) when it is not possible to define a class using unit probabilities.

and upper limits on the air temperature (apart from the zero point for thermodynamics). An alternative, and much simpler approach, would consists in neglecting the stochastic component of the temperature, and only considering the annual variation. In this case the probability $\mathbb{P}(T_{\text{air}} \leq T^*)$ becomes

$$\mathbb{P}(T_{\text{air}} \leq T^*_{\text{air}}) = F_{T_{\text{air}}}\left(T^*_{\text{air}}; \mu_T, T_{\text{y}}\right) \approx \frac{1}{2} + \frac{1}{\pi} \arctan\left(\frac{T^*_{\text{air}} - \mu_T}{\sqrt{T_{\text{y}}^2 - (\mu_T - T^*_{\text{air}})^2}}\right), \quad (69)$$

while the constraint on the lower and upper absolute limits may be expressed mathematically as

$$\mu_T - T_{\text{y}} \geq T^*_{\text{min}}, \quad (70a)$$
$$\mu_T + T_{\text{y}} \leq T^*_{\text{max}}. \quad (70b)$$

Equations (69) and (70) may be used in combination to provide a feasible set of parameters satisfying the conditions for the operating classes. In particular, it is worth mentioning that the different levels specified by the GTA system only need (70).

C. ADDITIONAL DATA AND TABLES

1) DATA FOR INDIVIDUAL MISSIONS

The values for the traveled distance and the standard deviation σ_Y of the topography for the missions in the example of Section IV are listed in Table 11.

2) sOC PARAMETERS

The estimated parameters for the sOCs in the example of Section IV-C are listed below. See Tables 12–17.

ACKNOWLEDGMENT

The authors kindly acknowledge the support from the COVER Project Member Anders Jensen at Scania, who supplied information on the User Factor Description (UFD). Authors Contribution: Luigi Romano—conceptualization, formalization, theory, methodology, formal analysis, implementation, data analysis, and writing—original draft; Pär Johannesson—methodology and supervision; Erik Nordström—implementation and data analysis; Fredrik Bruzelius—conceptualization and supervision; Rickard Anderson—funding acquisition; and Bengt Jacobson—supervision and funding acquisition. All the authors read and approved the original version of the manuscript.

REFERENCES

[1] P. Pettersson, "Operating cycle representation for road vehicles," Ph.D. dissertation, Dept. Mech. Maritime Sci., Chalmers Univ. Technol., Gothenburg, Sweden, 2019.
[2] S. Edlund and P.-O. Fryk, "The right truck for the job with global truck application descriptions," in *Proc. SAE Tech. Paper Ser.*, Oct. 2004, pp. 344–351, doi: 10.4271/2004-01-2645.
[3] G. Fontaras, M. Rexeis, P. Dilara, S. Hausberger, and K. Anagnostopoulos, "Development of a simulation tool for monitoring heavy-duty vehicle CO_2 emissions and fuel consumption in Europe," in *Proc. 11th Int. Conf. Engines Vehicles*, 2013, pp. 1–11.
[4] H. Achour and A. G. Olabi, "Driving cycle developments and their impacts on energy consumption of transportation," *J. Cleaner Prod.*, vol. 112, pp. 1778–1788, Jan. 2016, doi: 10.1016/j.jclepro.2015.08.007.
[5] J. Liu, X. Wang, and A. Khattak, "Customizing driving cycles to support vehicle purchase and use decisions: Fuel economy estimation for alternative fuel vehicle users," *Transp. Res. C, Emerg. Technol.*, vol. 67, pp. 280–298, Jun. 2016, doi: 10.1016/j.trc.2016.02.016.
[6] D. W. Wyatt, H. Li, and J. E. Tate, "The impact of road grade on carbon dioxide (CO_2) emission of a passenger vehicle in real-world driving," *Transp. Res. D, Transp. Environ.*, vol. 32, pp. 160–170, Oct. 2014, doi: 10.1016/j.trd.2014.07.015.
[7] K. M. Sentoff, L. Aultman-Hall, and B. A. Holmén, "Implications of driving style and road grade for accurate vehicle activity data and emissions estimates," *Transp. Res. D, Transp. Environ.*, vol. 35, pp. 175–188, Mar. 2015, doi: 10.1016/j.trd.2014.11.021.
[8] D. Llopis-Castelló, A. M. Pérez-Zuriaga, F. J. Camacho-Torregrosa, and A. García, "Impact of horizontal geometric design of two-lane rural roads on vehicle co 2 emissions," *Transp. Res. D, Transp. Environ.*, vol. 59, pp. 46–57, Mar. 2018, doi: 10.1016/j.trd.2017.12.020.
[9] A. Sciarretta, *Energy-Efficient Driving of Road Vehicles*, 1st ed. Cham, Switzerland: Springer, 2020, doi: 10.1007/978-3-030-24127-8.
[10] P. Johannesson, K. Podgórski, I. Rychlik, and N. Shariati, "AR(1) time series with autoregressive gamma variance for road topography modeling," *Probabilistic Eng. Mech.*, vol. 43, pp. 106–116, Jan. 2016, doi: 10.1016/j.probengmech.2015.12.006.
[11] P. Johannesson, K. Podgórski, and I. Rychlik, "Laplace distribution models for road topography and roughness," *Int. J. Vehicle Perform.*, vol. 3, no. 3, p. 224, 2017. [Online]. Available: http://www.inderscience.com/offer.php?id=85032
[12] A. Donkers, D. Yang, and M. Viktorović, "Influence of driving style, infrastructure, weather and traffic on electric vehicle performance," *Transp. Res. D, Transp. Environ.*, vol. 88, Nov. 2020, Art. no. 102569, doi: 10.1016/J.TRD.2020.102569.
[13] D. Akin, V. P. Sisiopiku, and A. Skabardonis, "Impacts of weather on traffic flow characteristics of urban freeways in Istanbul," *Proc. Social Behav. Sci.*, vol. 16, pp. 88–89, Jan. 2011, doi: 10.1016/J.SBSPRO.2011.04.432.
[14] E. Hooper, L. Chapman, and A. Quinn, "The impact of precipitation on speed–flow relationships along a U.K. motorway corridor," *Theor. Appl. Climatol.*, vol. 117, nos. 1–2, pp. 303–316, Jul. 2014, doi: 10.1007/s00704-013-0999-5.
[15] O. Travesset-Baro, M. Rosas-Casals, and E. Jover, "Transport energy consumption in mountainous roads. A comparative case study for internal combustion engines and electric vehicles in andorra," *Transp. Res. D, Transp. Environ.*, vol. 34, pp. 16–26, Jan. 2015, doi: 10.1016/J.TRD.2014.09.006.
[16] B. Y. Boroujeni and H. C. Frey, "Road grade quantification based on global positioning system data obtained from real-world vehicle fuel use and emissions measurements," *Atmos. Environ.*, vol. 85, pp. 179–186, Mar. 2014, doi: 10.1016/j.atmosenv.2013.12.025.
[17] P. Shen, Z. Zhao, J. Li, and X. Zhan, "Development of a typical driving cycle for an intra-city hybrid electric bus with a fixed route," *Transp. Res. D, Transp. Environ.*, vol. 59, pp. 346–360, Mar. 2018, doi: 10.1016/j.trd.2018.01.032.
[18] J. Brady and M. O'Mahony, "Development of a driving cycle to evaluate the energy economy of electric vehicles in urban areas," *Appl. Energy*, vol. 177, pp. 165–178, Sep. 2016, doi: 10.1016/j.apenergy.2016.05.094.
[19] L. Guzzella and A. Sciarretta, *Vehicle Propulsion Systems: Introduction to Modeling and Optimization*, 3st ed. Cham, Switzerland: Springer, 2013.
[20] T. Hofman, S. Ebbesen, and L. Guzzella, "Topology optimization for hybrid electric vehicles with automated transmissions," *IEEE Trans. Veh. Technol.*, vol. 61, no. 6, pp. 2442–2451, Jul. 2012, doi: 10.1109/TVT.2012.2196299.
[21] T. Ghandriz, J. Hellgren, M. Islam, L. Laine, and B. Jacobson, "Optimization based design of heterogeneous truck fleet and electric propulsion," in *Proc. IEEE 19th Int. Conf. Intell. Transp. Syst. (ITSC)*, Nov. 2016, pp. 328–335.
[22] T. Ghandriz, "Transportation mission based optimization of heavy vehicle fleets including propulsion tailoring," Licentiate thesis, Dept. Mech. Maritime Sci., Chalmers Univ. Technol., Gothenburg, Sweden, 2018.
[23] T. Ghandriz, B. Jacobson, L. Laine, and J. Hellgren, "Impact of automated driving systems on road freight transport and electrified propulsion of heavy vehicles," *Transp. Res. C, Emerg. Technol.*, vol. 115, Jun. 2020, Art. no. 102610, doi: 10.1016/j.trc.2020.102610.

[24] T. Ghandriz, B. Jacobson, L. Laine, and J. Hellgren, "Optimization data on total cost of ownership for conventional and battery electric heavy vehicles driven by humans and by automated driving systems," *Data Brief*, vol. 30, Jun. 2020, Art. no. 105566, doi: 10.1016/j.dib.2020.105566.

[25] T. Ghandriz, B. Jacobson, M. Islam, J. Hellgren, and L. Laine, "Transportation-mission-based optimization of heterogeneous heavy-vehicle fleet including electrified propulsion," *Energies*, vol. 14, no. 11, p. 3221, May 2021, doi: 10.3390/en14113221.

[26] T. Ghandriz, "Transportation mission-based optimization of heavy combination road vehicles and distributed propulsion, including predictive energy and motion contro," Ph.D. dissertation, Dept. Mech. Maritime Sci., Chalmers Univ. Technol., Gothenburg, Sweden, 2020.

[27] M. Åsbogård, L. Johannesson, D. Angervall, and P. Johansson, "Improving system design of a hybrid powertrain using stochastic drive cycles and dynamic programming," in *Proc. SAE Tech. Paper Ser.*, Apr. 2007, p. 10, doi: 10.4271/2007-01-0304.

[28] P. Nyberg, "Evaluation, generation and transformation of driving cycles," Ph.D. dissertation, Dept. Elect. Eng., Linköping Univ. Electronic Press, Linköping, Sweden, 2015.

[29] A. Ashtari, E. Bibeau, and S. Shahidinejad, "Using large driving record samples and a stochastic approach for real-world driving cycle construction: Winnipeg driving cycle," *Transp. Sci.*, vol. 48, no. 2, pp. 170–183, May 2014, doi: 10.1287/trsc.1120.0447.

[30] E. Tazelaar, J. Bruinsma, B. Veenhuizen, and P. Bosch, "Driving cycle characterization and generation, for design and control of fuel cell buses," *World Electr. Veh. J.*, vol. 3, no. 1, pp. 812–819, 2009, doi: 10.3390/wevj3040812.

[31] J. Lin and D. A. Niemeier, "An exploratory analysis comparing a stochastic driving cycle to California's regulatory cycle," *Atmos. Environ.*, vol. 36, no. 38, pp. 5759–5770, 2002, doi: 10.1016/S1352-2310(02)00695-7.

[32] T.-K. Lee and Z. S. Filipi, "Synthesis of real-world driving cycles using stochastic process and statistical methodology," *Int. J. Vehicle Des.*, vol. 57, no. 1, pp. 17–36, 2011. [Online]. Available: http://www.inderscience.com/offer.php?id=43590

[33] T.-K. Lee, B. Adornato, and Z. S. Filipi, "Synthesis of real-world driving cycles and their use for estimating PHEV energy consumption and charging opportunities: Case study for midwest/U.S.," *IEEE Trans. Veh. Technol.*, vol. 60, no. 9, pp. 4153–4163, Nov. 2011, doi: 10.1109/TVT.2011.2168251.

[34] G. Amirjamshidi and M. J. Roorda, "Development of simulated driving cycles for light, medium, and heavy duty trucks: Case of the Toronto waterfront area," *Transp. Res. D, Transp. Environ.*, vol. 34, no. 1, pp. 255–266, 2015, doi: 10.1016/j.trd.2014.11.010.

[35] S. H. Kamble, T. V. Mathew, and G. K. Sharma, "Development of real-world driving cycle: Case study of Pune, India," *Transp. Res. D, Transp. Environ.*, vol. 14, no. 2, pp. 132–140, 2009, doi: 10.1016/j.trd.2008.11.008.

[36] E. Silvas, "Integrated optimal design for hybrid electric vehicles," Ph.D. dissertation, Dept. Mech. Eng., Technische Universiteit Eindhoven, Eindhoven, The Netherlands, 2015.

[37] E. Silvas, K. Hereijgers, H. Peng, T. Hofman, and M. Steinbuch, "Synthesis of realistic driving cycles with high accuracy and computational speed, including slope information," *IEEE Trans. Veh. Technol.*, vol. 65, no. 6, pp. 4118–4128, Mar. 2016, doi: 10.1109/TVT.2016.2546338.

[38] X. Liu, J. Ma, X. Zhao, J. Du, and Y. Xiong, "Study on driving cycle synthesis method for city buses considering random passenger load," *J. Adv. Transp.*, vol. 2020, pp. 1–21, Feb. 2020, doi: 10.1155/2020/3871703.

[39] S. Shi, S. Wei, H. Kui, L. Liu, C. Huang, and M. Liu, "Improvements of the design method of transient driving cycle for passenger car," in *Proc. IEEE Vehicle Power Propuls. Conf.*, Sep. 2009, pp. 1581–1586, doi: 10.1109/VPPC.2009.5289594.

[40] L. Liu, C. Huang, M. Liu, and S. Shi, "Study on the combined design method of transient driving cycles for passenger car in Changchun," in *Proc. IEEE Vehicle Power Propuls. Conf.*, Sep. 2008. [Online]. Available: https://ieeexplore.ieee.org/stamp/stamp.jsp?arnumber=4677594

[41] W. T. Hung, H. Y. Tong, C. P. Lee, K. Ha, and L. Y. Pao, "Development of a practical driving cycle construction methodology: A case study in Hong Kong," *Transp. Res. D, Transp. Environ.*, vol. 12, no. 2, pp. 115–128, 2007, doi: 10.1016/j.trd.2007.01.002.

[42] K. S. Nesamani and K. P. Subramanian, "Development of a driving cycle for intra-city buses in Chennai, India," *Atmos. Environ.*, vol. 45, no. 31, pp. 5469–5476, 2011, doi: 10.1016/j.atmosenv.2011.06.067.

[43] S.-H. Ho, Y.-D. Wong, and V. W.-C. Chang, "Developing Singapore driving cycle for passenger cars to estimate fuel consumption and vehicular emissions," *Atmos. Environ.*, vol. 97, pp. 353–362, Nov. 2014, doi: 10.1016/j.atmosenv.2014.08.042.

[44] K. Kivekäs, J. Vepsäläinen, and K. Tammi, "Stochastic driving cycle synthesis for analyzing the energy consumption of a battery electric bus," *IEEE Access*, vol. 6, pp. 55586–55598, 2018, doi: 10.1109/ACCESS.2018.2871574.

[45] K. Kivekas, J. Vepsalainen, K. Tammi, and J. Anttila, "Influence of driving cycle uncertainty on electric city bus energy consumption," in *Proc. IEEE Vehicle Power Propuls. Conf. (VPPC)*, Dec. 2017, pp. 1–5, doi: 10.1109/VPPC.2017.8331014.

[46] F. Guo and F. Zhang, "A study of driving cycle for electric cars on Beijing urban and suburban roads," in *Proc. IEEE Int. Conf. Power Renew. Energy (ICPRE)*, Oct. 2016, pp. 319–322, doi: 10.1109/ICPRE.2016.7871224.

[47] S. Ou, Y. Zhou, J. Lian, P. Jia, and B. Tian, "Development of hybrid city bus's driving cycle," in *Proc. Int. Conf. Electr. Inf. Control Eng.*, Apr. 2011, pp. 2112–2116, doi: 10.1109/ICEICE.2011.5777149.

[48] L. Berzi, M. Delogu, and M. Pierini, "Development of driving cycles for electric vehicles in the context of the city of Florence," *Transp. Res. D, Transp. Environ.*, vol. 47, pp. 299–322, Aug. 2016, doi: 10.1016/j.trd.2016.05.010.

[49] S. Shi, N. Lin, Y. Zhang, C. Huang, L. Liu, B. Lu, and J. Cheng, "Research on Markov property analysis of driving cycle," in *Proc. IEEE Vehicle Power Propuls. Conf. (VPPC)*, Oct. 2013, pp. 1–5, doi: 10.1109/VPPC.2013.6671737.

[50] X. Hu, N. Murgovski, L. M. Johannesson, and B. Egardt, "Optimal dimensioning and power management of a fuel cell/battery hybrid bus via convex programming," *IEEE/ASME Trans. Mechatronics*, vol. 20, no. 1, pp. 457–468, Feb. 2015, doi: 10.1109/TMECH.2014.2336264.

[51] E. Silvas, T. Hofman, N. Murgovski, L. F. P. Etman, and M. Steinbuch, "Review of optimization strategies for system-level design in hybrid electric vehicles," *IEEE Trans. Veh. Technol.*, vol. 66, no. 1, pp. 57–70, Jan. 2017, doi: 10.1109/TVT.2016.2547897.

[52] X. Hu, S. J. Moura, N. Murgovski, B. Egardt, and D. Cao, "Integrated optimization of battery sizing, charging, and power management in plug-in hybrid electric vehicles," *IEEE Trans. Control Syst. Technol.*, vol. 24, no. 3, pp. 1036–1043, May 2016, doi: 10.1109/TCST.2015.2476799.

[53] M. Pourabdollah, N. Murgovski, A. Grauers, and B. Egardt, "Optimal sizing of a parallel PHEV powertrain," *IEEE Trans. Veh. Technol.*, vol. 62, no. 6, pp. 2469–2480, Jul. 2013, doi: 10.1109/TVT.2013.2240326.

[54] Z. Zou, S. Davis, K. Beaty, M. O'Keefe, T. Hendricks, R. Rehn, S. Weissner, and V. K. Sharma, "A new composite drive cycle for heavy-duty hybrid electric class 4–6 vehicles," in *Proc. SAE Tech. Paper Ser.*, Mar. 2004, pp. 1–10, doi: 10.4271/2004-01-1052.

[55] M. Montazeri-Gh and M. Naghizadeh "Development of car drive cycle for simulation of emissions and fuel economy," in *Proc. 15th Eur. Simulation Symp. Alexander Verbraesk*, V. Hlupic, Ed. SCS European Council/SCS Europe BVBA, 2003.

[56] Z. Jing, G. Wang, S. Zhang, and C. Qiu, "Building Tianjin driving cycle based on linear discriminant analysis," *Transp. Res. D, Transp. Environ.*, vol. 53, pp. 78–87, Jun. 2017, doi: 10.1016/j.trd.2017.04.005.

[57] J. Vepsäläinen, K. Kivekäs, K. Otto, A. Lajunen, and K. Tammi, "Development and validation of energy demand uncertainty model for electric city buses," *Transp. Res. D, Transp. Environ.*, vol. 63, pp. 347–361, Aug. 2018, doi: 10.1016/j.trd.2018.06.004.

[58] P. Pettersson, P. Johannesson, B. Jacobson, F. Bruzelius, L. Fast, and S. Berglund, "A statistical operating cycle description for prediction of road vehicles' energy consumption," *Transp. Res. D, Transp. Environ.*, vol. 73, pp. 205–229, Aug. 2019, doi: 10.1016/j.trd.2019.07.006.

[59] L. Romano, P. Johannesson, F. Bruzelius, and B. Jacobson, "An enhanced stochastic operating cycle description including weather and traffic models," *Transp. Res. D, Transp. Environ.*, vol. 97, Aug. 2021, Art. no. 102878, doi: 10.1016/j.trd.2021.102878.

[60] P. Pettersson, S. Berglund, B. Jacobson, L. Fast, P. Johannesson, and F. Santandrea, "A proposal for an operating cycle description format for road transport missions," *Eur. Transp. Res. Rev.*, vol. 10, no. 2, pp. 1–19, Jun. 2018, doi: 10.1186/s12544-018-0298-4.

[61] L. Romano, "Mathematical modelling of operating cycles for road vehicles," Licentiate thesis, Dept. Mech. Maritime Sci., Chalmers Univ. Technol., Gothenburg, Sweden, 2021.

[62] M. Karlsson, "Load modelling for fatigue assessment of vehicles—A statistical approach," Ph.D. dissertation, Dept. Math. Sci., Chalmers Univ. Technol., Göteborg, Sweden, 2007.

[63] M. Karlsson, "Evaluation of approximative methods for rainflow damage of broad-banded non-Gaussian random loads," in *Proc. Design Eng., A B*, Jan. 2005, pp. 79–87, doi: 10.1115/IMECE2005-79868.
[64] M. Karlsson, "Evaluation of road load classification for fatigue assessments," *Int. J. Vehicle Des.*, vol. 47, nos. 1–4, pp. 250–268, 2013, doi: 10.1504/IJVD.2008.020890.
[65] K. Bogsjö, "Coherence of road roughness in left and right wheel-path," *Vehicle Syst. Dyn.*, vol. 46, no. sup1, pp. 599–609, Sep. 2008, doi: 10.1080/00423110802018289.
[66] P. Johannesson, K. Podgórski, and I. Rychlik, "Modelling roughness of road profiles on parallel tracks using roughness indicators," *Int. J. Vehicle Des.*, vol. 70, no. 2, p. 183, 2016.
[67] K. Bogsjö, K. Podgórski, and I. Rychlik, "Models for road surface roughness," *Vehicle Syst. Dyn.*, vol. 50, no. 5, pp. 725–747, 2012, doi: 10.1080/00423114.2011.637566.
[68] G. Box, G. Jenkins, G. Reinsel, G. Ljung, and G. Ljung, *Time Series Analysis: Forecasting and Control*, 5th ed. San Francisco, CA, USA: Wiley, 2015.
[69] C. J. J. Beckers, I. J. M. Besselink, and H. Nijmeijer, "Modeling of energy losses during cornering for electric city buses," in *Proc. IEEE Intell. Transp. Syst. Conf. (ITSC)*, Oct. 2019, pp. 4164–4169, doi: 10.1109/ITSC.2019.8917232.
[70] C. Beckers, I. Besselink, and H. Nijmeijer, "On-line test of a real-time velocity prediction for E-bus energy consumption estimation," in *Proc. IEEE Vehicle Power Propuls. Conf. (VPPC)*, Oct. 2021, pp. 1–5, doi: 10.1109/VPPC53923.2021.9699205.
[71] C. J. J. Beckers, I. J. M. Besselink, and H. Nijmeijer, "Assessing the impact of cornering losses on the energy consumption of electric city buses," *Transp. Res. D, Transp. Environ.*, vol. 86, Sep. 2020, Art. no. 102360, doi: 10.1016/j.trd.2020.102360.
[72] C. J. Dodds and J. D. Robson, "The description of road surface roughness," *J. Sound Vibrat.*, vol. 31, no. 2, p. 2, 1973, doi: 10.1016/S0022-460X(73)80373-6.
[73] *Mechanical Vibration—Road Surface Profiles—Reporting of Measured Data*, document ISO 8608, 1995.
[74] F. Pellicano, Z. Li, W. Yu, and X. Cui, "Online classification of road roughness conditions with vehicle unsprung mass acceleration by sliding time window," *Shock Vib.*, vol. 10, no. 3, pp. 1–14, 2018, doi: 10.1109/TVT.2012.2196299.
[75] S. Kotz, T. Kozubowski, and K. Podgorski, *The Laplace Distribution and Generalizations*, 2nd ed. Basel, Switzerland: Birkhäuser, 2001, doi: 10.1007/978-1-4612-0173-1.
[76] M. Guiggiani, *The Science of Vehicle Dynamics*, 2nd ed. Cham, Switzerland: Springer, 2018.
[77] H. B. Pacejka, *Tire and Vehicle Dynamics*, 3rd ed. Amsterdam, The Netherlands: Elsevier, 2012.
[78] L. Romano, F. Timpone, F. Bruzelius, and B. Jacobson, "Analytical results in transient brush tyre models: Theory for large camber angles and classic solutions with limited friction," *Meccanica*, vol. 57, no. 1, pp. 165–191, Jan. 2022, doi: 10.1007/s11012-021-01422-3.
[79] L. Romano, *Advanced Brush Tyre Modelling*. Cham, Switzerland: Springer, 2022, doi: 10.1007/978-3-030-98435-9.
[80] G. Grimmett and D. Stirzaker, *Probability and Random Processes*, 4th ed. London, U.K.: Oxford Univ. Press, 2020.
[81] H. P. Hsu, *Schaum's Outline of Probability, Random Variables, and Random Processes*, 4th ed. New York, NY, USA: McGraw-Hill, 2020.
[82] R. Griego and R. Hersh, "Theory of random evolutions with applications to partial differential equations," *Trans. Amer. Math. Soc.*, vol. 156, pp. 405–418, Jan. 1971, doi: 10.2307/1995620.
[83] K. L. Chungr, *Markov Chains With Stationary Transition Probabilities*, 2nd ed. Berlin, Germany: Springer, 1967, doi: 10.1007/978-3-642-62015-7.
[84] A. R. Babu, J. Andric, B. Minovski, and S. Sebben, "System-level modeling and thermal simulations of large battery packs for electric trucks," *Energies*, vol. 14, no. 16, p. 4796, Aug. 2021, doi: 10.3390/en14164796.
[85] G. J. Marshall, C. P. Mahony, M. J. Rhodes, S. R. Daniewicz, N. Tsolas, and S. M. Thompson, "Thermal management of vehicle cabins, external surfaces, and onboard electronics: An overview," *Engineering*, vol. 5, no. 5, pp. 954–969, Oct. 2019, doi: 10.1016/j.eng.2019.02.009.
[86] M. M. Ahmed and A. Ghasemzadeh, "The impacts of heavy rain on speed and headway behaviors: An investigation using the SHRP2 naturalistic driving study data," *Transp. Res. C, Emerg. Technol.*, vol. 91, pp. 371–384, Jun. 2018, doi: 10.1016/j.trc.2018.04.012.
[87] J. Yeo, J. Lee, and K. Jang, "The effects of rainfall on driving behaviors based on driving volatility," *Int. J. Sustain. Transp.*, vol. 15, pp. 435–443, Mar. 2021, doi: 10.1080/15568318.2020.1756543.
[88] B. N. J. Persson, U. Tartaglino, O. Albohr, and E. Tosatti, "Rubber friction on wet and dry road surfaces: The sealing effect," *Phys. Rev. B, Condens. Matter*, vol. 71, no. 3, Jan. 2005, Art. no. 035428, doi: 10.1103/PhysRevB.71.035428.
[89] K. R. Gabriel and J. Neumann, "A Markov chain model for daily rainfall occurrence at tel aviv," *Quart. J. Roy. Meteorolog. Soc.*, vol. 88, no. 375, pp. 90–95, Jan. 1962, doi: 10.1002/qj.49708837511.
[90] E. H. Chin, "Modeling daily precipitation occurrence process with Markov chain," *Water Resour. Res.*, vol. 13, no. 6, pp. 949–956, Dec. 1977, doi: 10.1029/WR013i006p00949.
[91] G. J. Husak, J. Michaelsen, and C. Funk, "Use of the gamma distribution to represent monthly rainfall in Africa for drought monitoring applications," *Int. J. Climatol.*, vol. 27, no. 7, pp. 935–944, Jun. 2007, doi: 10.1002/joc.1441.
[92] V. Kumar and S. Jahangeer, "Statistical distribution of rainfall in Uttarakhand, India," *Appl. Water Sci.*, vol. 7, no. 8, pp. 4765–4776, Dec. 2017, doi: 10.1007/s13201-017-0586-5.
[93] *MANOBS (Manual of Surface Weather Observations)*, Metereological Service of Canada, Toronto, ON, Canada, 2013.
[94] P. A. Brodtkorb, P. Johannesson, G. Lindgren, I. Rychlik, J. Rydén, and E. Sjö, "WAFO—-A MATLAB Toolbox for the analysis of random waves and loads," *Proc. 10th Int. Offshore Polar Eng. Conf., (ISOPE)*, vol. 3, 2000, pp. 343–350.
[95] *WAFO—A MATLAB Toolbox for Analysis of Random Waves and Loads—A Tutorial*, WAFO-Group, Mathematics & Statistics, Centre for Mathematical Sciences, Lund Univ., Lund, Sweden, 2000. [Online]. Available: http://www.maths.lth.se/matstat/wafo
[96] E. Nordström, "Advanced modelling and energy efficiency prediction for road vehicles," M.S. thesis, Dept. Phys., Umeå Univ., Umeå, Sweden, 2020.
[97] *Volvotrucks.se*. Accessed: Jul. 7, 2022. [Online]. Available: https://www.volvotrucks.se/sv-se/trucks/trucks/volvo-fh16/specifications/data-sheets.html
[98] *VehProp*. Accessed: Jul. 7, 2022. [Online]. Available: https://www.chalmers.se/en/departments/m2/research/veas/Pages/VehProp.aspx
[99] L. Ntziachristos and Z. Samaras, *EMEP/EEA Air Pollutant Emission Inventory Guidebook 2016 Part B.1.A.3.B.I-Iv Road Transport 2018*. Copenhagen, Denmark: European Environment Agency, Chalmers Univ. Technology, 2018.

LUIGI ROMANO received the M.Sc. degree in mechanical engineering from the University of Naples Federico II, Italy, in 2018. He is currently pursuing the Ph.D. degree with the Vehicle Dynamics Group, Chalmers University of Technology, Gothenburg, Sweden, within the COVER Project. After graduation, he worked as an Independent Consultant on the Feel-Tire Unina Project, developing model-based estimators for intelligent tire technologies. His research interests include sustainable transportation systems, vehicle state estimation and control, and tire dynamics and modeling. In 2016, he was awarded the prize "Buon Compleanno Federico II" as the Best Mechanical Engineering Student.

PÄR JOHANNESSON received the Ph.D. degree in mathematical statistics from the Lund Institute of Technology, with a thesis on statistical load analysis for fatigue, and the joint postdoctoral degree in mathematical statistics from the Chalmers University of Technology and PSA Peugeot Citroën, France. He currently works as a Senior Researcher in mechanical reliability, fatigue, and load analysis at RISE Research Institute of Sweden, Gothenburg. He is a Docent in mathematical statistics with the Chalmers University of Technology. He has more than 20 years of experience in research and development in fatigue and loads analysis with a focus on engineering statistics and reliability in industrial applications. He has published more than 20 articles in international journals and is a Co-Editor of the handbook *Guide to Load Analysis for Durability in Vehicle Engineering*.

ERIK NORDSTRÖM received the degree in engineering physics from Umeå University, Sweden, in 2020. He carried out his master's thesis work at the Chalmers University of Technology, Gothenburg, Sweden, where he was also involved in the COVER Project. He is currently a Post Graduate Student at Umeaå University and a QA Test Engineering at Nasdaq, Stockholm.

FREDRIK BRUZELIUS received the M.Sc. degree in applied mathematics from Linköping University, in 1999, and the Ph.D. degree in control theory from the Chalmers University of Technology, in 2004. He worked for five years at Volvo developing vehicle dynamics estimation and control strategies in cars and trucks. Currently, he is a Senior Researcher in vehicle dynamics with the Department of Mechanics and Maritime Sciences, Chalmers University of Technology. His research interests include vehicle state estimation and control, tire modeling and simulation, driving simulators, and vehicle testing.

RICKARD ANDERSSON graduated in physics at the University of Gothenburg, Sweden, in 1996. Since then, he has worked in many positions, within automotive and aerospace companies. In 2005, he joined Volvo Trucks, where he currently holds the position as a Lead Research Engineer within the simulation and analysis area, and where he is leading strategic development activities within the field of energy predictive management for vehicles. He has held a large number of positions in Swedish research foundations and EU projects. He is currently the Project Leader of the COVER Project, founded by the Swedish Energy Authority (FFI frame), managing customer operation research with the objective to lower CO_2 emissions.

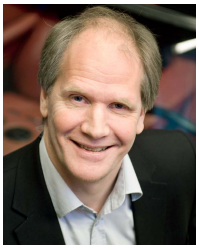

BENGT JACOBSON received the Ph.D. degree in machine elements from the Chalmers University of Technology, Gothenburg, Sweden, in 1993. He was a Technical Expert with Volvo Car Corporation, Gothenburg, from 2001 to 2010, with a focus on vehicle dynamics control and active safety. He is currently a Senior Professor with the Department of Mechanics and Maritime Sciences, Chalmers University of Technology; and the Head of the Vehicle Dynamics Group.